
Molecules of astrochemical interest: theoretical and experimental studies

Domenico Prudenzano



München 2020

Molecules of astrochemical interest: theoretical and experimental studies

Domenico Prudenzano

Dissertation
an der Physik
der Ludwig–Maximilians–Universität
München

vorgelegt von
Domenico Prudenzano
aus Italien

München, den 16 January 2020

Erstgutachter: Prof. Dr. Paola Caselli

Zweitgutachter: Prof. Dr. Dieter Braun

Tag der mündlichen Prüfung: 27 February 2020

Inhaltsverzeichnis

Zusammenfassung	xi
Summary	xiii
1 Introduction	1
1.1 Overview	1
1.2 Classes of molecules	2
1.2.1 Sulphur bearing molecules	3
1.2.2 Complex Organic Molecules (COMs)	4
1.3 Molecules as Swiss-Army knives: the perfect multi-purpose tools	6
1.4 Molecules in the gas phase	8
1.4.1 Rotational spectroscopy	8
1.4.2 Asymmetric-top rotors	11
1.4.3 Line intensity and selection rules	13
1.4.4 Centrifugal distortion	15
1.4.5 Nuclear quadrupole coupling	16
1.4.6 Line profile	18
1.5 Molecules in the solid phase	20
1.5.1 Vibrational spectroscopy	20
1.5.2 Normal modes	21
1.5.3 Column density	22
1.6 Collisional excitation	22
1.6.1 Basis set functions	22
1.6.2 Electronic Schrödinger equation	23
1.6.3 Nuclear Schrödinger equation	24
2 Instrumentation	27
2.1 Absorption cell spectrometer	27
2.1.1 Discharge cell	27
2.1.2 Pyrolysis cell	29
2.1.3 Spectrometer	30
2.2 Infrared spectrometer for photoionization	31

3 Rotational spectroscopy and solid-phase study of dithioformic acid, HCSSH	33
3.1 Introduction	33
3.2 Accurate millimetre and submillimetre rest frequencies for <i>cis</i> - and <i>trans</i> -dithioformic acid, HCSSH	35
3.2.1 Experimental setup	35
3.2.2 Results and data analysis	35
3.2.3 Discussion and conclusions	37
3.3 Dithioformic acid formation in ion irradiated ice analogues	39
3.3.1 Experimental setup	39
3.3.2 Results and data analysis	40
3.3.3 Discussion and conclusions	41
4 Accurate millimetre and submillimetre rest frequencies for <i>E</i>- and <i>Z</i>-propargylimine, HCCCHNH	45
4.1 Introduction	45
4.2 Experimental setup	46
4.3 Results and data analysis	46
4.4 Discussion and conclusions	50
5 Collisional excitation of NH(${}^3\Sigma^-$) by Ar: a new <i>ab initio</i> 3D Potential Energy Surface and scattering calculations	53
5.1 Introduction	53
5.2 Potential energy surface	54
5.2.1 Analytical representation of the potential energy surface	55
5.2.2 NH–Ar bound states and dissociation energy	57
5.3 Scattering calculations	58
5.4 Comparison with experiments	61
5.5 Conclusions	63
6 Conclusions	65
A HCSSH: theoretical calculations	67
B HCCCHNH: theoretical calculations	71
Bibliography	86

Abbildungsverzeichnis

1.1	Life-cycle of interstellar medium objects (van Dishoeck, 2017)	2
1.2	Schematic overview of molecules formation in solid-phase and consequent passage into the gas phase due to energetic processes (Whittet, 2017)	7
1.3	Distribution of rotational levels for prolate (left), asymmetric (center) and oblate (right) rotors. The asymmetric top levels are labelled with the subscript τ corresponding to $K_{-1} - K_1$ (Gordy and Cook, 1984)	12
1.4	quadrupolevectors	16
2.1	Different regimes of self sustaining discharges, depending of the current-to-voltage ratio. The image is taken from Piel (2017)	28
2.2	(a) Regions of a glow discharge. (b) Electric potential Φ and axial electric field (E) variation in the normal regime. The image is taken from Piel (2017)	29
2.3	General scheme of the discharge and pyrolisys cells connected to the FM spectrometer. Full description of each component is given in the text.	30
2.4	Scheme of the high vacuum chamber for the IR study of ion irradiated ice analogues.	32
3.1	Molecular structures of the two planar isomers of HCSSH. Details concerning the geometries of the two species are given in Section 3.2.2 and Appendix A. Yellow spheres indicate sulphur atoms, the dark grey sphere indicates carbon, and hydrogen atoms are shown in light grey.	34
3.2	(Left panel) Experimental spectra of the $54_{7,*} - 53_{7,*}$ transitions of <i>trans</i> -HCSSH, with total integration time of 146 s and 3 ms of time constant. (Right panel) Experimental spectra of the $53_{7,*} - 52_{7,*}$ transitions of <i>cis</i> -HCSSH with total integration time of 87 s and 3 ms of time constant. (Both panels) The $K_a=7$ asymmetry doublet is not resolved. The red traces indicate the resulting line profile fitted with the proFFit code (see text).	36
3.3	Intensities and line distributions of rotational transitions at 10 and 100 K, for <i>trans</i> and <i>cis</i> dithioformic acid isomers. Most of the bandheads above 250 GHz are produced by <i>b</i> -type transitions.	39
3.4	IR trasmittance spectra of the mixture of H ₂ S:CO with ratio 1:1.	40
3.5	IR trasmittance spectra of the mixture of H ₂ S:CO with ratio 1:6.	41

3.6	Column densities plotted as a function of fluence during irradiation of the ice mixture for H ₂ S, CS ₂ and HCSSH.	43
3.7	Column densities of CS ₂ and HCSSH plotted as a function of dose and normalized over the initial H ₂ S abundance.	44
4.1	Molecular structure and principal inertial axes of the Z and E isomers of propargyl imine. The orange arrow indicates the direction of the electric dipole moment μ and points towards the displacement of the notional negative charge.	47
4.2	Recording of the $J_{K_a,K_c} = 8_{2,10} - 7_{2,9}$ of Z-HCCCHNH showing the two weak $\Delta F = 0$ hyperfine components symmetrically separated from the central blended $\Delta F = +1$ triplet by 1.3 MHz (<i>upper panel</i>). Total integration time 47 s with time constant $RC = 3$ ms. The area enclosed in the dashed box is plotted with expanded y-axis in the <i>lower panel</i>	48
4.3	Recordings of two b-type transitions for E-propargyl imine showing the typical hyperfine structure produced by the quadrupole coupling of the ¹⁴ N nucleus. <i>Left panel</i> : $J_{K_a,K_c} = 5_{1,5} - 4_{0,4}$; integration time 180 s. <i>Right panel</i> : $J_{K_a,K_c} = 5_{2,3} - 6_{1,6}$; integration time 165 s. The adopted scan rate is 0.2 MHz s ⁻¹ with time constant $RC = 3$ ms.	49
5.1	Definition of the Jacobi coordinate system. The origin of the coordinate system corresponds with the NH center of mass. R is the distance between the origin and the Ar atom, θ is the angle at which the Ar approach the NH molecule and r is the NH bond length.	54
5.2	Contour plot (in cm ⁻¹) of the NH–Ar PES averaged over the ground vibrational state $v = 0$ as a function of Jacobi coordinates R and θ	56
5.3	Collisional excitation cross sections of NH by Ar from $N = 0, F_1$. The upper panel is for fine-structure conserving transitions while the two other panels are for fine-structure changing transitions.	60
5.4	Thermal dependence of the rate coefficients of NH by Ar from $N = 0, F_1$. The upper panel is for fine-structure conserving transitions while the two other panels are for fine-structure changing transitions.	62

Tabellenverzeichnis

1.1	Most abundant elements in the Milky Way, based on their cosmic elemental abundances (Asplund et al., 2009).	3
1.2	Matrix elements of the angular momentum operators in the symmetric-top basis, for the body-fixed axes system.	13
3.1	Spectroscopic parameters of the two conformers of HCSSH. The results of this study are compared with those of Bak et al. (1978).	37
3.2	Partition functions of <i>trans</i> -HCSSH and <i>cis</i> -HCSSH at various temperatures.	38
3.3	Band strength values, A , for each corresponding vibrational band used to calculate the column densities.	42
4.1	Summary of the transitions with resolved hyperfine structure recorded for both propargyl imine isomers.	50
4.2	Experimental and theoretical spectroscopic parameters of E and Z isomers of propargyl-imine. Number in parentheses are 1σ statistical uncertainties in the units of the last quoted digit.	51
5.1	NH–Ar bound energy levels (in cm^{-1}) obtained excluding the NH fine structure. Energies are relative to the ground-state energy of NH. All the levels correspond to the approximate quantum numbers $N = 0$. J and l correspond to the total and orbital angular momentum of the complex, respectively.	57
5.2	NH–Ar bound energy levels (in cm^{-1}) obtained with the inclusion of the NH fine structure. Energies are relative to the ground-state energy of NH. All the levels correspond to the approximate quantum numbers $N = 0, F_1$. J and l correspond to the total and orbital angular momentum of the complex, respectively.	58
5.3	Comparison between experimental and our theoretical cross sections at a collisional energy of 410 cm^{-1} and for transitions out of the $N = 0, F_1$ rotational level. All the values are normalized with respect to the cross section for the $N = 0, F_1 \rightarrow N' = 1, F_1$ transition. Experimental error in parenthesis are in units of the last quoted digit.	63

5.4	Comparison between experimental and convolved theoretical cross sections at a collisional energy of 410 cm^{-1} and for transitions out of the $N = 0, F_1$ rotational level. All the values are normalized with respect to the cross section of the $N = 0, F_1 \rightarrow N' = 1, F_1$ transition. Experimental error in parenthesis are in units of the last quoted digit. The convolution of the theoretical values is described in Section 5.4. As a comparison, we also included the relative values obtained without the elastic contributions in the $N = 0, F_1 \rightarrow N' = 1, F_1$ and $N = 0, F_1 \rightarrow N' = 1, F_2$ cross sections.	64
A.1	Equilibrium geometries and energies of <i>trans</i> -HCSSH and <i>cis</i> -HCSSH are reported. All the values were computed at the CCSD(T) level of theory.	68
A.2	Dipole moments of <i>trans</i> -HCSSH and <i>cis</i> -HCSSH. All the values were computed at the CCSD(T) level of theory.	69

Zusammenfassung

Moleküle sind wichtige Träger von einer großen Anzahl an Informationen. Im besonderen innerhalb des astrochemischen Feldes können sie genutzt werden, um abhängig von der involvierten Technik, Chemie und Physik Details über die untersuchte Quelle zu gewinnen.

Moleküle im Gaszustand können mittels der Rotationsspektroskopie durch Signale im elektromagnetischen Spektralbereich der Radio- und Mikrowellen detektiert werden. Um dabei zu helfen, die komplexen Spektren einer Quelle zu entschlüsseln und die detektierten Signale zu verstehen, arbeiten Forscher in der labortechnischen Spektroskopie ununterbrochen mit Beobachtern zusammen, um eine Datenbank molekularer Spektren bereitzustellen. Studien im Labor sind in der Tat das beste Mittel, um unbekannte Spektren zu verstehen, welche dann an die Beobachter weitergereicht werden und dazu verwendet werden, das chemische Wissen einer astronomischen Quelle zu vervollständigen. Abhängig vom ausgewählten Molekül können verschiedene Instrumentierungen und Experimente verwendet werden. Ganz besonders exotische Spezies, die nicht unter irdischen Bedingungen produziert werden können, können durch hochenergetische Techniken wie etwa der Entladung oder Pyrolyse erzeugt werden.

Um zusätzlich Informationen über den festen Zustand zu erhalten, müssen Infrarotspektren ebenfalls studiert werden. Diese Studien nutzen die Vibrationsspektroskopie, welche innerhalb des interstellaren Mediums (ISM) die Anwesenheit einer infraroten (IR) Quelle benötigt, um detektierbare Absorptionssignale zu erzeugen. Auch wenn die direkte Erforschung von Staub und Eiskörnern im ISM eine Herausforderung darstellt, so können im Labor unter der Simulation von Bedingungen ähnlich denen im ISM Nachbildung von Eis erzeugt und charakterisiert werden. Mittels hochenergetischer Interaktionen wie etwa Protonenbeschuss oder Erhitzung können Eisnachbildungen chemische Prozesse durchlaufen, die für das Verständnis über die Formung und Zerstörung von Molekülen in der festen Phase hilfreich sind.

Sobald die Spektren gesammelt und entschlüsselt wurden, ist es ebenfalls wichtig zu verstehen, wie einzelne Moleküle miteinander sowie mit Strahlung interagieren. Das Wissen um Kollisionen und Energieübertragung im besonderen ist relevant, um die beobachteten Rotationsübergänge richtig zu modellieren, um Informationen über die lokalen physikalischen Bedingungen zu erhalten.

Um Theoretikern und Beobachtern bei dieser Herausforderung zu helfen, müssen die sogenannten Ratenkoeffizienten bereitgestellt werden, um zuverlässige Ergebnisse zu erhalten. Solche Koeffizienten beschreiben, wie einzelne Kollisionen ein bestimmtes Molekül rotational anregen können. Sie können berechnet werden, indem rechnergestützt eine große Anzahl von Techniken und Methoden, die sich der Simulationen von Streuung widmen, angewandt werden.

All diese Studien (spektroskopische und solche der Kollisionen) fallen unter die Klassifizierung von Astrochemie im Labor und sie stellen sich auf täglicher Basis beobachtender und theoretischer Astrochemie zur Seite, um die chemische Charakterisierung einer Zielquelle zu vervollständigen und ihre zeitliche Evolution zu verstehen.

Spektroskopische Studien im Labor sind somit ununterbrochen notwendig, um mit der großen Menge an Daten, die jeden Tag von Beobachtern gesammelt werden, Schritt zu halten und Modellierern dabei zu helfen, eine höhere Verlässlichkeit ihrer Simulationen zu erhalten. Dieses fortwährende Zwischenpiel und die gemeinsamen Bemühungen haben in den letzten Dekaden wertvolle Ergebnisse geliefert, aber es muss immer noch viel getan werden, um unser Verständnis vom ISM zu vervollständigen.

Der Fokus dieser Arbeit: Spektroskopie zweier Moleküle von astrochemischem Interesse im Labor, namentlich Dithiomethansäure (HCSSH), eine schwefelhaltige Verbindung, und Proparaglymin (HCCCHNH), ein sogenanntes komplexes organisches Molekül (COM) sowie Berechnungen zur Streuung von NH in Kollision mit Argon, ein Vergleichstest für eine neu entwickelte Methode, die Vibrationsbewegungen des kollidierenden Moleküls miteinbezieht.

Summary

Molecules are important carrier of a large number of information. Within the astrochemistry field, in particular, they can be employed to retrieve details on the studied source depending on the technique, the chemistry and the physics involved.

Molecules in the gas phase can be detected by means of rotational spectroscopy, with signals falling within the radio and microwave domain of the electromagnetic spectrum. To help decoding the complex spectra of a source and understand the detected signals, laboratory spectroscopists work constantly in cooperation with observers to provide databases of molecular spectra. Laboratory studies are in fact, the best tool to understand unknown spectra which can then be passed to observers and used to complete the chemical knowledge of an astronomical source. Depending on the targeted molecule, different instrumentations and experiments can be carried out. In particular, exotic species that cannot be produced on terrestrial conditions, can be created employing high energetic techniques such as the discharge or the pyrolysis.

In addition, to obtain information on the solid phase, infrared spectra must be studied, too. These studies make use of vibrational spectroscopy, which within the interstellar medium (ISM) requires the presence of an infrared (IR) source to produce detectable absorption signals. However given the challenges for direct studies of ISM dust and ice grains, ice analogues can be produced and characterized in the laboratory, simulating similar ISM conditions. By means of high energetic interactions, such as proton bombardment and heating, ice analogues can undergo chemical processes, helpful to understand how molecules form and are destroyed in the solid phase.

Once the spectra have been collected and deciphered, it is also important to understand how the single molecules interact with each other and with the radiation. In particular, knowledge of collisions and energy transfer are relevant to model correctly the observed rotational transitions, to obtain information on the local physical conditions.

To help theoreticians and observers in this challenge, the so-called rate coefficients must be provided to obtain reliable results. Such coefficients describe how the single collisions can rotationally excite a certain molecule and can be calculated computationally employing a large number of techniques and methods dedicated to scattering simulations.

All of these studies (spectroscopic and collisional) fall under the classification of laboratory astrochemistry, which side on a daily basis with observational and theoretical astrochemistry to complete the chemical characterization of a target source and fully understand its evolution through time.

Laboratory spectroscopy studies are hence constantly required to keep pace with the large

pool of data collected every day by observers and to help modellers to achieve higher reliability with the simulations. This constant interplay and joint effort have produced valuable results within the last decades, but much is still needed to be done to complete our understanding of the ISM.

This thesis focus on: laboratory spectroscopy of two molecules of astrochemical interest, namely dithioformic acid (HCSSH), a sulphur-bearing species, and propargyl imine (HCCCHNH), a so-called Complex Organic Molecule (COM), and on scattering calculations of NH in collision with Argon, benchmark test for a newly developed method involving vibrational motions of the colliding molecule.

Kapitel 1

Introduction

1.1 Overview

Of all the matter present in the universe known so far, only a modest quantity, namely less than 5%, is baryonic (Persic and Salucci 1992, Planck et al. 2013) and only a small, almost insignificant fraction of it is in the form of molecules. Despite their "low abundance, molecules are what constitute our daily life: each colour we see is linked to a different molecular species; the food we eat everyday is taken apart and metabolized by our body as proteins, aminoacids, fats and so on; H₂O is responsible of the existence of cellular life itself, while similar compounds such as H₂S could be easily responsible for its complete disappearance.

For this reason, molecules have been and still are the main scaffold around which many different fields of science are born and built. Among these, astrochemistry has been able to grow exponentially within the last decades, making use of every possible characteristic of molecules to retrieve a variegated amount of information regarding the observed astrophysical objects.

Astrochemistry is a melting pot of chemistry, astronomy and, more in general, molecular physics, and can be essentially defined as the study of "the formation, destruction, and excitation of molecules in astronomical environments and their influence on the structure, dynamics, and evolution of astronomical objects." (Dalgarno, 2008).

The molecular material in the interstellar medium (ISM), in fact, follows a path of cyclic evolution which sees formation of specific molecules within only certain types of objects. Most of the molecules are not ubiquitous and therefore can be easily linked to certain characteristics of the ISM, probing specific moments in its life-cycle. In addition, some chemical compounds are also carrier of supplementary physical information, such as local temperatures and dynamics and can be used to probe such features.

Starting from the diffuse clouds, the ISM life-cycle proceeds through formation of dense molecular clouds which constitute the birthplace for stars and planetary systems and ends with the release of their chemical content as a consequence of many possible events, such as stars explosion.

Thus, probing the ISM searching for molecular signals both in the gas and solid phase, and the consequent understanding of its chemical composition, is necessary to fully characterize a

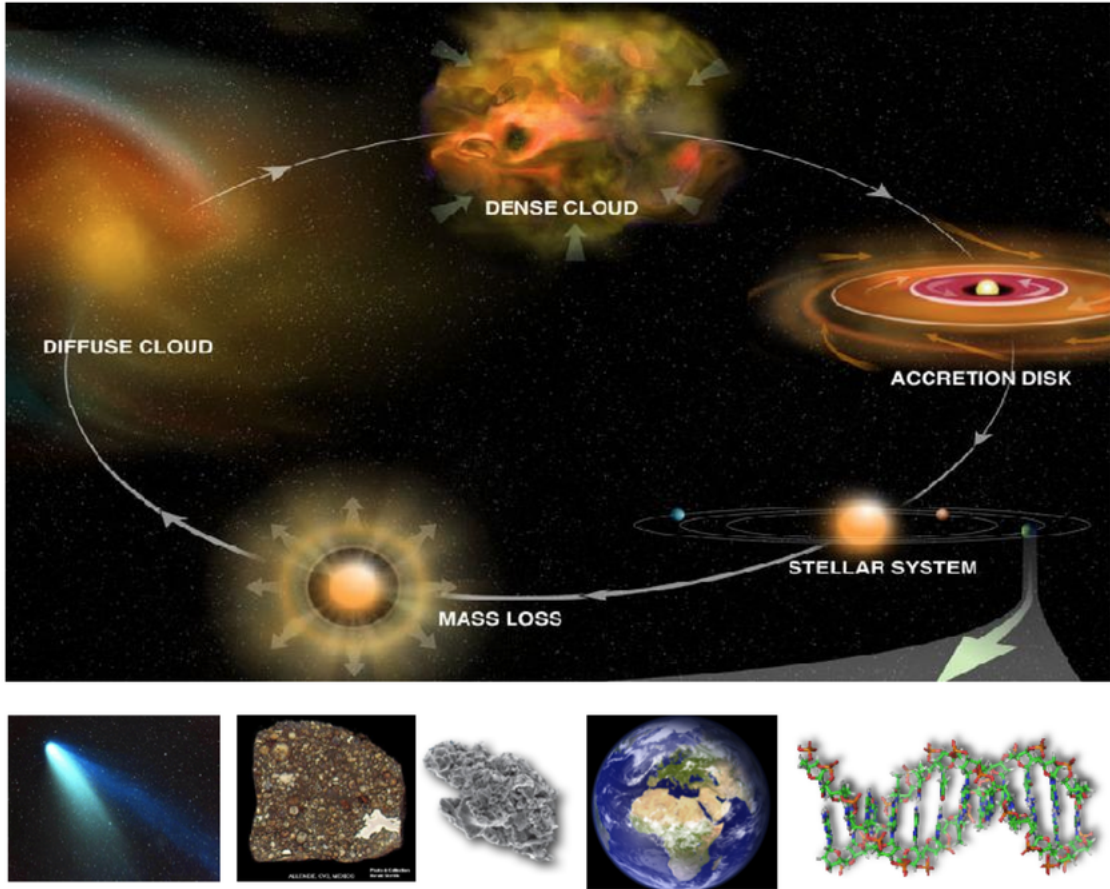


Abbildung 1.1: Life-cycle of interstellar medium objects (van Dishoeck, 2017).

source. Once a first overview of the chemical network is obtained, chemical models can then be used to simulate and reproduce the observed chemistry to understand the source pathways and evolution. To achieve higher reliability and better reproduce energy transfer, these models ideally require information on both chemical reactions and scattering for every species taken into account.

As a result, molecules can unveil the past and the present of our species, and of the universe itself. Astrochemistry, in a way, is the translation of an encoded language based on a complex vocabulary made of molecules.

1.2 Classes of molecules

Each stage within the evolution of the ISM has specific physical properties and since each molecule forms and survives only under certain conditions, we can choose among a large number of compounds depending on the source we want to focus on and depending on our final goal.

However, given the large number of candidates for further and new studies, the best place to

begin with is to consider the cosmic abundance of the chemical elements and their propensity to form molecules of astronomical interest. Table 1.1, shows the ten most abundant elements in our galaxy (Asplund et al., 2009).

Tabelle 1.1: Most abundant elements in the Milky Way, based on their cosmic elemental abundances (Asplund et al., 2009).

Element	Relative abundance
Hydrogen	1
Helium	8.51×10^{-2}
Oxygen	4.90×10^{-4}
Carbon	2.69×10^{-4}
Neon	8.51×10^{-5}
Nitrogen	6.76×10^{-5}
Magnesium	3.98×10^{-5}
Silicon	3.24×10^{-5}
Iron	3.16×10^{-5}
Sulphur	1.32×10^{-5}

A combination of these, then, can be taken into account and many classes of species can be formed depending not only on the elements involved, but also on the total number of atoms of the compound, on the molecular stability and depending on their electronic structure. Two groups of molecules are of interest for the scope of this thesis, namely the sulphur-bearing ones and the Complex Organic Molecules.

1.2.1 Sulphur bearing molecules

Sulphur chemistry has attracted interest since the early 70s, when the first S-bearing molecule, CS, was detected in the interstellar medium (Penzias et al., 1971), followed by observations of other sulphur species in the same decade, such as OCS, H₂S, and CH₃SH (Jefferts et al. 1971, Thaddeus et al. 1972, Linke et al. 1979 and references therein).

In diffuse clouds sulphur is mainly found in the gas phase in the form of S⁺ and has cosmic abundances of $\sim 10^{-5}$ with respect to the H nuclei (Jenkins 1987, Savage and Sembach 1996). However, to reproduce the observed abundances of S-bearing molecules in dark clouds (Oppenheimer and Dalgarno 1974, Tieftrunk et al. 1994), chemical models typically assume that sulphur is highly depleted, using an initial elemental abundance of 8×10^{-8} (Wakelam and Herbst, 2008). A possible explanation of this problem is given by Ruffle et al. (1999), who proposed that during collapse of translucent gas, sulphur tends to freeze-out more than other elements, due to its predominant ionized form, S⁺, which is subject to strong electrostatic attraction to negatively charged grains.

Many studies have discussed the problem and some have suggested that most of the missing sulphur in the ISM dense regions could be trapped in the solid phase as either polysulphanes, having the formula H_xS_y (Jiménez-Escobar and Muñoz Caro 2011, Druard and Wakelam 2012),

or refractory sulphur polymers, such as S₈ (Wakelam et al., 2004, 2005; Shingledecker et al., 2020). However, the main reservoirs of solid sulphur are still unknown.

Some laboratory studies, focused on dust and ice analogues, proposed carbon disulfide (CS₂), as a major sink of sulphur (Ferrante et al. 2008, Garozzo et al. 2010, Jiménez-Escobar et al. 2014). Recently, CS₂ has been found in the comas of some comets through the identification of its emission spectra in the UV and visible region (Jackson et al., 2004), or in situ by ROSINA (Calmonte et al., 2016). In particular, Calmonte et al. (2016) have found that the amount of CS₂ in the coma of 67P/Churyumov-Gerasimenko accounted for the 0.35% of the total sulphur content, resulting more abundant than thioformaldehyde (H₂CS, 0.14%), a well-known S-bearing molecule, detected for the first time in SgrB2 by Sinclair et al. (1973). Nevertheless, carbon disulfide is still undetected in interstellar ices. Furthermore, in warm and shocked regions, where this compound could be transferred in the gas phase as a result of evaporation and sputtering of the grains, its detection by means of radio telescopes is unfeasible because it has no permanent dipole moment. Therefore, S-bearing molecules chemically related to CS₂ should be alternatively sought.

Recently, many steps have been taken towards improving our understanding of interstellar sulphur chemistry, as highlighted by the detection of new S-bearing compounds, such as S₃, S₄, and ethyl mercaptan (CH₃CH₂SH) in the comas of 67P/Churyumov-Gerasimenko (Calmonte et al., 2016) and a tentative detection of CH₃CH₂SH in Orion KL (Kolesniková et al., 2014). Moreover, chemical models have been significantly improved through expansion of the sulphur chemical network by the inclusion of these compounds and many other reactions and species (Woods et al. 2015, Vidal et al. 2017, Laas and Caselli 2019, Shingledecker et al. 2020).

Notwithstanding this progresses, a number of important species are still not considered in the current picture of sulphur chemistry and further studies are required to expand and possibly complete our understanding of these molecules.

1.2.2 Complex Organic Molecules (COMs)

By terrestrial standard most of the detected and studied ISM molecules are considered small and simple. However, the point of view towards these species changes drastically within the astronomical environment. In dense objects the most abundant species is molecular hydrogen (H₂), followed by carbon monoxide (CO), which has a typical fractional abundance of 10⁻⁴ with respect to H₂ (Bolatto et al., 2013). By increasing the number of atoms the abundances decrease drastically, with fractional values ranging between 10⁻⁵ and 10⁻¹¹, even for simple species such as ammonia (NH₃) and methanol (CH₃OH) (Pratap et al. 1997, Suzuki et al. 1992).

Hence, molecules such as methanol can be already considered complex from an astrochemical point of view. As a matter of fact, as stated by Herbst and van Dishoeck (Herbst and Van Dishoeck, 2009) “we arbitrarily refer to species with six atoms or more as complex”. In addition, since all of the complex species detected up to date contain at least one atom of carbon, the term “complex molecules” has always been coupled with “organic”.

These compounds, have received an increasing attention in the last decade in a effort of unveiling how chemical complexity builds up, from the earlier phases of the star formation —

where simple species dominate — to the much larger molecular structures required to establish biological processes on planets where appropriate conditions are met.

Among the over 220 molecules detected in the ISM and circumstellar shells (as of February 2020), approximately 70 are Complex Organic Molecules (COMs) (Endres et al., 2016).

Given this fairly large sample, sub-groups can be easily arranged. In first place, depending on the hydrogen content, we can have saturated and unsaturated COMs, i.e. rich or poor in hydrogen, respectively. Both these two groups contain all the detected hydrocarbons, which can be mainly found within cold clouds or in circumstellar envelopes. COMs containing oxygen are typical of molecular rich regions of the Galactic center (such as SgrB2) and hot regions more in general, while nitrogen-containing COMs are ubiquitous (Herbst and Van Dishoeck, 2009).

The latter are particularly interesting as they can be regarded as an intermediate step towards the formation of biologically important species, such as nucleobases and amino acids.

As protein constituents, amino acids are prime targets for astrobiological studies, and their extra-terrestrial formation is a highly debated topic. Numerous compounds of this class have been found in carbonaceous chondrites (see e.g., Cobb and Pudritz, 2014, and references therein), where they are thought to form by aqueous alteration (see Burton et al. 2012 for a review on meteoritic prebiotic compounds).

Glycine, the simplest amino acid, has not been firmly detected in the ISM to date (Snyder et al., 2005), however it was found in the aerogel samples returned to Earth by the *Stardust* mission after 81P/Wild 2 comet flyby (Elsila et al., 2009) and, more recently, it has also been unambiguously identified in the coma of the P67 comet through *in situ* mass spectrometry (Altweig et al., 2016). The presence of glycine in the volatile cometary material thus strongly suggests the existence of a process able to generate amino acids in absence of liquid water.

Many theoretical and laboratory studies have been devoted to the investigation of the chemical routes which may lead to amino acids in diverse extra-terrestrial environments (see e.g., Woon, 2002; Koch et al., 2008; Aponte et al., 2017, and references therein). The most promising pathways in interstellar ice analogues involve, as the last step, the hydration of an amino-nitrile compound which, in turn, may be generated by cyanide ($\text{R}-\text{CN}$) hydrogenation, or through the Strecker-cyanohydrin mechanism, i.e., via addition of ammonia to an aldehyde ($\text{R}-\text{CHO}$, Danger et al., 2011; Theulé et al., 2011).

In either cases, the process involves a species containing the iminic moiety ($\text{RC}=\text{NH}$) as reactive intermediate (Aponte et al., 2017).

Imines are a class of molecules that are well represented in the ISM with six members detected to date. Four are simple chains: methanimine (CH_2NH , Godfrey et al., 1973; Dickens et al., 1997), ethanimine (CH_3CHNH , Loomis et al., 2013), ketenimine (CH_2CNH , Lovas et al., 2006), and 3-imino-1,2-propadienylidene (CCCNH , Kawaguchi et al., 1992); but there are also the substituted C-cyano-methanimine (NCCHNH , Zaleski et al., 2013; Rivilla et al., 2018), and the cumulated “dimer” carbodiimide (HNCNH , McGuire et al., 2012).

These observational evidences point to a preponderance of unsaturated chains and suggest a common formation route from simple nitriles via tautomerisation (Lovas et al., 2006) or by partial hydrogenation on dust grain surface (Theulé et al., 2011; Krim et al., 2019).

Hence, new imines can be chosen as targets for new and further studies, to better understand and complete our knowledge of the COMs chemistry and, in particular of the pathways towards

amino acids formation.

1.3 Molecules as Swiss-Army knives: the perfect multi-purpose tools

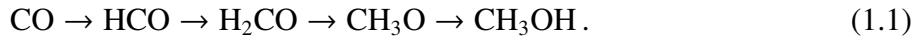
Until the 40s it was thought that molecules in space were something extremely rare and nearly impossible to form, mostly because only small ionized or radical compounds had been observed, such as CH, CH⁺ and CN, and only as absorption signals within the visible range of the electromagnetic spectrum (McKellar 1940, Douglas and Herzberg 1941).

The birth of radio-telescopes allowed for the first time detection of interstellar molecular signals first within the centimetre domain and later on also in the millimetre and sub-millimetre range, opening a whole new region to astronomers (Sullivan, 2004). Many new molecules were detected across the sky in the gas phase and rotational spectroscopy became a new and perfectly suitable tool for astronomy.

In particular within the last decades, rotational spectroscopists have also been regularly involved to provide large databases of molecular spectra (Endres et al., 2016), helping the astrochemistry community to identify as many unknown signals as possible. Laboratory studies are constantly required for molecules never studied before, to keep pace with the increasing number of observational data collected every year.

This joint effort have produced valuable results, and, especially in the last 20-30 years, thanks to the large advances in terms of theory and technology, it has resulted in more than 220 molecules detected in the ISM, with many more to be found.

In addition, given that rotational spectroscopy is limited to gas-phase chemistry, these works are often followed by, or coupled with solid-phase studies. Surface chemistry becomes indeed highly relevant when gas-phase reactions alone cannot justify formation and abundances of certain species. Most of the molecules, in fact, are born on dust grains coated with ice mantles, where processes like hydrogenation are faster and more efficient. For instance, the main formation path for CH₃OH rely on the progressive hydrogenation of CO locked onto solid-phase, as follows (Watanabe and Kouchi, 2002):



In addition, in presence of cosmic rays, UV radiation and other high energy interactions, simple molecules can easily fragment and recombine forming new compounds, which can then be released into gas-phase through different processes, such as thermal heating, shock heating, non-thermal desorption (photodesorption or excess chemical reaction energy) and sputtering (Whittet, 2017).

This constant interplay between the gas and the solid phases makes necessary the knowledge of grains chemical composition and abundances, obtainable by means of absorption features corresponding to molecular vibrational transitions. In the ISM the detection of such signals requires the presence of an infrared source embedded in the target or an intense background source, thus collect solid-phase data for starless clouds is a difficult task. In addition, direct detection of

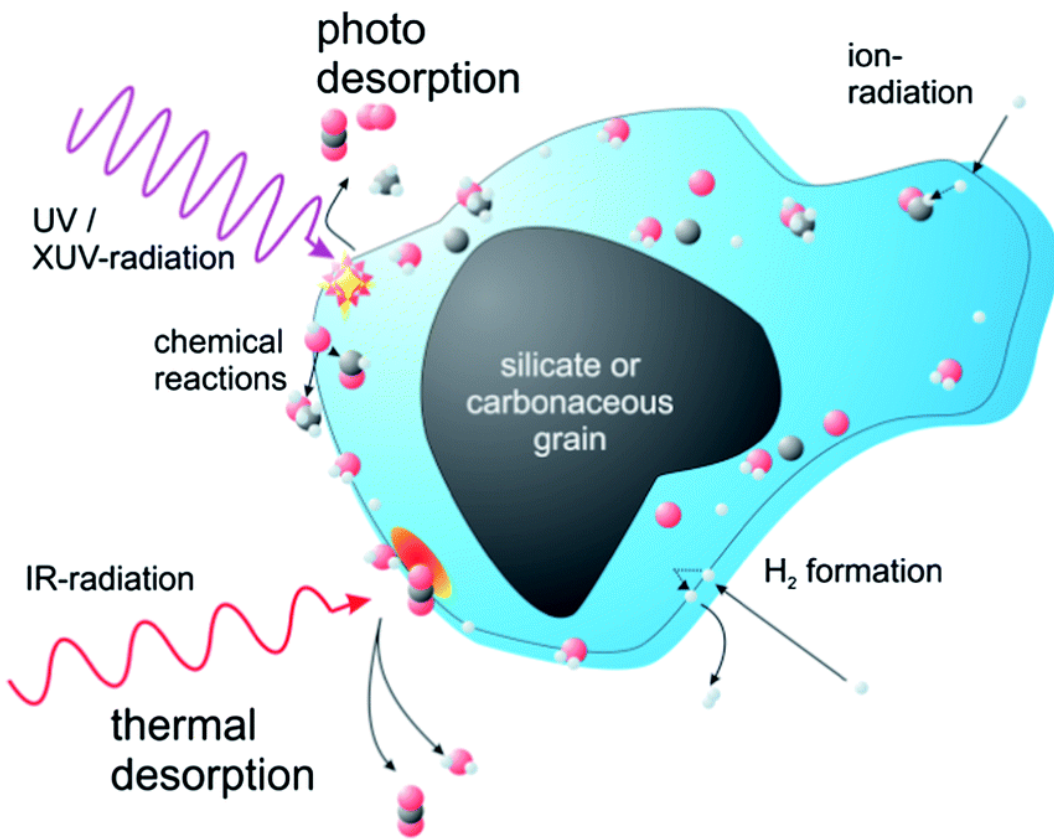


Abbildung 1.2: Schematic overview of molecules formation in solid-phase and consequent passage into the gas phase due to energetic processes (Whittet, 2017).

solid-phase species can be challenging due to intrinsically weak signals or due to the presence of vibrational bands that interfere and overlaps with each other. As a consequence, in most cases we cannot directly study or observe in detail the interstellar grains.

A reasonable solution to this problem is to reproduce and observe dust and ice analogues in the laboratory, which provides a controlled environment. In particular, ice analogues with different chemical compositions can be easily studied by means of vibrational spectroscopy while undergoing high energetic processes, such as proton bombardment or heating, to simulate similar ISM conditions.

All the data coming with these laboratory studies, both in the gas and solid phase, account for a large number of useful information. However, to complete the picture, the molecular rotational spectra can also be employed to obtain further and more detailed results by modelling their excitation scheme.

In fact, once a source has been chemically outlined at the best of our possibilities, it is important to understand how the single species interact with each other. On one side, chemical composition and reactions play a central role to fully model the evolution of the ISM, while scattering studies are important to understand molecular excitations and to obtain informations on the local physical conditions. Molecular collisions are, in fact, highly sensitive to properties such

as density or gas kinematic temperature, making certain molecules good and reliable tracers for the physics of the interstellar gas.

Knowledge of energy transfer due to inelastic collisions is, therefore, required to model the observed interstellar rotational transitions and with more and more molecules detected every year, computational studies have become the best choice to keep pace with the observers, being able to provide reliable results. In particular, new methods must always be benchmarked and a simple procedure to ensure reliable results is to start from simpler systems, i.e. involving Argon, Neon and Helium as colliding atoms, and then proceed with the one of astronomical interest but also more complex from a quantum mechanics point of view, i.e. molecular hydrogen.

The final results, i.e. the state-to-state rate coefficients, can then be employed to model all the observational data through radiative transfer simulations which make use of every single information retrieved by means of both laboratory and observational studies.

1.4 Molecules in the gas phase

Molecules are subject to different kind of motions depending on the energies involved and their physical state. While in solid and liquid phase motions are limited due to strong molecular interactions and hindrance, in gas-phase all the species can be considered free and isolated. Hence, rotational motions become always possible and, being unique of the gas phase, they are a perfect tool to study species in such a state.

Rotational spectroscopy makes use of signals rising from transitions between rotational levels, which are quantized and organized depending on the properties of each molecule. By experimental detection of such signals and by application of the theory, also through computational studies, is then possible to achieve an overall and complete knowledge of the different molecules considered.

Given that one of the main scope of this thesis is the study of molecules in the gas phase, here we will give a detailed overview of the main theoretical concepts of rotational spectroscopy, applied to the works presented in Chapter 3, 4 and 5.

1.4.1 Rotational spectroscopy

A convenient starting point for the understanding of rotational spectroscopy is the study of the motion of a rigid body. In fact, at a zero-th order of approximation a molecule can be considered as a system of point-like atoms, rigidly connected through chemical bonds. In classical mechanics the total angular momentum of such a system can be expressed as (Landau and Lifšits, 1978)

$$\mathbf{P} = \mathbf{I}\boldsymbol{\omega}, \quad (1.2)$$

where ω is the angular velocity and I is the moment of inertia tensor, a 3×3 matrix having as diagonal elements the moments of inertia (Gordy and Cook, 1984):

$$I_{\alpha\alpha} = \sum_i m_i(\beta_i^2 + \gamma_i^2), \quad (1.3)$$

and as off-diagonal elements the products of inertia:

$$I_{\alpha\beta} = I_{\beta\alpha} = - \sum_i m_i \alpha_i \beta_i, \quad (1.4)$$

in which α, β, γ are the coordinates x, y, z chosen cyclically and m_i is the mass of the i -th atom.

The cartesian (x, y, z) axis system is fixed in the body of the molecule and its origin is placed at the center of mass to allow separation of the translational and rotational motions.

Being real and symmetric, the I matrix is Hermitian. By the solution of the secular equation (Gordy and Cook, 1984)

$$\begin{vmatrix} I_{xx} - I & I_{xy} & I_{xz} \\ I_{yx} & I_{yy} - I & I_{yz} \\ I_{zx} & I_{zy} & I_{zz} - I \end{vmatrix} = 0, \quad (1.5)$$

it is possible to find the eigenvalues of the inertia tensor. This process corresponds to a rotation of the original axis system into the so-called principal axis system (a, b, c) . The products of inertia, i.e. the off-diagonal elements, are now equal to zero and the diagonal elements are the principal moments of inertia, $I_a \leq I_b \leq I_c$.

To identify the rotational spectral frequencies we need to solve the Schrödinger equation and find the energies of the rotational levels, i.e. the eigenvalues of the corresponding Hamiltonian operator. To do so, first it is important to define an appropriate classical Hamiltonian. Since no torque is applied, we define the classical Hamiltonian as the only kinetic component:

$$H = T = \frac{1}{2} P \omega. \quad (1.6)$$

Given equation (1.2) and considering each separate component of the angular momentum:

$$P_a = I_a \omega_a, \quad P_b = I_b \omega_b, \quad P_c = I_c \omega_c, \quad (1.7)$$

we can rewrite the classical Hamiltonian for a rigid rotor as:

$$H = \frac{1}{2} \omega \mathbf{I} \omega = \frac{1}{2} \left(\frac{P_a^2}{I_a} + \frac{P_b^2}{I_b} + \frac{P_c^2}{I_c} \right). \quad (1.8)$$

The next step is to replace each classical observable in (1.8) with its corresponding operator (Papousek and Aliev, 1982). For the angular momentum we have that:

$$P_x \rightarrow \hat{P}_x = \sum_n \frac{\hbar}{i} \left(y \frac{\partial}{\partial z} - z \frac{\partial}{\partial y} \right) \quad (1.9)$$

$$P_y \rightarrow \hat{P}_y = \sum_n \frac{\hbar}{i} \left(z \frac{\partial}{\partial x} - x \frac{\partial}{\partial z} \right) \quad (1.10)$$

$$P_z \rightarrow \hat{P}_z = \sum_n \frac{\hbar}{i} \left(x \frac{\partial}{\partial y} - y \frac{\partial}{\partial x} \right). \quad (1.11)$$

The resulting Hamiltonian operator is:

$$\hat{H} = \frac{4\pi^2}{\hbar} \left(A \hat{P}_a^2 + B \hat{P}_b^2 + C \hat{P}_c^2 \right), \quad (1.12)$$

where A , B and C are the rotational constants defined as

$$A = \frac{\hbar}{8\pi^2 I_a}, \quad B = \frac{\hbar}{8\pi^2 I_b}, \quad C = \frac{\hbar}{8\pi^2 I_c}. \quad (1.13)$$

Depending on the values of the moments of inertia we can define different classes of rotors, such as:

1. Linear, $I_a = 0, I_b = I_c$
2. Spherical, $I_a = I_b = I_c$
3. Symmetric prolate, $I_a < I_b = I_c$
4. Symmetric oblate, $I_a = I_b < I_c$
5. Asymmetric, $I_a < I_b < I_c$

All the non-asymmetric species have closed expressions for the energies as solution of the Schrödinger equation. For prolate symmetric-top molecules, the corresponding Hamiltonian is:

$$\hat{H} = \frac{\pi^2}{2I_b} + \frac{1}{2} \left(\frac{1}{I_a} - \frac{1}{I_b} \right) \hat{P}_a^2. \quad (1.14)$$

In this case \hat{H} commutes with the angular momentum operators \hat{P}^2 (total) and \hat{P}_z^2 (body-fixed); in addition it commutes also with the space-fixed operator \hat{P}_Z^2 (Gordy and Cook, 1984). Hence, an appropriate common set of eigenfunctions $|J, K, M\rangle$ must be considered. J , K and M are called good quantum numbers. J is the rotational quantum number labelling the total angular momentum, K is the quantum number for the projection of the total angular momentum onto the z (a) body-fixed (BF) axis and M is used for the projection of the angular momentum onto the space-fixed axis Z . Both K and M can assume integer values between $-J$ and J . Levels with $-K$ and $+K$ are degenerate, giving for each J a total of $J + 1$ non degenerate sub-levels, while the M sub-states are always degenerate for a given J and K , unless an external field is applied.

The set of eigenfunctions $|J, K, M\rangle$ is most easily obtained by expressing the angular momentum operators in Euler's angles θ, ϕ and χ and setting up the proper Hamiltonian operator (Gordy and Cook, 1984). The resulting wavefunction can be written as:

$$|J, K, M\rangle = \Theta_{J,K,M}(\theta) e^{iK\phi} e^{iM\chi}. \quad (1.15)$$

The functions $\Theta_{J,K,M}$ can be obtained as solutions of the Legendre equation:

$$\frac{1}{\sin \theta} \frac{\partial}{\partial \theta} \left(\sin \theta \frac{\partial \Theta(\theta)}{\partial \theta} \right) - \left[\frac{m^2}{\sin^2 \theta} + \left(\frac{\cos^2 \theta}{\sin^2 \theta} + \frac{A}{B} \right) K^2 - \frac{2 \cos \theta}{\sin^2 \theta} KM - \frac{E_r^0}{B} \right] \Theta(\theta) = 0 \quad (1.16)$$

and are Legendre polynomials $P_J^0(\cos \theta)$ if $K = M = 0$, or associated Legendre polynomials if $M \neq 0$. The only physically acceptable solutions correspond to the eigenvalues:

$$E_r^0 = E_{J,K} = BJ(J+1) + (A-B)K^2, \quad (1.17)$$

with E_r^0 being diagonal in J and K .

1.4.2 Asymmetric-top rotors

While the Schrödinger equation is easy to solve for symmetric rotors and gives analytical solutions for the energies, such as (1.17), this is not possible for asymmetric molecules. Having all of the three principal moments of inertia different from zero and from each other, the corresponding Hamiltonian operator:

$$\hat{H} = A\hat{P}_a^2 + B\hat{P}_b^2 + C\hat{P}_c^2, \quad (1.18)$$

does not commute with any body-fixed angular momentum operator. With only J and M left as good quantum numbers, to better identify the rotational levels we need to employ the so-called pseudo-quantum numbers. First we define the Ray's parameter, κ (Gordy and Cook, 1984):

$$\kappa = \frac{2B - A - C}{A - C}, \quad (1.19)$$

as an indication of the asymmetry of the molecule. With $\kappa = -1$, the rotor is prolate symmetric; $\kappa = 1$ corresponds to an oblate symmetric-top; $\kappa = 0$ equals the higher level of asymmetry. Furthermore, for asymmetric rotors, a value close to -1 or 1 identifies two particular types of asymmetric rotors, namely the near-prolate and the near-oblate.

In this situation, together with J , two pseudo-quantum numbers, i.e. K_{-1} e K_1 , are required to label the energy levels, which describe the quantum number K in the prolate and oblate limits for the symmetric case. Therefore, each energy level is labelled as $J_{K_{-1}K_1}$ and the degeneracy of $-K$ and K level is lost, giving for each J a total of $2J + 1$ rotational sub-levels. A schematic view of such rotational level is shown in 1.3.

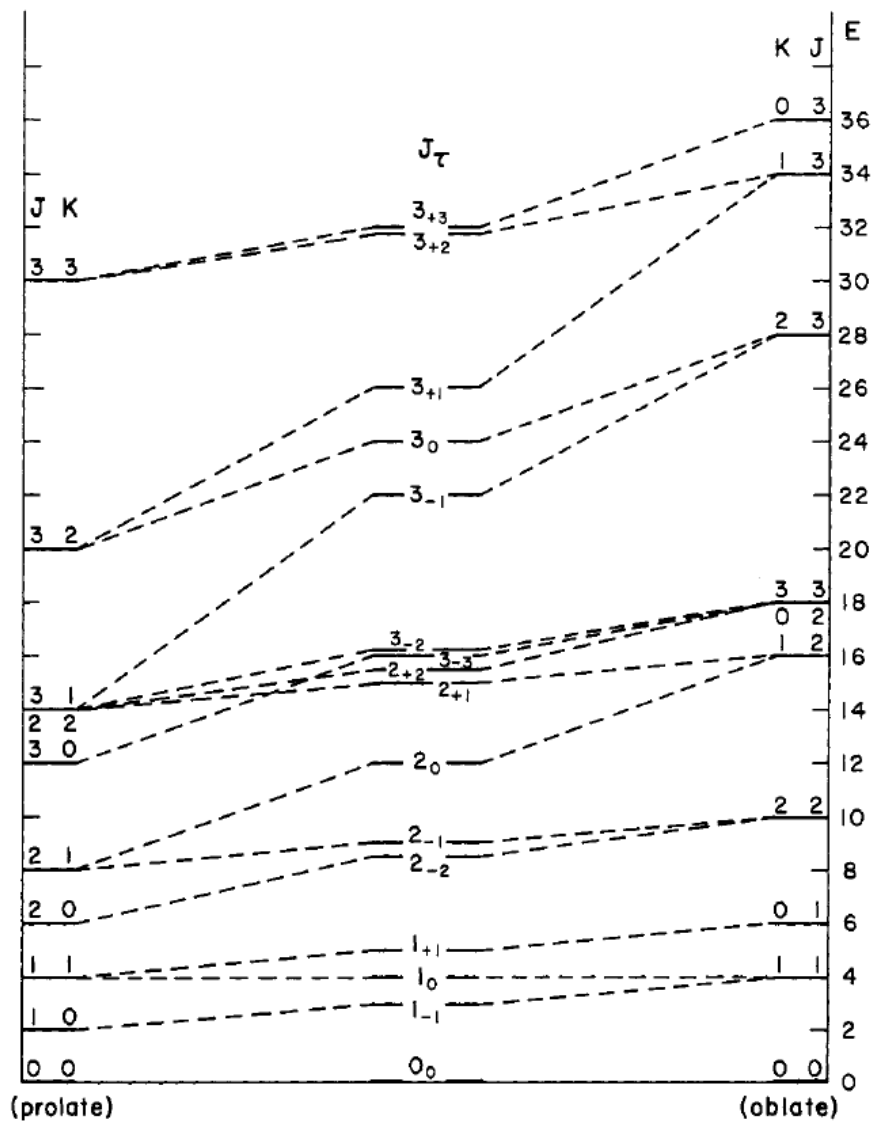


Abbildung 1.3: Distribution of rotational levels for prolate (left), asymmetric (center) and oblate (right) rotors. The asymmetric top levels are labelled with the subscript τ corresponding to $K_{-1} - K_1$ (Gordy and Cook, 1984)

To obtain the energies for the asymmetric case, we must consider the asymmetric eigenfunctions as a linear combination of the symmetric rotor functions (Gordy and Cook, 1984):

$$|J_{K-1} K_1 M\rangle = \sum_{J,K,M} a_{J,K,M} |J, K, M\rangle . \quad (1.20)$$

Here $a_{J,K,M}$ are numerical constants and can be calculated. It is possible then to obtain the asymmetric-top energies by diagonalization, as follows:

$$V^{-1} H_{K'K} V = E , \quad (1.21)$$

where E are the eigenvalues of $H_{K'K}$, i.e. the matrix representation of the asymmetric rotor Hamiltonian (1.18), expressed in the form:

$$H_{K'K} = \langle J, K', M | \hat{H} | J, K, M \rangle , \quad (1.22)$$

which is a tridiagonal matrix of size $(2J + 1) \times (2J + 1)$ with off-diagonal elements having $\Delta K = \pm 2$. V is the orthogonal eigenvector matrix containing the $a_{J,K,M}$ coefficients. Since (1.18) is a function of the angular momentum operators P_x^2 , P_y^2 and P_z^2 , we need to employ the corresponding matrix elements in the symmetric-top representation. These values are shown in Table 1.2.

Tabelle 1.2: Matrix elements of the angular momentum operators in the symmetric-top basis, for the body-fixed axes system.

$$\langle J, K, M | \hat{P}^2 | J, K, M \rangle = J(J + 1)$$

$$\langle J, K, M | \hat{P}_z^2 | J, K, M \rangle = K$$

$$\langle J, K, M | \hat{P}_y^2 | J, K, M \rangle = \langle J, K, M | \hat{P}_x^2 | J, K, M \rangle = \frac{1}{2}[J(J + 1) - K^2]$$

$$\begin{aligned} \langle J, K, M | \hat{P}_y^2 | J, K \pm 2, M \rangle &= \langle J, K, M | \hat{P}_x^2 | J, K \pm 2, M \rangle = \\ &= \frac{1}{4}[J(J + 1) - K(K \pm 1)][J(J + 1) - (K \pm 1)(K \pm 2)]^{1/2} \end{aligned}$$

1.4.3 Line intensity and selection rules

For the rotational transitions to be visible it is important that the molecule have an electric dipole moment different from zero and permanent. The electric dipole moment, μ , is given in Debye (D) and represents the magnitude of the separation of charges along the molecular principal axis system. To be present, the molecule must not be centrosymmetric, therefore molecules such as H_2 or NCCN cannot be studied by means of sole rotational spectroscopy. From Time-Dependent Perturbation Theory we know that the transition rate is proportional to the square of the modulus of the transition dipole moment and to the intensity of the incident radiation, as follows:

$$W_{f \leftarrow i} = \frac{|\mu_{fi}|^2 \rho_R(\nu_{fi})}{6\epsilon_0 \hbar^2} , \quad (1.23)$$

where $\rho_R(\nu_{fi})$ is the energy density for a given transition frequency ν_{fi} and μ_{fi} is the transition dipole moment:

$$\mu_{\mathbf{f}} = \int \Psi_f^* \mu \Psi_i d\tau, \quad (1.24)$$

with μ being the electric dipole moment operator and Ψ_f and Ψ_i the wavefunctions of the final and initial rotational states. As a consequence, a larger value of μ means more intense rotational transitions signals.

Non-zero values are given if the product in the (1.24) transforms according to the total symmetric representation. In particular, for the asymmetric rotor we must refer to the Four-group operations which characterize the symmetry of the inertia ellipsoid (Gordy and Cook, 1984). For some combinations of the initial and final states, however, $\mu_{\mathbf{f}}$ vanishes, leading to the so-called forbidden transitions.

The resulting specific selection rules and corresponding changes in the quantum numbers for the allowed transitions are $\Delta J = 0, \pm 1$ and:

$$\Delta K_{-1} = 0, \pm 2 \quad \Delta K_1 = \pm 1, \pm 3$$

for the *a*-type transitions (component of the dipole moment along the *a* axis);

$$\Delta K_{-1} = \pm 1, \pm 3 \quad \Delta K_1 = \pm 1, \pm 3$$

for the *b*-type transitions (component of the dipole moment along the *b* axis);

$$\Delta K_{-1} = \pm 1, \pm 3 \quad \Delta K_1 = 0, \pm 2$$

for the *c*-type transitions (component of the dipole moment along the *c* axis);

If there is no component of the dipole moment along one of the principal axes, meaning that its projection onto that axis is zero, the corresponding transitions have zero probability.

The line intensity is a bulk property, thus it is strictly related to the population distribution. This distribution is related to the temperature, the degeneracy and the energy of the rotational levels considered, and according to the Boltzmann equation, can be described as (Gordy and Cook, 1984)

$$N_f = \frac{g_f}{Q} e^{-\frac{E_f}{kT}}. \quad (1.25)$$

Q is the so-called partition function, which takes the general form

$$Q = \sum_i g_i e^{-\frac{E_i}{kT}}. \quad (1.26)$$

For an asymmetric rotor this sum can be approximated through the closed expression

$$Q = 5.34 \times 10^6 \left(\frac{T^3}{ABC} \right)^{1/2}, \quad (1.27)$$

where k is the Boltzmann constant and A, B and C are the rotational constants in MHz (Gordy and Cook, 1984).

1.4.4 Centrifugal distortion

Since molecules are not rigid, during rotation their structure is influenced by centrifugal forces. This centrifugal distortion is directly related to the angular momentum and it produces a small shift of the rotational energies with respect to the ones computed with the rigid rotor approximation. This effect can be treated as a series of perturbation terms, as follows (Papousek and Aliev, 1982):

$$H' = H'_r + H'_d^4 + H'_d^6, \quad (1.28)$$

with H'_r being the rigid rotor Hamiltonian. H'_d^4 and H'_d^6 are the Hamiltonian including the fourth and sixth power of the angular momentum, respectively and take the general form (Papousek and Aliev, 1982):

$$H'_d^4 = \frac{\hbar^4}{4} \sum_{\alpha\beta\gamma\delta} \tau_{\alpha\beta\gamma\delta} \hat{J}_\alpha \hat{J}_\beta \hat{J}_\gamma \hat{J}_\delta, \quad (1.29)$$

$$H'_d^6 = \hbar^6 \sum_{\alpha\beta\gamma\delta\epsilon\eta} \nu_{\alpha\beta\gamma\delta\epsilon\eta} \hat{J}_\alpha \hat{J}_\beta \hat{J}_\gamma \hat{J}_\delta \hat{J}_\epsilon \hat{J}_\eta, \quad (1.30)$$

where $\alpha, \beta, \gamma, \delta, \epsilon, \eta = x, y \text{ or } z$. $\tau_{\alpha\beta\gamma\delta}$ and $\nu_{\alpha\beta\gamma\delta\epsilon\eta}$ are the quartic and sextic centrifugal distortion constants, respectively.

For asymmetric rotors, these constants amounts to a total number of 81 quartic and 729 sextic coefficients. However, appropriate reduced Hamiltonians can be employed, namely the A - and the S -reduced Hamiltonians, originally developed by Watson (Watson, 1977a), which bring the number of coefficients to a total of five independent quartic constants, seven sextics and nine octics, to use when appropriate according to the measured transitions. The quartic and sextic contributions for both the S - and A -reduced Hamiltonians are:

$$\tilde{H}_d^4(A) = -\Delta_J \hat{J}^4 - \Delta_{JK} \hat{J}^2 \hat{J}_z^2 - \Delta_K \hat{J}_z^4 - \frac{1}{2} [(\delta_J \hat{J}^2 + \delta_K \hat{J}_z^2), (\hat{J}_+^2 + \hat{J}_-^2)]_+, \quad (1.31)$$

$$\tilde{H}_d^6(A) = \Phi_J \hat{J}^6 + \Phi_{JK} \hat{J}^4 \hat{J}_z^2 + \Phi_{KJ} \hat{J}^2 \hat{J}_z^4 + \Phi_K \hat{J}_z^6 + \frac{1}{2} [(\phi_J \hat{J}^4 + \phi_{JK} \hat{J}^2 \hat{J}_z^2 + \phi_K \hat{J}_z^4), (\hat{J}_+^2 + \hat{J}_-^2)]_+, \quad (1.32)$$

$$\tilde{H}_d^4(S) = -D_J \hat{J}^4 - D_{JK} \hat{J}^2 \hat{J}_z^2 - D_K \hat{J}_z^4 + d_1 \hat{J}^2 (\hat{J}_+^2 + \hat{J}_-^2) + d_2 (\hat{J}_+^4 + \hat{J}_-^4), \quad (1.33)$$

$$\tilde{H}_d^6(S) = H_J \hat{J}^6 + H_{JK} \hat{J}^4 \hat{J}_z^2 + H_{KJ} \hat{J}^2 \hat{J}_z^4 + H_K \hat{J}_z^6 + h_1 \hat{J}^4 (\hat{J}_+^2 + \hat{J}_-^2) + h_2 \hat{J}^2 (\hat{J}_+^4 + \hat{J}_-^4) + h_3 (\hat{J}_+^6 + \hat{J}_-^6). \quad (1.34)$$

Here $\hat{J}_\pm = \hat{J}_x \pm i \hat{J}_y$ are the angular momentum ladder operators and the symbol $[A, B]_+$ represents the anticommutator of the two operators A and B , i.e. $AB + BA$.

1.4.5 Nuclear quadrupole coupling

If a molecule contains an atom with nuclear spin $I > \frac{1}{2}$, i.e. non-spherical distribution of the nuclear charge, the molecular electric field gradient and the nuclear quadrupole moment interact, giving rise to the so-called nuclear quadrupole coupling, described as

$$\mathbf{F} = \mathbf{J} + \mathbf{I}, \quad (1.35)$$

where \mathbf{J} is the end-to-end rotation angular momentum, \mathbf{I} is the nuclear spin and \mathbf{F} is the resulting total angular momentum. 1.4 shows the coupling of the vectors.

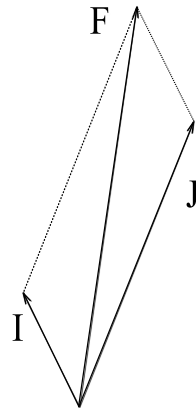


Abbildung 1.4: Vectorial diagram of the quadrupole coupling, between the rotational end-to-end angular momentum \mathbf{J} and the nuclear spin \mathbf{I} , resulting in the total angular momentum \mathbf{F} .

As a consequence of this coupling is the splitting of each rotational level in $(2I+1)$ sub-levels, each denoted by the quantum number F :

$$F = J + I, J + I - 1, \dots, |J - I|. \quad (1.36)$$

The rotational transitions will then occur between these sub-levels and the spectra for each J level will show multiplets of lines known as the hyperfine structure. The general form of the quadrupole Hamiltonian is:

$$H_Q = \frac{eQq_j}{2J(2J-1)I(2I-1)} [3(\mathbf{I} \cdot \mathbf{J})^2 + \frac{3}{2}\mathbf{I} \cdot \mathbf{J} - \mathbf{I}^2 \mathbf{J}^2]. \quad (1.37)$$

Here Q is the quadrupole moment of the nucleus, q_j is the electric field gradient and e is the elementary charge. The quantity eQq_j takes the name of quadrupole coupling constant, denoted by the symbol χ . The resulting general expression for the first-order energies is (Gordy and Cook, 1984):

$$E_Q = \sum_{g=a,b,c} \chi_{gg} \langle J_{K_{-1}K_1}, M = J | \Phi_{Zg}^2 | J_{K_{-1}K_1}, M = J \rangle \frac{\frac{3}{4}C(C+1) - I(I+1)J(J+1)}{2(2J-1)I(2I-1)}, \quad (1.38)$$

where Φ_{Zg} is the direction cosine between the axes Z and g , i.e the space-fixed and the body-fixed principal axes, respectively. C is the Casimir function:

$$C = F(F + 1) - J(J + 1) - I(I + 1), \quad (1.39)$$

and χ_{gg} are in the form:

$$\chi_{gg} = eQq_{gg} \quad \text{with } g = a, b, c, \quad (1.40)$$

with q_{gg} being the diagonal values of the tensor matrix of the electric field gradient in the principal axes system. These energies represent the diagonal elements of the corresponding matrix representation of the Hamiltonian (1.37).

It is important to underline that, from the Laplace equation, we have $\chi_{aa} + \chi_{bb} + \chi_{cc} = 0$, hence only two of the constants are independent. In addition, the matrix elements of the direction cosines differ depending on the molecules. For linear molecules, we have that:

$$q_{xx} = q_{yy} = -\frac{1}{2}q_{zz} = q, \quad (1.41)$$

due to simmetry of the electric field gradient along the bond axis. This allows calculation of the first-order energies in the form:

$$E_Q = -eQq \frac{\frac{3}{4}C(C + 1) - I(I + 1)J(J + 1)}{2(2J - 1)(2J + 3)I(2I - 1)} = -eQqY(J, I, F). \quad (1.42)$$

However, (1.42) and (1.38) are not really diagonal matrixes, even though in most molecular systems the off-diagonal elements can be neglected. When this is not possible, a second-order term can be considered, which takes the form:

$$E_Q^{(2)} = \sum_{J', i'} \frac{|\langle J, i, I, F | H_Q | J', i', I, F \rangle|^2}{E_{J, i} - E_{J', i'}} \quad (1.43)$$

and contains off-diagonal elements in i , with i being either the quantum number K or the pseudo quantum numbers K_{-1}, K_1 .

For asymmetric molecules, a simple evaluation of the first- and second-order energies through a closed formula cannot be achieved. In this case, the quadrupole energies can be calculated numerically employing a direction cosines matrix expressed in the symmetric-top representation (see section 1.4.2).

The selection rules for the hyperfine transitions are $\Delta F = 0, \pm 1$ and $\Delta I = 0$. The magnitude of the hyperfine splitting for each transition is directly dependent on the χ value, as follows:

$$\nu = \nu_0 - eQq[Y(J + 1, I, F') - Y(J, I, F)], \quad (1.44)$$

with ν_0 being the central frequency, i.e. the frequency of the rotational transition without any hyperfine splitting. This equation underlines the fact that with increasing J the hyperfine splitting become less resolvable until complete overlapping of the hyperfine components onto one single line.

1.4.6 Line profile

To obtain an accurate description of the rotational energies of the molecule, the measured signals must provide accurate centre frequencies for the corresponding transitions. The centre frequency can be retrieved by analysis of the profile of the detected transition, whose shape is determined by many different factors. In fact, experimental spectral signals always appear to be broader than an ideal sharp and narrow line, due to a series physical reasons.

The first cause of line broadening is the natural line width: even though a transition between two states should involve a specific quanta $h\nu_{fi} = E_f - E_i = \Delta E_{fi}$, a quantum mechanical system is always changing with time and in principle no excited state has infinite lifetime due to the Heisenberg's Uncertainty Principle (Heisenberg, 1927). Hence, there will always be an associated finite lifetime $\delta\tau$, so that the energies will have an uncertainty:

$$\delta E \delta\tau \sim \frac{h}{2\pi} \rightarrow \delta\nu = \frac{\delta E}{h} \sim \frac{1}{2\pi\delta\tau}, \quad (1.45)$$

meaning that the photon associated with the transition will assume all the possible frequencies within the range $\nu_{fi} \pm \delta\nu$.

The lifetime is the main indicator of how broad a line can be. The natural width broadening of a certain transition is a fixed value, since it depends on the spontaneous decay associated with the corresponding Einstein's coefficient for the spontaneous emission, A , as follows:

$$\delta\tau = \frac{1}{A}, \quad (1.46)$$

with:

$$A = \frac{16\pi^3\nu^3}{3\epsilon_0hc^3} |\mu_{fi}^2|, \quad (1.47)$$

where ν is the line frequency, ϵ_0 is the vacuum permittivity and μ_{fi} is the transition moment of the molecule. As a result the natural broadening $\delta\nu$ is proportional to A .

In addition, the lifetime can also be influenced by interaction with other particles through collisions. These collisions can shorten significantly the lifetime of a given transition by induced decay, causing the so-called pressure broadening (Birnbaum, 1967). In this case the broadening will be:

$$\delta\nu = \Gamma p \sim Nv\sigma, \quad (1.48)$$

where p is the pressure, Γ is the pressure broadening parameter, N is the density, v is the average thermal velocity and σ is the cross section.

The lineshape associated with both the natural and pressure broadenings can be described by a Lorentzian profile:

$$\Xi_L(\nu) = \frac{\delta\nu/2\pi}{(\delta\nu/2)^2 + (\nu - \nu_0)^2}, \quad (1.49)$$

where ν_0 is the rest frequency.

A third factor influencing the line width is the Doppler broadening. Molecules in gas-phase are not stationary but move with a velocity \mathbf{v} . As a consequence the observer will detect a shifted signal with frequency:

$$\nu = \nu_0 \left(1 \pm \frac{v_z}{c}\right), \quad (1.50)$$

where \pm indicate a source approaching or moving away and v_z is the component of molecular velocity parallel to the radiation. When in thermal equilibrium, molecular velocities follow a Maxwell-Boltzmann distribution. The resulting Doppler line width is:

$$\delta\nu_D = \frac{2\nu_0}{c} \sqrt{\frac{2kT \ln 2}{m}}, \quad (1.51)$$

where k is the Boltzmann constant, T is the system temperature and m is the mass of the molecule. The corresponding line profile is a Gaussian function in the form:

$$\Xi_G(\nu) = \frac{2}{(\delta\nu_D)} \sqrt{\frac{\ln 2}{\pi}} \exp \left[-4 \ln 2 \left(\frac{(\nu - \nu_0)}{\delta\nu_D} \right)^2 \right]. \quad (1.52)$$

For rotational spectroscopy within the microwave regime, the pressure and the Doppler broadenings are of the same order of magnitude and must be taken into account when analyzing a signal. In these cases, the line profile can be considered as a convolution of the two Lorentzian and Gaussian profile. The resulting function takes the name of Voigt profile (Posener, 1959).

The instrumentation described in Chapter 2 employs the frequency modulation technique (Gordy, 1948) and the detection at twice the modulating frequency, $2f$ (King and Gordy, 1954). For the full treatment, see Dore (2003) and references therein. Within this technique, the $2f$ line profile can be modelled as:

$$F_2(\bar{\omega}) \propto \text{Re} \int_0^\infty J_2(mt) \Phi(t) e^{-i\bar{\nu}t} dt, \quad (1.53)$$

which is the real part of the Fourier transform of the dipole correlation function, $\Phi(t)$, times a 2nd order Bessel function of the first kind, i.e. $J_2(z)$. Here m is the modulation depth and $\bar{\nu}$ is the time-independent frequency detuning, expressed as:

$$\bar{\nu} = \nu - \nu_0, \quad (1.54)$$

where ν_0 is the transition frequency.

The time dependent correlation function, $\Phi(t)$, contains information on the relaxation of the dipole moment oscillations, the latter occurring as a consequence of radiation absorption. Hence, if both broadening and Doppler effects are responsible for the relaxation, the correlation function employed to model the line profile can be written as

$$\Phi(\Gamma, \alpha_D, t) = \exp \left[-\Gamma t - \frac{(\alpha_D t)^2}{4} \right], \quad (1.55)$$

with

$$\alpha_D = \delta\nu_D \left(\frac{2\pi}{\sqrt{\ln 2}} \right). \quad (1.56)$$

The experimental rest frequency can be easily retrieved by means of the `proFFit` code described in Dore (2003).

1.5 Molecules in the solid phase

Being strongly bound to each other or to a substrate, solid-phase molecules lose their property to rotate freely and, therefore, cannot be studied by means of rotational spectroscopy anymore. However, their vibrational motions will still be present, making vibrational spectroscopy a complementary technique.

Vibrational spectroscopy is based on similar principle already introduced for rotational spectroscopy, involving finding the solutions of the Schrödinger equation with a suitable Hamiltonian. Here we will briefly introduce the general concepts and give the solutions for diatomic and polyatomic molecules energies within the harmonic approximation, applied to part of the work described in Section 3.3. For the detailed theoretical treatment, see Wilson et al. (1992) and Papousek and Aliev (1982).

1.5.1 Vibrational spectroscopy

The vibrational energies are obtained treating a molecule as a harmonic oscillator. In the case of a simple diatomic molecule they can be expressed as:

$$E_\nu = \left(\nu + \frac{1}{2} \right) h\nu_0, \quad (1.57)$$

with ν_0 being:

$$\nu_0 = \frac{1}{2\pi} \sqrt{\frac{k}{\mu}}, \quad (1.58)$$

where μ is the reduced mass, ν is the vibrational quantum number and k is the force constant which increases proportionally with the bond strength, defined as:

$$k = \left(\frac{d^2V}{dx^2} \right)_0, \quad (1.59)$$

with x being the displacement from the equilibrium position equal to $r - r_e$. For polyatomic molecules, with N atoms, first we need to provide a total of $3N$ coordinates to define their locations. Since we need 3 coordinates to fix the centre of mass and 3 angles to fix the orientation of the

molecule, a total of $3N - 6$ independent coordinates are left. Displacements along these coordinates identify the vibrational motions. For linear molecules, this number is $3N - 5$, since only two angles are required.

In general, the vibrational motions can be classified as the stretching, i.e. increasing and decreasing of the length of a two atoms bond, and the bending, i.e. change in the bond angle defined by three atoms. Most of the functional groups, i.e. a specific moiety such as the hydroxylic one (-OH), have characteristic vibrational energies for each of these motions. However, depending on the other adjacent atoms and functional groups, these energies can vary slightly from molecule to molecule. Since each motion is not isolated and all the atoms participate, the energy is always partially transferred to other bonds.

As a consequence, each vibrational signal becomes characteristic of a specific species, allowing and simplifying the molecular identification within the solid phase in presence of complex mixtures.

1.5.2 Normal modes

To better define the vibrations involving more than two atoms, a new system of coordinates must be introduced.

First we redefine the force constant, including displacements over two coordinates:

$$k_{ij} = \left(\frac{\partial^2 V}{\partial x_i \partial x_j} \right)_0 , \quad (1.60)$$

where the partial derivative of the two displacements x_i and x_j reflects the change in the force constant experienced by one atom when an adjacent displacement is happening.

Then we introduce the mass-weighted coordinates for i -th atom:

$$q_i = \sqrt{m_i} x_i . \quad (1.61)$$

With these terms, the total energy of the system, sum of the potential and kinetic energies, becomes:

$$E = \frac{1}{2} \sum_i \dot{q}_i^2 + \frac{1}{2} \sum_{i,j} k_{i,j} q_i q_j . \quad (1.62)$$

It is possible then to find linear combinations Q_i of q_i such that we have:

$$E = \frac{1}{2} \sum_i \dot{Q}_i^2 + \frac{1}{2} \sum_i \lambda_i Q_i^2 , \quad (1.63)$$

with no cross-terms, i.e. $i \neq j$ and with λ_i being the effective force constant. These linear combinations are called normal coordinates and the corresponding vibrations involving displacements along these coordinates are the normal modes of the species, each with a given energy.

Employing the appropriate radiation source is then possible to excite the molecule vibrationally and detect the corresponding signals, if allowed by the selection rules. A given vibrational

transition of a polyatomic molecule is allowed if there is a variation of the total dipole moment μ . Hence, the transition is visible even if the molecule do not have a permanent electric dipole moment, μ_0 , since

$$\mu = \mu_0 + \sum_i \left(\frac{\partial \mu}{\partial Q_i} \right)_0 Q_i + \dots . \quad (1.64)$$

In addition, within the harmonic approximation, is required that $\Delta\nu = \pm 1$.

1.5.3 Column density

Together with the detection of a molecule, it is important to get quantitative informations. For a given signal of area S retrieved after subtraction of the underlying continuum, the column density (molecules cm^{-2}) will be:

$$N = \frac{S}{A}, \quad (1.65)$$

where A is the integrated band strength (cm molecule^{-1}). For most of the molecules A has been obtained experimentally in previous studies and is tabulated.

1.6 Collisional excitation

Interactions between molecules and consequent energy transfer due to inelastic collision are described by the so-called collisional state-to-state rate coefficients.

The calculation of such coefficients for inelastic collisions requires the solution of the Schrödinger equation for both the electronic and nuclear energies. The best approach for this kind of problem is to apply the Born-Oppenheimer approximation (Born and Oppenheimer, 1927), which allows full separation of the Schrödinger equation into electronic and nuclear parts. This approximation relies on the fact that nuclear motions are much slower than electron motions and therefore, nuclei can be considered fixed compared to the electrons.

Hence, this separation allows splitting of the calculations in two parts: 1) the calculation of the Potential Energy Surface (PES), i.e. electronic energy as a function of fixed nuclear coordinates; 2) calculation of state-to-state cross sections by solution of the nuclear part of the Schrödinger equation, starting from the previously calculated PES. Here we will give an overview of the main concepts and the basic theoretical approaches applied to the work described in Chapter 5 and in the appendix.

1.6.1 Basis set functions

The first requirement to solve the Schrödinger equation is to employ appropriate wavefunctions.

The largely employed LCAO (Linear Combination of Atomic Orbitals) method allows calculation of the molecular wavefunctions, ϕ , from the atomic orbitals functions, φ_i . The set of

functions φ_i is called basis set and many different types have been developed within the last decades (Schuchardt et al., 2007). An appropriate basis set has to be chosen depending on the level of the results required and mostly depending on the calculation method employed. Larger basis sets produce more accurate results, but also require higher computational costs.

In theory, an infinitely large basis set should carry out the most accurate results possible. Since such a set does not exist, extrapolation schemes can be employed to retrieve values at the so-called Complete Basis Set (CBS) limit. These schemes work using hierarchical basis sets, i.e. a series of basis sets belonging to the same type but with increasing size. Depending on the size and the number of the sets employed and depending on the value we would like to retrieve, different schemes can be applied.

1.6.2 Electronic Schrödinger equation

Many computational methods have been developed in the past years to produce optimal results for the electronic Schrödinger equation. The simplest approach for a multi-electron system, such as a molecule, is the Hartree Fock (HF) method (Slater 1951 and references therein, Hehre 1986). This method approximate the multi-electron to a one-electron problem averaging the electron-electron interaction energy and considering each electron as moving within the average total field. This approximation help to simplify the Schrödinger equation, making it a one-electron equation in the form:

$$\hat{F}\Phi_i = E_i\Phi_i. \quad (1.66)$$

Here \hat{F} is the Fock operator, a one-electron effective Hamiltonian operator, and Φ_i is a set of one-electron wave functions representing the molecular orbitals, obtained through the LCAO method described in 1.6.1.

Being one of the first method ever developed, the HF is a starting point for other more accurate methods, such as the coupled cluster (CC) (Purvis III and Bartlett 1982, Raghavachari et al. 1989, Hampel et al. 1992, Deegan and Knowles 1994). The CC method expresses the molecular wave-function as:

$$\Psi_{CC} = \exp(\hat{T})\Psi_{HF}, \quad (1.67)$$

with:

$$\exp(\hat{T}) = 1 - \hat{T} + \frac{\hat{T}^2}{2!} + \frac{\hat{T}^3}{3!} + \dots = \sum_{k=0}^{\infty} \frac{\hat{T}^k}{K!}. \quad (1.68)$$

\hat{T} is the cluster operator and can be defined as:

$$\hat{T} = \hat{T}_1 + \hat{T}_2 + \hat{T}_3 + \dots, \quad (1.69)$$

with:

$$\hat{T}_m = \frac{1}{(m!)^2} \sum_{i,j,k,\dots} \sum_{a,b,c,\dots} t_{i,j,k,\dots}^{a,b,c,\dots} a^+ i b^+ j c^+ k \dots \quad (1.70)$$

Here i, j, k, \dots denote electrons in occupied orbitals and a, b, c, \dots electrons in virtual orbitals. The terms a^+, b^+, \dots and i, j, \dots are the creation and annihilation operators and when coupled they describe the single excitation of an electron, e.g. the transfer of an electron from the occupied orbital i to the orbital a and so on. The terms $t_{i,j,k,\dots}^{a,b,c,\dots}$ are the Cluster amplitudes. These coefficients are necessary to define the molecular wavefunctions and have to be determined to solve the Schrödinger equation.

The more terms in the \hat{T} operator are taken into account, the more accurate the results will be. However, due to high computational costs, it is common to truncate the operator after the double excitation term, i.e. \hat{T}_2 , and treat the triple excitations as a perturbation, resulting in the so-called single and double excitation couple cluster method with triple perturbation (CCSD(T)).

By means of this method is then possible to calculate energies for a given molecular system. In particular, to obtain the final PES of a collisional system made of one molecule and one colliding atom, calculations must be carried out for a grid of points, corresponding to different relative positions of the two species.

This grid of energies can then be converted into an analytical version of the PES, employing an appropriate expression, such as the one given in chapter 5.

1.6.3 Nuclear Schrödinger equation

Once the PES is available, it can be employed to solve the second part of the problem and retrieve the cross sections. For the purpose of this thesis, we will just consider an atom-diatom interacting system. The full treatment can be found in Flower (2007).

The nuclear Hamiltonian in a body-fixed (BF) frame takes the form:

$$\hat{H} = -\frac{1}{2\mu R} \frac{\partial^2}{\partial R^2} R + \frac{\hat{J} + \hat{j}^2 - 2\hat{\mathbf{j}} \cdot \hat{\mathbf{J}}}{2\mu R^2} + V(R, \theta, r) + \hat{H}_{diatom}, \quad (1.71)$$

with

$$\hat{H}_{diatom} = -\frac{1}{2\mu_{diatom} r} \frac{\partial^2}{\partial r^2} r + \frac{\hat{j}^2}{2\mu_{diatom} r^2} + V_{diatom}(r). \quad (1.72)$$

Here μ is the reduced mass of the atom-diatom complex, r is the bond length of the diatom, R is the length of the \mathbf{R} vector that connects the molecular centre of mass with the atom and θ is the angle between the \mathbf{R} vector and the molecular bond. These coordinates correspond to the so-called Jacobi coordinates system. $V(R, \theta, r)$ and $V_{diatom}(r)$ are the previously calculated PESs of the collisional system and the diatomic molecule, respectively. Lastly, J is the total angular momentum, sum of j , which describes the rotational angular momentum of the molecule, and the orbital angular momentum, l .

An appropriate form of the wave functions expanded in the body-fixed (BF) angular basis functions $|\mathbf{n}\rangle$ must be employed, expressed as:

$$\Phi = \frac{1}{R} \sum_n |\mathbf{n}\rangle \Psi_n(R), \quad (1.73)$$

with $\Psi_n(R)$ being functions of the radial coordinates. After substitution in the Schrödinger equation and projection with $\langle \mathbf{n}' |$ we obtain:

$$\frac{\partial^2}{\partial R^2} \Psi_{n'}(R) = \sum_n \langle \mathbf{n}' | \hat{W} | \mathbf{n} \rangle \Psi_n(R), \quad (1.74)$$

with the operator \hat{W} expressed as:

$$\hat{W} = 2\mu(\hat{H} - \hat{T}_{rad} - E). \quad (1.75)$$

Here E is the total energy of the system, \hat{H} is the Hamiltonian defined in (1.71) and \hat{T}_{rad} is the radial kinetic energy:

$$\hat{T}_{rad} = -\frac{1}{2\mu R} \frac{\partial^2}{\partial R^2} R. \quad (1.76)$$

The eigenvalues of the Hamiltonian \hat{H}_{diatom} (1.72) contained in the operator \hat{W} are the energies ϵ_j for a given rotational level of the diatomic molecule. These energies give the collisional energies, E_j , since:

$$E_j = E - \epsilon_j. \quad (1.77)$$

Solution of the equations (1.74) produces a matrix, S_l , which can be used to retrieve the partial cross sections $\sigma_l(j \leftarrow j')$ for each value of the orbital angular momentum l , using the expression

$$\sigma_l(j \leftarrow j') = \frac{\pi}{k_{j'}^2(2j'+1)} \sum_{\Omega} (2l+1) |S_l(j\Omega, j'\Omega)|^2 \quad (j \neq j'). \quad (1.78)$$

Here Ω is the projection of both j and J on the BF z-axis and $k_{j'}^2$ has the form

$$k_{j'}^2 = \frac{\mu E_j}{\hbar^2}. \quad (1.79)$$

The total cross sections can then be obtained by sum over l . The corresponding thermal rate coefficients for excitation and de-excitation transitions are calculated by averaging the cross sections over a Maxwellian distribution of collisional velocities, as described in section 5.3.

Kapitel 2

Instrumentation

2.1 Absorption cell spectrometer

The rotational spectroscopy studies have been realized employing the CASAC (Center for Astrochemical Studies Absorption Cell) frequency modulation (FM) spectrometer at the Max-Planck-Institut für extraterrestrische Physik in Garching (Germany). The central body of the instrumentation consist of two Pyrex tubes, each 3 m long and 5 cm wide in diameter. These tubes work as separate cells, each devoted to one of two molecular production systems employed in the laboratory, namely the DC-plasma and the pyrolysis system, described in section 2.1.1 and 2.1.2. These two different methods are complementary to each other in terms of produced species.

The two absorption cells can be kept under appropriate vacuum by means of a rotative and a diffusion pump, connected in series. Between the cells and the pumping system lay a series of valves to isolate completely the pumps or partially reduce the flow rate. In addition, there is a cold trap that can be properly cooled down at 77 K to collect and condensate the chemical products. The full system is shown in figure 2.3.

2.1.1 Discharge cell

The discharge system consist of a cell containing two cylinder-shaped electrodes at each end. These electrodes are connected to a power supply capable of a voltage of 5000 V and used to form the plasma, in presence of proper gas mixtures.

The high voltage, in fact, can cause an electric breakdown of the gas which ignite a current flow. Under certain conditions, the current stabilizes at a fixed value, producing different regimes of discharge depending on the ratio between current and potential, as shown in figure 2.1.

For spectroscopic purposes, only the normal and the anomalous glow discharges are relevant and can be chosen depending on the target molecule. These two regimes show glowing and dark regions depending on the relative position to the anode (negative electrode) and cathode (positive electrode), as shown in figure 2.2.

The first region of interest is the *Aston dark space*. In this section of the discharge, if the voltage is properly adjusted to reach the breakdown value, an avalanche of electrons is formed

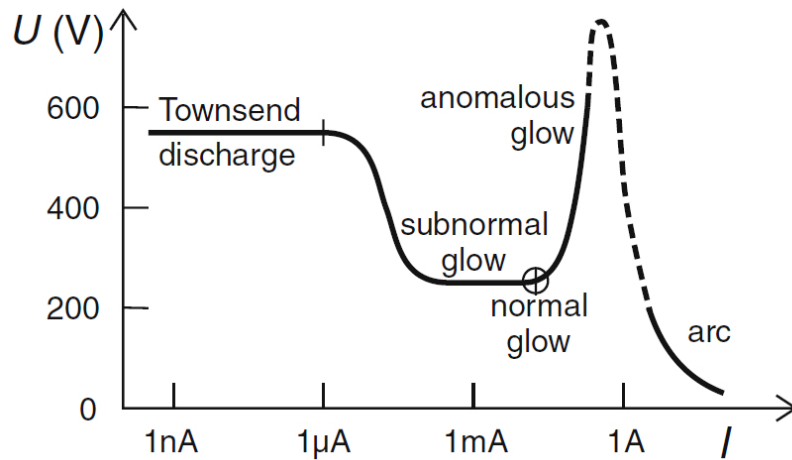


Abbildung 2.1: Different regimes of self sustaining discharges, depending of the current-to-voltage ratio. The image is taken from Piel (2017).

and the plasma formation is triggered. The required voltage depends on the structure and properties of the cell and electrodes, but also on the gas composition. Long cylindrical electrodes are more efficient, hence they have been largely employed in this kind of experiments. In addition, noble gases can be employed as buffer gas in larger quantities with respect to the sample mixture, helping to lower the minimum breakdown voltage and stabilize the discharge.

Due to the electric field applied, the newly released electrons will gain enough energy to excite atoms and molecules, which will emit light producing the first cathodic glowing region. After a cathodic dark space, where ionization processes become more frequent than the excitation ones due to higher electrons energy, the *negative glow* region is formed, followed by the *Faraday dark space*. Here electrons lose part of their energy before reaching the *positive column*, where the electrons will slowly drift towards the anode as a consequence of the weak electric field present.

Depending on the target molecule, the region of interest can either be the *negative glow* or the *positive column*. Due to higher electron density, the first is relevant for protonated species and most of the ions. The molecular production within this region can be enhanced by means of a variety of methods, e.g. by application of a magnetic field, which will reduce the collisions of the electrons with the cell walls favoring electron-molecules interactions.

The *positive column* has lower electron density and energies than the *negative glow* but is more extended and responsible for formation of most of the non-ionized species. A larger positive column results in enhanced molecular production, given that the current stays constant (constant voltage drop per unit length). To some extent, this improvement can be obtained by increasing the cell dimensions and adjusting the voltage.

Since the whole system can warm up due to the current flowing through the electrodes, a series of teflon pipes are wrapped around the cell and are connected to a 200 L dewar containing liquid nitrogen to allow cooling of the cell. This system can be operated manually or through a Programmable Logic Controller (PLC) which can automatically keep the temperature within a

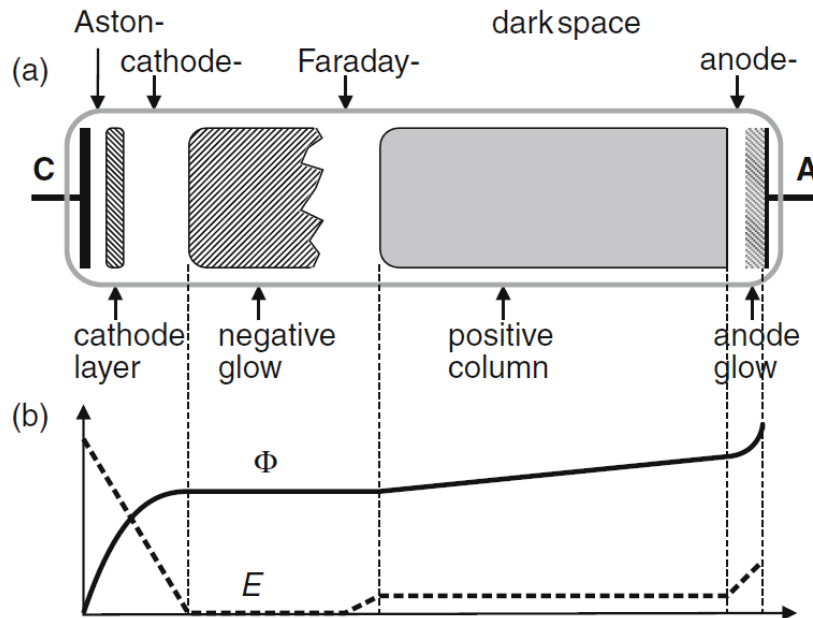


Abbildung 2.2: (a) Regions of a glow discharge. (b) Electric potential Φ and axial electric field (E) variation in the normal regime. The image is taken from Piel (2017).

fixed chosen range. In addition, around the cooling system, lay a copper solenoid employed to produce a magnetic field.

It's possible to employ a multi-channel computer-driven flow regulator to inject up to 4 different gases and 3 additional manual Alicatt flow regulators, to create the appropriate gas mixture for the experiment. All the flow regulators are connected to a common glass inlet placed at the cathodic side of the cell. The overall pressure is then controlled by means of two "Baratron"¹ pressure gauges, placed one on each end of the cell.

2.1.2 Pyrolysis cell

The pyrolysis system consist of a cell connected to a quartz tube, 70 cm long and 1 cm wide in diameter, going through an electric oven (Carbolite Gero Type 3216), which can reach temperature as high as 1600 Cdeg. However, given the material of the tube, the temperatures for the experiments cannot exceed 1200 Cdeg. One end of the quartz tube is used to introduce the sample or to create gas mixtures. Here, a first "Baratron" pressure gauge allows measurement of the inlet gas pressure. After leaving the oven, the quartz pipe is then connected to the absorption cell through a valve.

The pyrolyzed gas is then expanded in the cell, properly kept under flow, and the final pressure can be monitored through a second "Baratron" pressure gauge placed at opposite end of the absorption cell, with respect to the gas inlet. The pressures at the inlet range from 100 mTor to

¹"Baratron" is the commercial name of a capacitance pressure gauge.

1 Torr, while after expansion the cell pressure is reduced by two orders of magnitude and ranges between 0.5 and 10 mTorr about.

2.1.3 Spectrometer

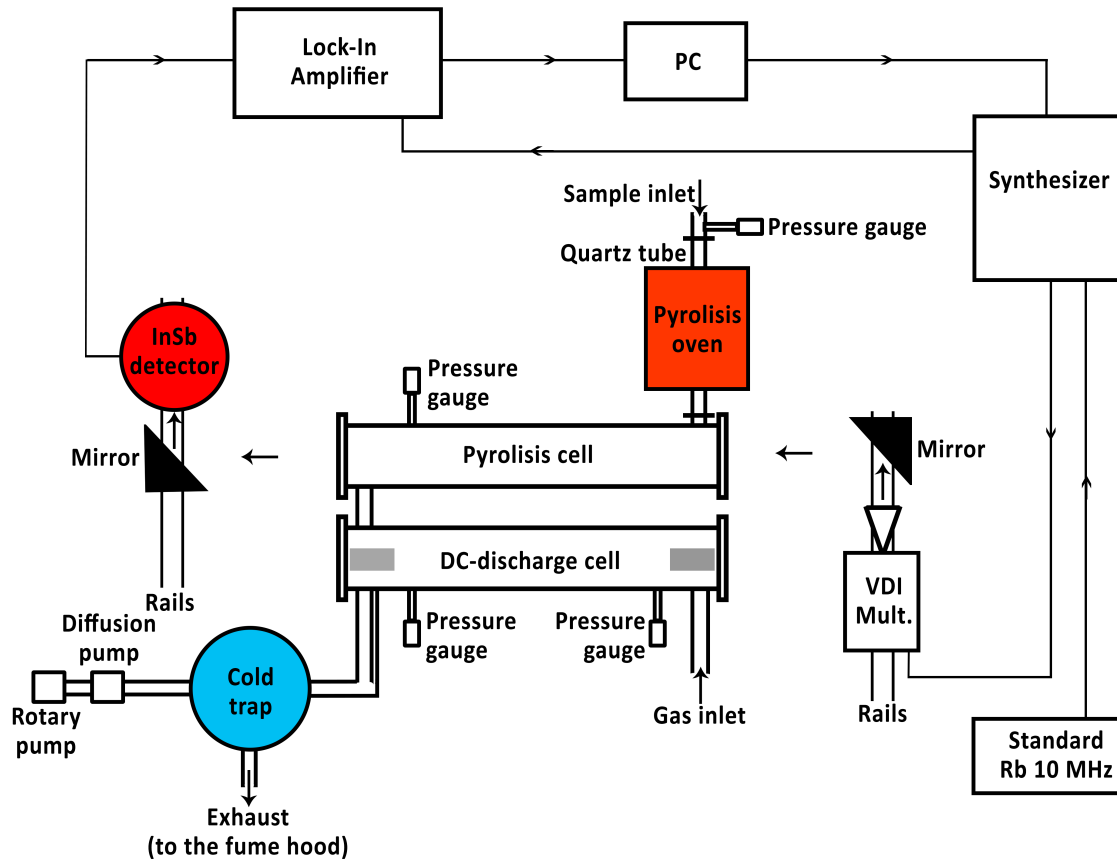


Abbildung 2.3: General scheme of the discharge and pyrolysis cells connected to the FM spectrometer. Full description of each component is given in the text.

The spectrometer operates in the millimeter and submillimeter range (80-1600 GHz). The radiation is generated in the cm-wave range by a frequency synthesizer, operating in the interval of 250 kHz to 67 GHz (Agilent E8257D), and then multiplied to higher frequencies through a VDI multiplier chain (9.0 SGX). A Rubidium atomic clock is used as primary frequency standard, providing a reference signal at 10 MHz. Parabolic mirrors are used to guide the radiation through the cell and to focus it in the detector, an Indium-Antimonide (InSb) hot electron bolometer, which is kept at the operating temperature of 4 K by a closed-cycle He refrigerator. The multiplier, the mirrors and the detector are positioned on rails and can be moved to adjust the optical path.

To enhance the signal-to-noise ratio (SNR), the frequency modulation technique is employed (Gordy, 1948). The sine-wave modulation is applied to the carrier signal by the synthesizer. The modulating signal is chosen with frequency between 15 and 50 kHz and variable amplitude. The output signal recovered from the detector is pre-amplified and then demodulated by the lock-in amplifier, tuned at twice the modulating frequency ($2f$). The resulting line profile is recorded as the second derivative of the actual absorption profile. In addition, a band-pass filter is applied to reduce undesired noise features.

2.2 Infrared spectrometer for photoionization

The solid phase work described in section 3.3 has been realized employing the experimental apparatus in the Laboratory of Experimental Astrophysics at the Osservatorio Astrofisico di Catania (Italy).

The instrumentation consist of a stainless steel high-vacuum chamber, which can reach pressures below 10^{-5} mTorr, containing a tail section of a closed-cycle helium cryostat in thermal contact with a KBr or silicon substrate. Ices can then be accreted on the substrate cooled down at the chosen temperature (10-300 K) by injection of gas mixtures through a needle valve.

The infrared spectrum is then recorded employing a FTIR spectrophotometer available commercially (Bruker Vertex 70) which works between 8000 and 400 cm^{-1} , with a resolution of 1 cm^{-1} .

The ion flux is provided by an ion implanter (Danfysik 1080–200) which can produce ions with energies up to 200 keV. To avoid macroscopic heating of the sample, current densities are kept below $1 \mu\text{A cm}^{-2}$. This system is interfaced with the vacuum chamber as shown in figure 2.4.

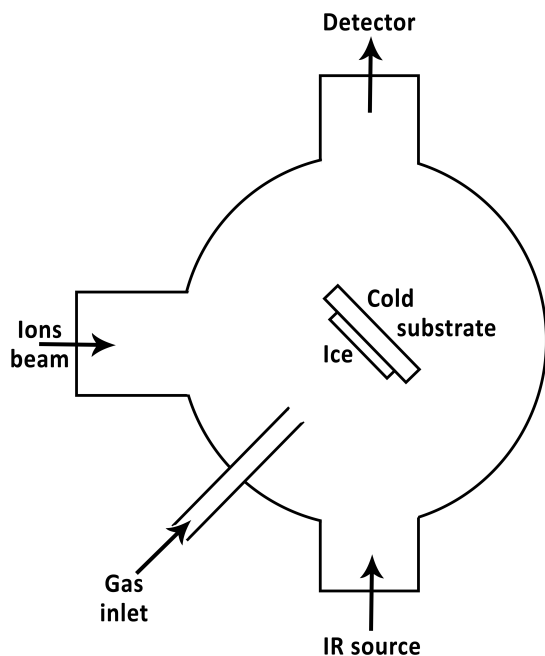


Abbildung 2.4: Scheme of the high vacuum chamber for the IR study of ion irradiated ice analogues.

Kapitel 3

Rotational spectroscopy and solid-phase study of dithioformic acid, HCSSH

Part of the content of this chapter (the gas-phase study of HCSSH) was published in the journal *Astronomy & Astrophysics*.

Credit: Prudenzano, D., et al., *Astronomy & Astrophysics*, 612 (2018): A56.

3.1 Introduction

As previously described in section 1.2.1, sulphur-related astrochemistry still requires a consistent number of molecules to be add in the general picture, including dithioformic acid, HCSSH.

This species is chemically related to CS_2 and is the S-bearing analogue of formic acid, HCOOH ; the latter was detected for the first time in SagittariusB2 (SgrB2) by Zuckerman et al. (1971) and in the dark cloud L134N by Irvine et al. (1990). Because it is isostructural with HCOOH , HCSSH exists in two different conformations, dubbed *cis* or *trans*, depending on the orientation of the S-H bond with respect to the C-H bond. These two conformers can be seen in Fig. 3.1.

The first gas-phase laboratory study of dithioformic acid was carried out by Bak et al. (1978). They measured transitions in the centimetre (cm) regime, between 18 and 40 GHz, for the *trans* and the *cis* conformers in the ground and in two low-lying vibrationally excited states. They also found an abundance ratio $\text{trans}/\text{cis}=5.43$, corresponding to an energy difference of 350 cm^{-1} . The molecules were produced by gas-phase pyrolysis of methanethiol, $\text{HC}(\text{SH})_3$, and the spectra were recorded with a Stark-modulated microwave spectrometer. In a subsequent work, the same authors carried out additional measurements of the two ^{34}S and one D isotopologues, leading to the experimental determination of the *trans*-HCSSH structure (Bak et al., 1979). However, the limited frequency range covered in these investigations prevented a satisfactory spectroscopic characterization of these species. In particular, the incomplete centrifugal distortion analysis and the rather high measurement errors caused by the interfering Stark lobes¹ led to high estimated uncertainties in the spectral predictions. The calculated rest frequencies are, in fact, affected by

¹Artefacts produced by the Stark modulation close to the centre frequency.

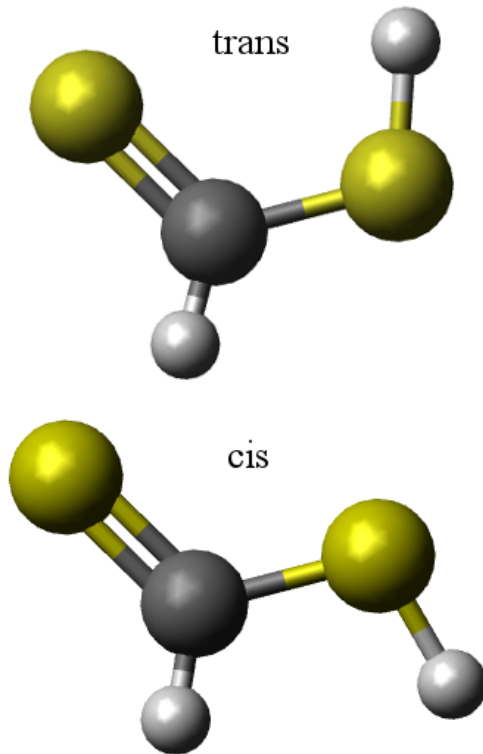


Abbildung 3.1: Molecular structures of the two planar isomers of HCSSH. Details concerning the geometries of the two species are given in Section 3.2.2 and Appendix A. Yellow spheres indicate sulphur atoms, the dark grey sphere indicates carbon, and hydrogen atoms are shown in light grey.

errors exceeding 0.7 MHz for the *trans* isomer and 1.1 MHz for the *cis*, already in the 3 mm region. In addition, no solid-phase studied have ever been produced on the topic.

Given the potential astronomical interest of this molecule, an improved knowledge of its rotational spectrum is desirable, together with information on its production onto solid phase. In this work we first present a thorough centrifugal distortion analysis of both *trans* and *cis* isomers of HCSSH. We extended the spectroscopic measurements well into the submillimetre (submm) domain, reaching a frequency as high as 478 GHz for the *trans*-HCSSH. High-level theoretical calculations were also carried out to provide a detailed description of the molecular properties, such as dipole moment components and equilibrium structures. We also present some preliminary data on the formation and presence of HCSSH in ion irradiated ice analogues.

3.2 Accurate millimetre and submillimetre rest frequencies for *cis*- and *trans*-dithioformic acid, HCSSH

3.2.1 Experimental setup

The measurements were performed using the CASAC (Center for Astrochemical Studies Absorption Cell) spectrometer at the Max-Planck-Institut für extraterrestrische Physik. Full details of the experimental apparatus can be found in Chapter 2. The instrument employs the frequency modulation technique in the mm and submm range and is equipped with a glow discharge cell for production of unstable species.

Measurements were carried out at room temperature to avoid condensation of the precursors. Dithioformic acid was produced by a 40 mA DC discharge (~ 0.8 kV) from a 1:1 mixture of CS_2 and H_2 , diluted in Ar buffer gas. The total pressure in the cell was 20–30 mTorr (27–40 μbar).

3.2.2 Results and data analysis

The HCSSH isomers are near-prolate asymmetric rotors ($\kappa_{trans}=-0.9901$ and $\kappa_{cis}=-0.9682$ ²) with C_s symmetry and planar structure. The a components of the dipole moment have been experimentally determined by Bak et al. (1978), where $\mu_a(trans)=1.53$ Debye (D) and $\mu_a(cis)=2.10$ D, while the b components were determined in our study (see Appendix A). We measured 204 new line frequencies for the *trans* conformer and 139 for the *cis*. We also detected seven b -type transitions for the *cis* conformer, which has a higher value of μ_b , equal to 1.67 D (see Table A.2). These new rotational transitions belong to the *R* branch ($\Delta J=+1$) and J values range from 14 to 74 and a maximum $K_a=20$.

We recovered the line central frequencies with the proFFit code (Dore, 2003), adopting a modulated Voigt profile. The estimated accuracy ranges between 25–50 kHz, depending on the line width, signal-to-noise ratio, and background continuum (standing waves produced between the two partially reflecting windows placed on either side of the cell). Examples of measured line and fitted profile of *trans* and *cis* isomers are shown in Figure 3.2. Both panels include lines corresponding to the blended $K_a=7$ asymmetry doublet, located at ca. 360 GHz.

We performed the spectral analysis using the Pickett SPFIT/SPCAT suit of programs (Pickett, 1991), adopting the Watson S-reduced Hamiltonian for asymmetric-top molecules (Watson, 1977a). The transitions measured by Bak et al. (1978) in the cm range were also included. To take into account the different experimental accuracies, we employed four distinct statistical weights ($1/\sigma^2$) for the two datasets. For the lines taken from literature, we assigned σ values of 75 kHz and 100 kHz to the *trans* and the *cis* isomers, respectively. A few lines showing very large deviation were removed from the final fit. Experimental uncertainties for our measurements are set to 25 or 50 kHz; the higher value is assigned only to lines broadened due to partially overlapped K doublets. The final fits lead to the determination of the complete set of quartic centrifugal distortion constants and four sextic constants, i.e. H_J , H_{JK} , H_{KJ} , and h_1 (energy contributions depending on

²Rey asymmetry parameter. It is an indication of the asymmetry of the molecule and can take values between -1, for a prolate symmetric top, and +1, for an oblate symmetric top. (Gordy and Cook, 1984)

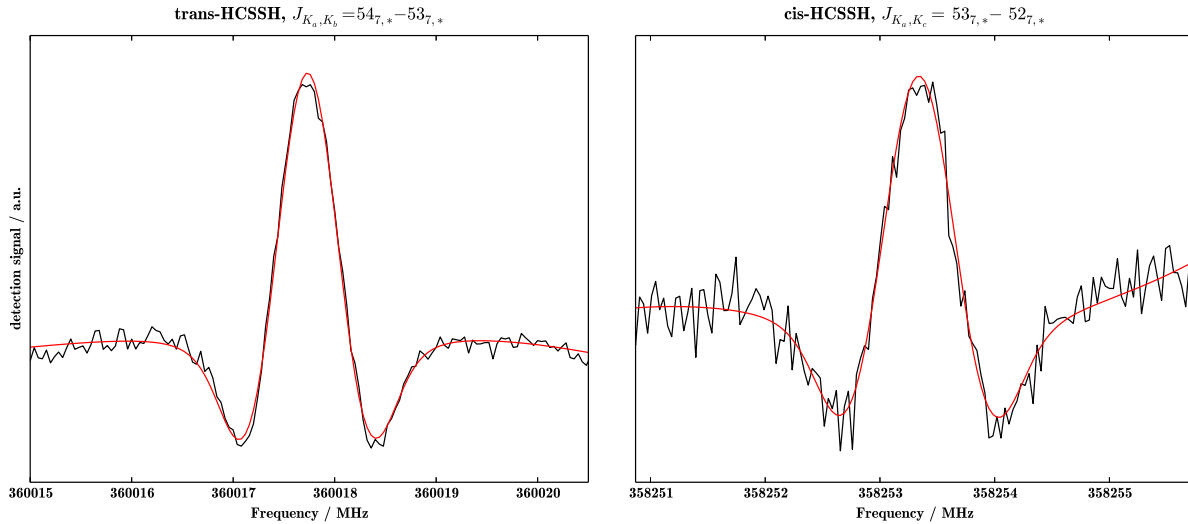


Abbildung 3.2: (*Left panel*) Experimental spectra of the $54_{7,*} - 53_{7,*}$ transitions of *trans*-HCSSH, with total integration time of 146 s and 3 ms of time constant. (*Right panel*) Experimental spectra of the $53_{7,*} - 52_{7,*}$ transitions of *cis*-HCSSH with total integration time of 87 s and 3 ms of time constant. (*Both panels*) The $K_a=7$ asymmetry doublet is not resolved. The red traces indicate the resulting line profile fitted with the proFFit code (see text).

J^6 , obtained from the rotational Hamiltonian). One octic constant, i.e. L_{KKJ} , was also determined for the *trans* isomer. The weighted root mean square (RMS) deviations are 0.936 and 0.933 for *trans* and *cis*, respectively. The resulting parameters are listed in Table 3.1. The lists of all the experimental frequencies are available at the CDS³ as supplementary data. Planarity of the species was confirmed by calculation of the inertial defect, $\Delta = I_c - (I_b + I_a)$ (Darling and Dennison, 1940), obtained using the moments of inertia I , derived from the ground-state rotational constants. The inertial defect values for *trans* and *cis* dithioformic acid are 0.0185 and 0.0173 amu Å², respectively, close to those of the two formic acid planar isomers, i.e. 0.0126 and 0.0102 amu Å² (Trambarulo et al. 1958, Davis et al. 1980 and references therein, Winnewisser et al. 2002).

The complete line catalogues, computed by using the spectroscopic parameters in Table 3.1, are provided as supplementary data at the CDS and also include the 1σ uncertainties, upper-state energies, line strength, and the Einstein A coefficient for spontaneous emission, all expressed in SI units as follows:

$$A_{ij} = \frac{16\pi^3\nu^3}{3\epsilon_0hc^3} \frac{1}{2J+1} S_{ij}\mu^2, \quad (3.1)$$

where ν is the line frequency, ϵ_0 is the vacuum permittivity, h is the Plank's constant, c is the speed of light, J is the quantum number of the upper state for the rotational angular momentum, and $S_{ij}\mu^2$ is the line strength. The lists consist of transitions with $E_u/k < 300$ K and predicted uncertainties lower than 50 kHz, resulting in lines between 0.2 and 300 GHz. All of these rest

³<http://cdsweb.u-strasbg.fr/>

Tabelle 3.1: Spectroscopic parameters of the two conformers of HCSSH. The results of this study are compared with those of Bak et al. (1978).

Constants	Units	<i>trans</i> -HCSSH ¹	<i>trans</i> -HCSSH ²	<i>cis</i> -HCSSH ¹	<i>cis</i> -HCSSH ²
A_0	MHz	49206.11(21) ³	49227.(86)	48572.439(66)	48947.(380)
B_0	MHz	3447.53432(37)	3447.5312(89)	3498.74789(67)	3498.719(24)
C_0	MHz	3219.47256(37)	3219.4954(96)	3261.42278(62)	3261.433(30)
D_J	kHz	1.063389(64)	1.10(10) ⁴	1.27724(14)	1.02(42) ⁴
D_{JK}	MHz	-0.0389438(19)	-0.03905(24) ⁴	-0.0470807(33)	-0.0484(12) ⁴
D_K	MHz	1.376(33)		1.412(17)	
d_1	Hz	-3.609(38)		4.343(28)	
d_2	kHz	-0.119787(80)		0.14900(20)	
H_J	Hz	0.0005714(64)		0.001169(25)	
H_{JK}	Hz	-0.00573(31)		-0.03601(50)	
H_{KJ}	Hz	-4.216(15)		-4.109(20)	
h_1	Hz	0.0001673(96)		0.000288(38)	
L_{KKJ}	Hz	0.000447(27)			
$I_c - (I_b + I_a)$	amu Å ²	0.0185		0.0173	
σ_w		0.936		0.933	
No. of lines		204	25	139	19

¹ This work.

² Bak et al. (1978).

³ Standard error in parentheses are in units of the last digit.

⁴ Calculated using the Watson A-reduction for asymmetric top molecules.

frequencies have at least a precision of 6×10^{-8} , corresponding to a radial velocity of 0.018 km s⁻¹ or even better. Partition functions at various temperatures for both isomers are listed in Table 3.2.

3.2.3 Discussion and conclusions

This laboratory study provides a comprehensive spectroscopic characterization of the two stable conformers of HCSSH in the ground state. Extension of the measurements up to 478 GHz and the resulting larger dataset lead to an overall improvement of the spectroscopic parameters with respect to that of Bak et al. (1978). In particular, the uncertainties on the A rotational constant and on the D_J centrifugal distortion constant were reduced by more than 3 orders of magnitude. We extended the centrifugal distortion analysis with all the quartic and four sextic constants. Additionally, the octic L_{KKJ} parameter was included for the *trans* conformer. Further improvements in the fit of the *cis* conformer were obtained through measurements of *b*-type transitions. These new sets of spectroscopic parameters made it possible to compute accurate rest frequencies. In comparison to previous studies, predicted uncertainties were significantly reduced and have values as low as 2 kHz (0.006 km s⁻¹) at 3 mm wavelength.

An astronomical search of these molecules can be carried out in the cm, mm, and submm

Tabelle 3.2: Partition functions of *trans*-HCSSH and *cis*-HCSSH at various temperatures.

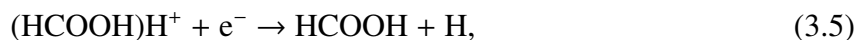
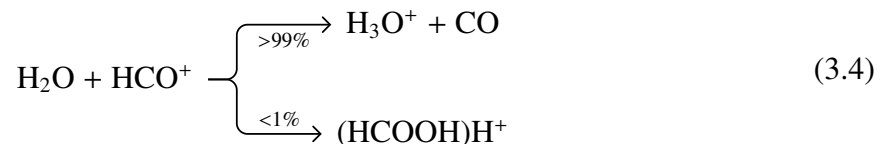
T (K)	Q (<i>trans</i> -HCSSH)	Q (<i>cis</i> -HCSSH)
300	37126.4660	36887.4922
200	20421.8656	20276.8962
100	7224.8408	7172.3000
50	2554.3700	2535.7348
20	647.0112	642.2926
10	229.3211	227.6550

bands, depending on the temperature of the source. As shown in figure 3.3, in cold environments with $T_{\text{kin}} \sim 10$ K or lower (such as the S-rich prestellar cores L183 and Barnard 1), assuming local thermal equilibrium, calculated line intensities and distribution for the *trans* isomer peak around 45 GHz. In warm regions with $T_{\text{kin}} \sim 100$ K, the peak shifts at higher frequencies, ca. 200 GHz. Owing to its larger b component of the dipole moment, the *cis* isomer shows a different intensity distribution. In this case the calculated peak lies at ~ 280 GHz in cold sources and at ~ 780 GHz in warm regions. However, the strongest lines above 300 GHz, i.e. b -type transitions with low E_u/k , present uncertainties higher than 1 MHz. These large errors are a consequence of the restricted number of measurable b -type transitions, strongly limited by the overall lower intensity of the *cis* lines with respect to the *trans*.

Work is also under way in our group to extend astrochemical modelling of sulphur to a number of new species, including HCSSH (Laas and Caselli, 2019). Although this molecule has not been previously studied in the context of astrochemical modelling, a number of reactions may be readily tested, based on standard grain surface rates (Hasegawa et al., 1992) or ion-neutral gas-phase kinetics (Troe, 1985). Analogous to many other interstellar complex organic molecules, it is likely that a series of barrierless radical-radical addition reactions might lead to its formation on grain surfaces, such as



in analogy with the efficient formation of the O-bearing counterpart formic acid. In the gas phase, HCOOH may be efficiently formed via the ionic route,



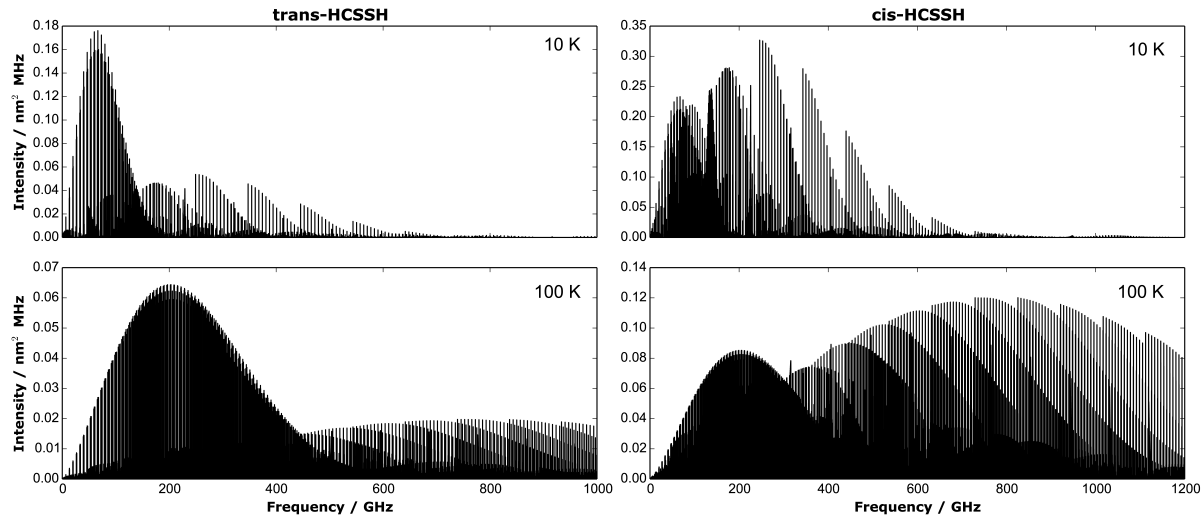


Abbildung 3.3: Intensities and line distributions of rotational transitions at 10 and 100 K, for *trans* and *cis* dithioformic acid isomers. Most of the bandheads above 250 GHz are produced by *b*-type transitions.

and the analogue of this route will also be tested for the gas-phase formation of HCSSH. If HCSSH is indeed found to be formed efficiently in a way similar to HCOOH, it is likely that the most promising sources for detection are S-rich regions, where formic acid can be routinely observed.

3.3 Dithioformic acid formation in ion irradiated ice analogues

3.3.1 Experimental setup

The measurements were performed using the instrumentation at the Osservatorio Astrofisico of Catania (Italy). Full details of the experimental apparatus can be found in Chapter 2.

Two different gas mixtures of H₂S and CO have been employed to produce two separated experiments: a mixture with ratio 1:1 and one with ratio 1:6. Once deposited, the ice analogues were irradiated with high energetic ions. During the irradiation the ion current is measured and then converted in ion fluence (ion cm⁻²), employing the so-called stopping power, i.e. the average depth reached by each ion within the solid ice. The stopping power is calculated by means of the SRIM software (Ziegler, 2004). The radiation dose is then obtained as a scale of eV per 16u molecule, with *u* being the atomic mass unit.

3.3.2 Results and data analysis

Mixture 1: The first mixture studied contains H₂S and CO with a ratio 1:1. The features of main interest before irradiation are the ν_1 stretching mode of H₂S at $\sim 2570\text{ cm}^{-1}$ and the ν_1 stretching mode of CO at $\sim 2139\text{ cm}^{-1}$ (Garozzo et al. 2010 and references therein).

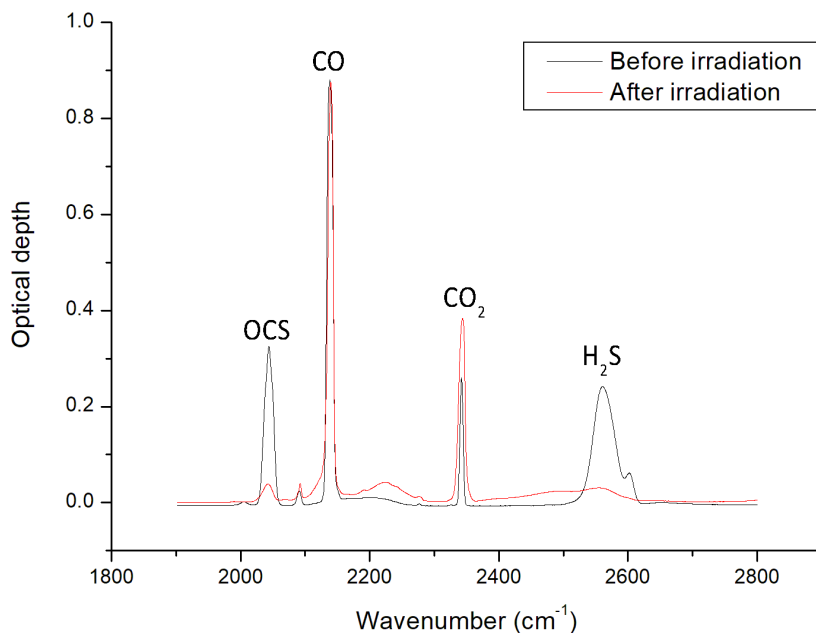


Abbildung 3.4: IR transmittance spectra of the mixture of H₂S:CO with ratio 1:1.

After irradiation new S-bearing species are formed, mainly SO₂ and CS₂. However, the main HCSSH feature, i.e. the band at $\sim 1166\text{ cm}^{-1}$ (Bohn et al., 1992), is not observed even at high doses (the higher dose reached is 47.7 eV/16u). The main reason could be that the large amounts of sulphur atoms lead to more sulphur-sulphur interactions, favouring the formation of the more stable undetectable sulphur polymers. Given that the focus of our work is HCSSH, no further investigations have been carried out on this mixture.

Figure 3.4 depicts the IR transmittance spectra of ice deposited at 20 K and irradiated with 200 keV H⁺.

Mixture 2: The second experiment involved a mixture 1:6 of H₂S and CO. The features of main interest before irradiation are the ν_3 and ν_1 stretching mode of H₂S at $\sim 2640\text{ cm}^{-1}$ and $\sim 2570\text{ cm}^{-1}$, respectively, and the ν_1 stretching mode of CO at $\sim 2139\text{ cm}^{-1}$ (Garozzo et al. 2010 and references therein).

Figure 3.5 depicts the IR transmittance spectra of ice deposited at 20 K and after irradiation with 200 keV H⁺.

The column densities for the molecules of interest have been calculated for the corresponding vibrational bands employing the band strength values listed in table 3.3.

As expected, our results follow the trend shown in Woods et al. (2015), with H₂S decreasing consistently within the starting phases of irradiation as it is quickly transformed in other com-

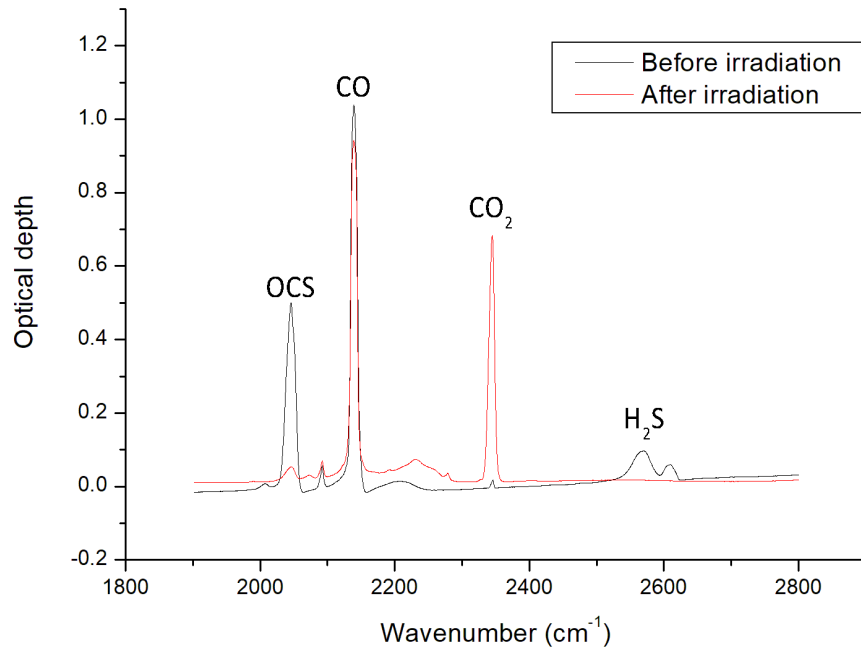


Abbildung 3.5: IR transmittance spectra of the mixture of H₂S:CO with ratio 1:6.

pounds. In particular, H₂S becomes undetectable at fluences between 120 and 150×10^{13} keV H⁺ cm⁻².

HCSSH, identified through the band at ~ 1166 cm⁻¹ (Bohn et al., 1992), is formed from the first phases of irradiation together with CS₂. Figure 3.6 plots the column densities of these molecules during the irradiation process as a function of ion fluence.

At the highest dose reached, i.e. 109 eV/16u, HCSSH is still forming. Since decomposition of HCSSH is never observed within the range of doses experimented, a possible explanation lies in the fact that CS₂ could work as a sink of sulphur for HCSSH formation.

3.3.3 Discussion and conclusions

Dithioformic acid is considered as a possible sink of sulphur in the ISM ice grains. As described by Laas and Caselli (2019), HCSSH should be indeed mainly formed onto solid phase, following the formation path



As shown in the previous section, HCSSH is indeed formed if specific ratio of sulphur-carbon atoms are respected, i.e. initial H₂S abundance lower than the CO one.

Woods et al. (2015) present a thorough analysis of some S-bearing species that, in solid phase, could account for the overall sulphur elemental abundance. They show that all the H₂S is rapidly consumed and transformed in other compounds, such as CS₂, OCS and SO₂. This is the

Tabelle 3.3: Band strength values, A , for each corresponding vibrational band used to calculate the column densities.

Molecule	Vibrational band (cm^{-1})	A (cm molecule^{-1})
HCSSH ¹	1166	1.00×10^{17}
CS_2 ²	1520	9.13×10^{17}
H_2S ³	2550	1.12×10^{17}

¹ Estimated value based on similar molecules employed when the experimental band strength is unknown.

² Pugh and Rao (1976).

³ Smith (1991).

case also for our experiment.

However, in their study the total amount of elemental sulphur carried by the detected molecules does not account for the starting sulphur introduced as H_2S , meaning that it is still in large part trapped as other undetected compounds, forming the so-called sulphur residue.

Within our experiment, HCSSH has also been considered to account for the missing sulphur. However as shown in figure 3.7, since HCSSH abundances are smaller by one to two orders of magnitude compared to CS_2 , its contribute to the overall sulphur elemental abundance is minimal and cannot fill the gap corresponding to the missing sulphur. Hence, further studies are required to find possible candidates and further expand our knowledge of solid phase sulphur chemistry.

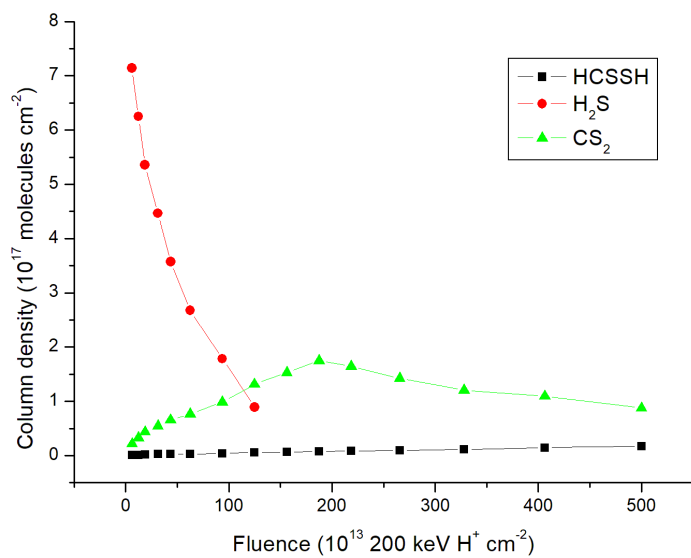


Abbildung 3.6: Column densities plotted as a function of fluence during irradiation of the ice mixture for H_2S , CS_2 and HCSSH.

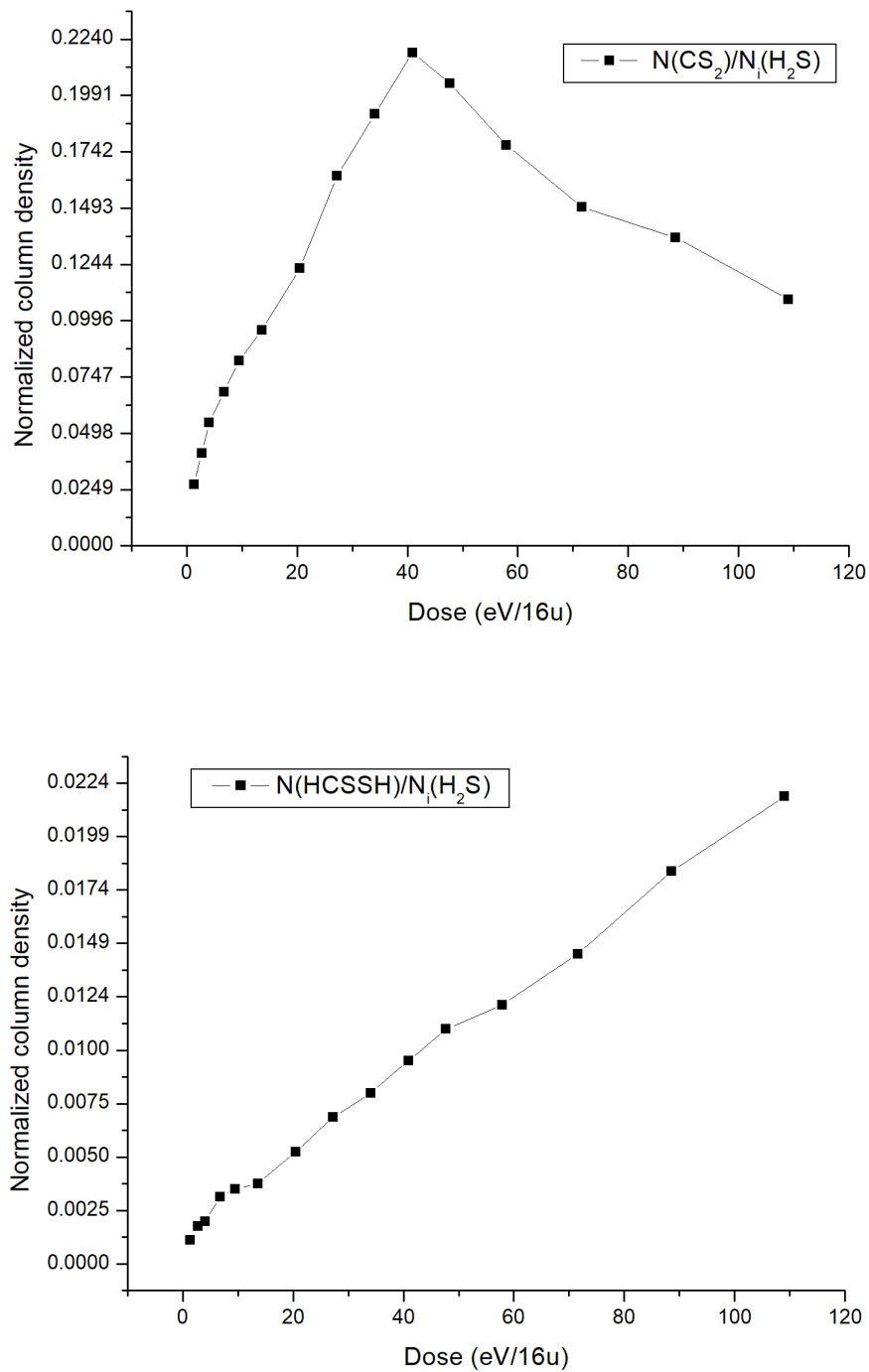


Abbildung 3.7: Column densities of CS_2 and HCSSH plotted as a function of dose and normalized over the initial H_2S abundance.

Kapitel 4

Accurate millimetre and submillimetre rest frequencies for *E*- and *Z*-propargylimine, HCCCHNH

The content of this chapter will be submitted to the journal *Astronomy & Astrophysics*.

4.1 Introduction

From the reasoning introduced in section 1.2.2, it results that, among 3-C-atom bearing imines, a new, promising candidate for the detection in the ISM is propargyl imine (HCCCHNH).

This species is a structural isomer of the well known astrophysical molecule acrylonitrile (Gardner and Winnewisser, 1975) and can be chemically related — through 2H addition — to cyanoacetylene (HC_3N), a nitrile species which is ubiquitous in the ISM (e.g., Bizzocchi et al., 2017, and references therein). Despite this, propargyl imine has not attracted a great deal of interest from laboratory spectroscopists and only a few, rather outdated works, are present in the literature. Its rotational spectrum was first observed in 1984 by Kroto et al. in the centimetre-wave (cm-wave) spectral region. Shortly after, the study was extended by Sugie et al. (1985) and by McNaughton et al. (1988), who also recorded a few rotational transitions for several isotopic variants. In the middle '80s, the low-resolution infrared (IR) spectrum had been also reported (Hamada et al., 1984; Osman et al., 1987).

These studies do not provide an exhaustive spectroscopic knowledge. In particular, the coverage of the rotational spectrum is sparse and limited to the cm-wave regime, thus the reliability of the rest-frequency computed at millimetre wavelengths is not suitable for the purpose of an effective astronomical search. With this in mind, we have undertaken an extensive laboratory investigation, recording the millimetre-wave (mm-wave) spectrum of the propargyl imine in its vibrational ground state.

4.2 Experimental setup

The rotational spectrum of propargyl imine has been recorded using the CASAC (Center for Astrochemical Studies Absorption Cell) spectrometer at the Max-Planck-Institut für extraterrestrische Physik in Garching. Full details of the setup can be found in chapter 2.

The spectral measurements have been performed using the frequency modulation (FM) technique: the carrier signal from the cm-wave synthesizer is sin-wave modulated at 50 kHz sine-wave and the detector output is demodulated at twice this frequency ($2f$) by a lock-in amplifier. The second derivative of the actual absorption profile is thus recorded by the computer controlled acquisition system.

Propargyl imine was produced as in Sugie et al. (1985), i.e., by pyrolysing dipropargyl amine ($\text{HC}\equiv\text{C}-\text{CH}_2\text{NH}$) vapours and flowing the gaseous reaction products through the absorption cell kept under continuous pumping. In our setup, the strongest absorption signals of the target molecules were obtained by setting the oven temperature at 950° . Typical pressure were 150-200 mTorr at the quartz tube inlet, which correspond to ca. 4 mTorr in the absorption cell. Multiple side-products are produced, as reported by McNaughton et al. (1988), which occasionally generated strong spectral features. This, however did not hamper the recording of the target spectrum, thus sample purification via selective trapping or condensation/re-vaporisation were not attempted in the present investigation.

4.3 Results and data analysis

Propargyl imine can be described as a molecule joining two basic subunits: the ethynyl group $\text{HC}\equiv\text{C}-$ and the iminic moiety $-\text{CH}=\text{NH}$. The presence of two conjugated multiple bonds forces the molecule to the planar configuration with all the seven atoms lying on the plane defined by the a and b principal axes. Owing to different relative position of the HCC group and of the iminic H with respect to the $\text{C}=\text{N}$ double bond: two structural isomers exist: *Z* and *E*. Their structures is depicted in Fig. 4.1.

From newly performed ab initio calculations (see § B) the energy difference between the *Z* (more stable) and *E* isomers is 0.00137 au (0.857 kcal mol $^{-1}$).

Both isomers are prolate-type slightly asymmetric tops ($\kappa \sim 0.98$). While the modulus of the dipole moment is similar ($|\mu| \sim 2$ D), the corresponding projections onto the principal axes are very different: $\mu_a = 2.20$ D and $\mu_b = 0.16$ D for the *Z* isomer; $\mu_a = 0.28$ D and $\mu_b = -1.92$ D for the *E* isomer. The dipole moment vectors are also shown in Fig. 4.1. In the mm region, *Z*-propargyl imine presents a typical *a*-type spectrum with groups of *R*-branch $\Delta K_a = 0$ transitions regularly separated by $\approx B + C$, while the *E* species exhibits a much more complex spectrum consisting on several $\Delta K_a \pm 1$ ladders overlapped each other and with some prominent *Q*-branch band-heads spaced by $\approx 2A - B - C$.

From the ab initio computed energy difference a relative *E/Z* isomer relative abundance of 0.24 can be estimated at 300 K.

Due to the presence of nitrogen, hyperfine coupling is generated between the molecular electric field gradient, averaged over the end-over-end rotation, and the quadrupole moment of ^{14}N

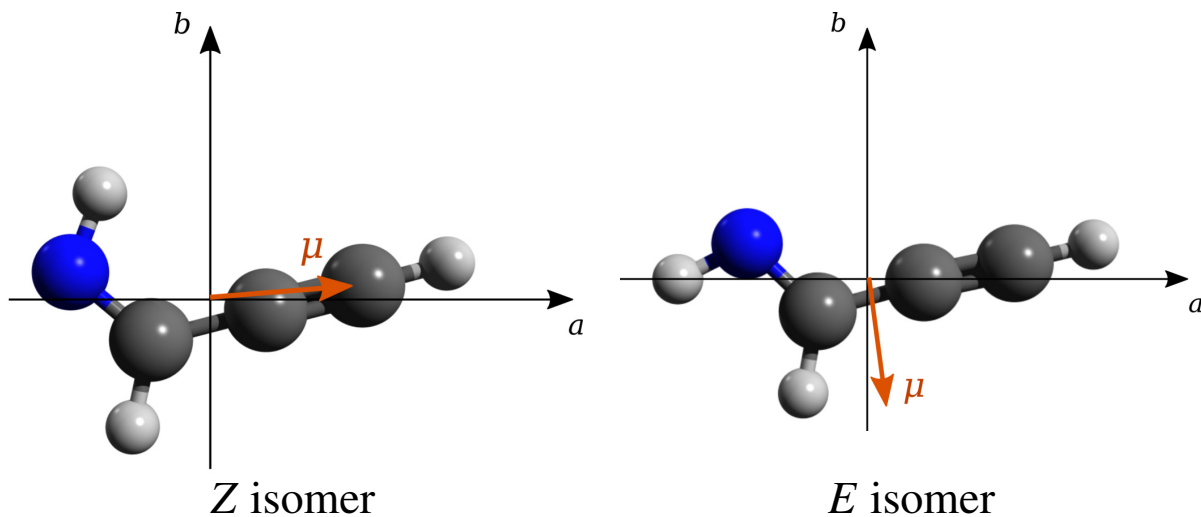


Abbildung 4.1: Molecular structure and principal inertial axes of the *Z* and *E* isomers of propargyl imine. The orange arrow indicates the direction of the electric dipole moment μ and points towards the displacement of the notional negative charge.

nucleus having spin $I = 1$. Thus, each rotational level with principal quantum number $J > 0$ is splitted into three hyperfine sublevels labelled with the total angular quantum number F , where $F = J - 1, J, J + 1$. As a consequence, the transitions are splitted into several components according the the selection rules $\Delta F = 0, \pm 1$, with the stronger features being those for which $\Delta F = \Delta J$. However, in the frequency interval covered by the present investigation the J quantum number reaches a value as high as 54, thus most of the $^aR_{0,+1}$ transitions¹ — which dominates the *Z* isomer spectrum — have the their hyperfine pattern collapsed into a single feature. Nevertheless, for a few low- J lines it was possible to detect the very weak $\Delta F = 0$ components, which form a widely separated doublet approximately centred at the frequency of the corresponding unsplit transition. An examples of such hyperfine patterns is given in Fig. 4.2. The situation is different for the b -type lines, typical of the *E* isomer spectrum. Due to the change in the K_a pseudo quantum number involved in these transitions, less close hyperfine patterns are produced and, for low J -values, triplets/doublets of lines have been typically recorded as shown in Figure 4.3. A summary of the transitions of both isomers for which the hyperfine structure have been resolved is presented in Table 4.1.

For the lines, the measured features were assigned to one or more quadrupole components depending on the actual pattern and taking into account the available spectral resolution. In case of multiple assignment (typically 2 or 3), the intensity-averaged calculated frequency was compared with the experimental data in the least-squares fit. Loose blends of unresolved components have been also observed. These lines appeared as broad and distorted features and were not used

¹The symbol ${}^xM_{\delta K_a, \delta K_c}$ is used to label in a compact form the transition type for an asymmetric rotor: x indicates the dipole moment component involved, $M = P, Q, R$ is the symbol for the transitions with $\Delta J = -1, 0, +1$, respectively, and δK_a and δK_c refer to the (signed) change of the K_a and K_c pseudo-angular quantum numbers (Gordy and Cook, 1984).

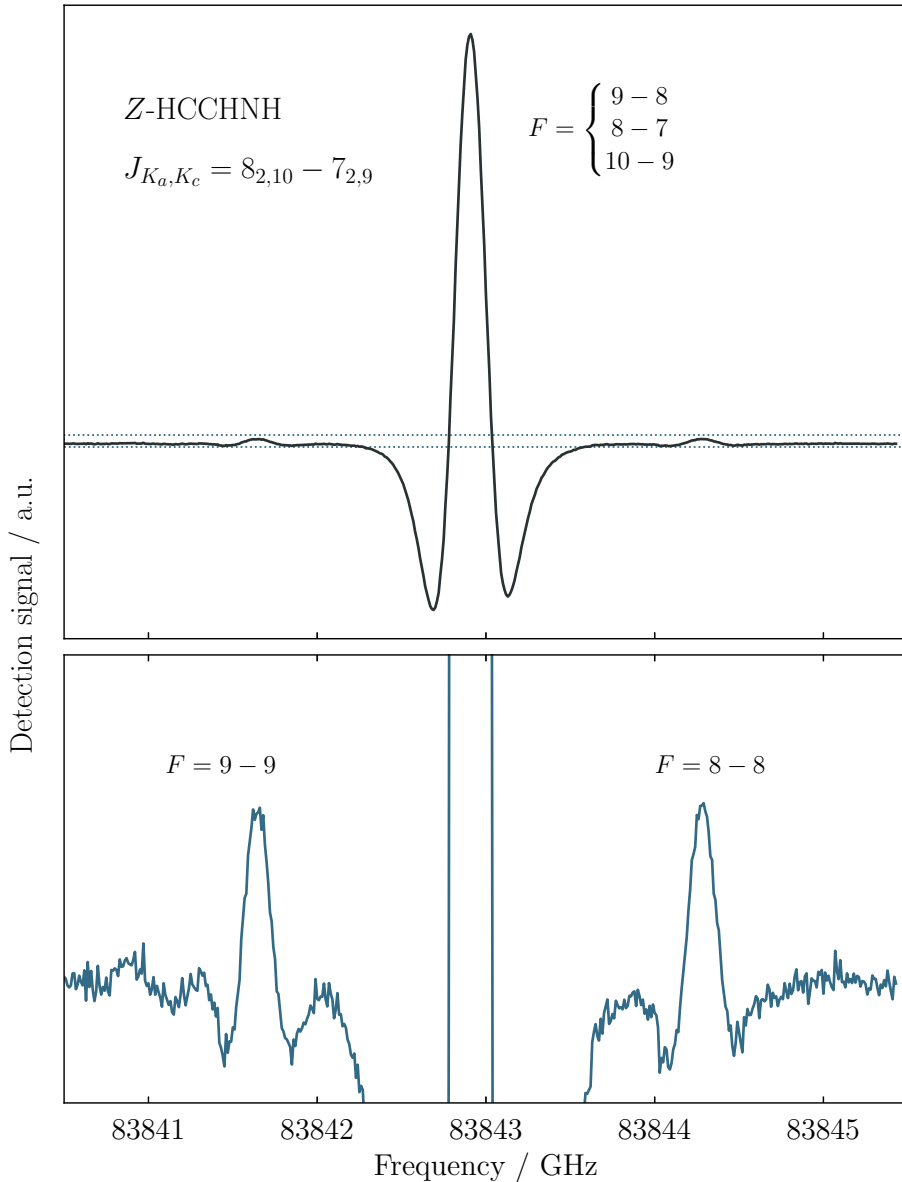


Abbildung 4.2: Recording of the $J_{K_a,K_c} = 8_{2,10} - 7_{2,9}$ of *Z*-HCCCHNH showing the two weak $\Delta F = 0$ hyperfine components symmetrically separated from the central blended $\Delta F = +1$ triplet by 1.3 MHz (*upper panel*). Total integration time 47 s with time constant $RC = 3$ ms. The area enclosed in the dashed box is plotted with expanded y-axis in the *lower panel*.

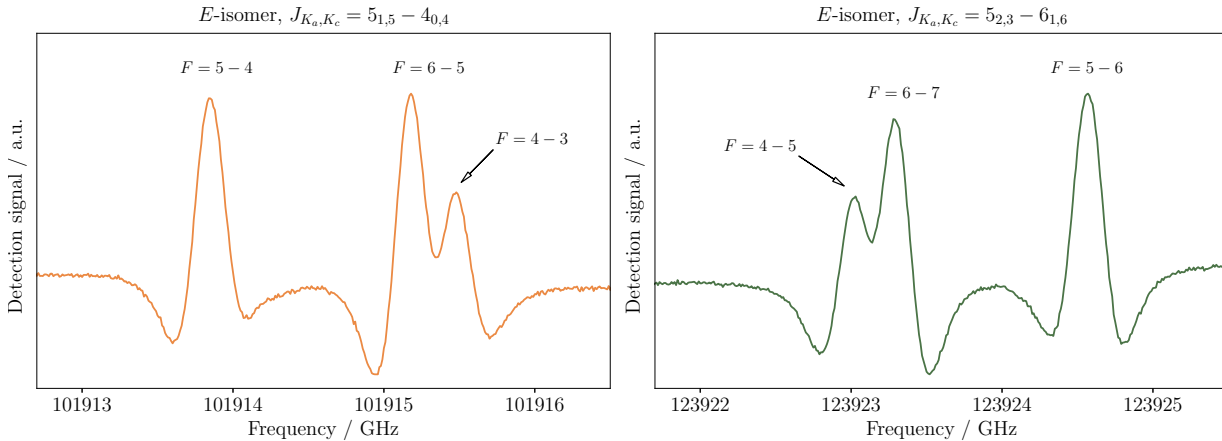


Abbildung 4.3: Recordings of two *b*-type transitions for *E*-propargyl imine showing the typical hyperfine structure produced by the quadrupole coupling of the ^{14}N nucleus. *Left panel*: $J_{K_a,K_c} = 5_{1,5} - 4_{0,4}$; integration time 180 s. *Right panel*: $J_{K_a,K_c} = 5_{2,3} - 6_{1,6}$; integration time 165 s. The adopted scan rate is 0.2 MHz s^{-1} with time constant $RC = 3 \text{ ms}$.

in the analysis. A sizeable number of recorded transitions did not show any hint of hyperfine splitting, namely 417 for the *Z* isomer and 241 for the *E* isomer. For these data, the contribution due to the nuclear quadrupole coupling were neglected, and the measured frequencies were assigned to the corresponding pure rotational transitions.

In total, our data sets comprise 566 lines for *Z*-HCCCHNH and 544 lines for *E*-HCCCHNH. They also included 46 and, respectively, 49 cm-wave transitions taken from the literature (Sugie et al., 1985; McNaughton et al., 1988). Different statistical weights $w = 1/\sigma^2$ were given to the various subsets to take into account the different measurement precision (σ). For the lines measured by Sugie et al. (1985) we retained the same weighting scheme of the original paper, while 50 kHz was given to the few transitions of the *Z*-propargyl imine reported by McNaughton et al. (1988). The average uncertainty of the frequencies measured in the present work is estimated to be 15 kHz.

The hyperfine energies were computed adopting the standard vector coupling scheme between the rotational angular momentum J and the nitrogen spins I_{N} :

$$\mathbf{J} + \mathbf{I}_{\text{N}} = \mathbf{F}. \quad (4.1)$$

The total Hamiltonian is thus expressed as the sum of a purely rotational part and a hyperfine contribution:

$$\hat{H} = \hat{H}_{\text{rot}} + \hat{H}_{\text{HFS}}. \quad (4.2)$$

The pure rotational levels are labelled with the quantum numbers J_{K_a,K_c} , the total angular momentum quanta F must be added when the hyperfine sublevels are considered.

The rotational Hamiltonian \hat{H}_{rot} is the S -reduced Watson-type Hamiltonian in its I' representation (Watson 1977b) and includes centrifugal distortion corrections up to the octic terms.

Tabelle 4.1: Summary of the transitions with resolved hyperfine structure recorded for both propargyl imine isomers.

isomer Z				isomer E			
type ^a	no. of lines	no. of comp.	K'_a	type ^a	no. of lines	no. of comp.	K'_a
^a $R_{0,+1}$	29	76	0,1,2,3	^b $P_{+1,-1}$	10	18	1
^b $R_{+1,+1}$	4	6	0	^b $R_{0,+1}$	73	140	0,1,2
^b $R_{-1,+1}$	3	6	1	^b $Q_{+1,-1}$	50	99	0,1,2
^b $Q_{+1,-1}$	6	12	0				

The hyperfine-structure Hamiltonian \hat{H}_{HFS} is expressed by the traceless tensor χ which has χ_{aa} and $\chi_{bb} - \chi_{cc}$ as determinable coefficients. The weak spin–rotation coupling do not produce any detectable effect in the recorded spectra and was thus neglected.

The resulting spectroscopic parameters are listed in table 4.2.

4.4 Discussion and conclusions

In our study we provide a complete characterization of the two propargyl imine isomers in their ground electronic state. Given the extension of the range in term of measured transitions, the new datasets result in very accurate and reliable spectroscopic parameters. The error on the rotational constants, in fact, is lower than the 0.00001% for *A* and even lower for *B* and *C*, for both the *E*- and *Z*-propargyl imine.

The centrifugal distortion analysis has been completed with inclusion of all the quartic, the sextic and some octic constants, when necessary. In addition, the hyperfine splitting have been resolved and included in the fit, leading to the experimental values of the quadrupole constants, as listed in table 4.2.

These new sets of spectroscopic parameters made it possible to compute accurate rest frequencies which can be largely employed for an astronomical search of the compound. Detection of these molecules should be indeed possible in the ISM and can be carried out in the cm, mm, and submm bands, depending on the temperature of the source.

Tabelle 4.2: Experimental and theoretical spectroscopic parameters of E and Z isomers of propargyl-imine. Number in parentheses are 1σ statistical uncertainties in the units of the last quoted digit.

Parameter	<i>E</i> isomer			<i>Z</i> isomer		
	experiment	theory	¹	experiment	theory	¹
<i>A</i>	/ MHz	63099.2227(25)	62982.386	54640.1484(46)	54733.840	
<i>B</i>	/ MHz	4766.557624(58)	4768.456	4862.362753(62)	4861.328	
<i>C</i>	/ MHz	4425.560989(62)	4426.522	4458.249982(56)	4457.883	
<i>D_J</i>	/ kHz	1.608437(51)	1.580	2.008287(40)	1.988	
<i>D_{JK}</i>	/ kHz	-108.8297(16)	-109.2	-101.1808(21)	-100.3	
<i>D_K</i>	/ kHz	6192.58(70)	6122.9	4170.0(32)	4003.9	
<i>d₁</i>	/ kHz	-0.3010606(87)	-0.2926	-0.410931(21)	-0.4022	
<i>d₂</i>	/ kHz	-0.0188115(26)	-0.1503	-0.027980(21)	-0.0233	
<i>H_J</i>	/ mHz	4.037(13)	3.925	5.5704(84)	5.688	
<i>H_{JK}</i>	/ Hz	-0.46708(84)	-0.4788	-0.4606(81)	-0.4464	
<i>H_{KJ}</i>	/ Hz	-3.678(52)	-3.192	-6.740(28)	-7.879	
<i>H_K</i>	/ kHz	1.073(50)	1.101	3.17(39)	0.7939	
<i>h₁</i>	/ mHz	1.5508(24)	1.486	2.1744(68)	2.188	
<i>h₂</i>	/ mHz	0.2052(11)	0.1645	0.3461(60)	0.2721	
<i>h₃</i>	/ mHz	0.06095(24)	0.04505	0.1197(45)	0.0733	
<i>L_{JJK}</i>	/ mHz	-	-	0.00301(38)	-	
<i>L_{JK}</i>	/ mHz	-0.343(10)	-	-0.3326(28)	-	
<i>L_{JKK}</i>	/ mHz	-2.15(35)	-	-	-	
χ_{aa}	/ MHz	1.26(23)	0.931	-4.0583(66)	-4.190	
$\chi_{bb} - \chi_{cc}$	/ MHz	-7.665(11)	-7.895	-2.658(16)	-2.776	
no. of lines		523		509		
σ_w		0.932		0.908		

¹ See appendix B for further details.

**4. Accurate millimetre and submillimetre rest frequencies for *E*- and *Z*-propargylimine,
52 HCCCHNH**

Kapitel 5

Collisional excitation of NH($^3\Sigma^-$) by Ar: a new *ab initio* 3D Potential Energy Surface and scattering calculations

The content of this chapter was published in *The Journal of chemical physics*.

Credit: Prudenzano, D., et al., *The Journal of chemical physics*, 150.21 (2019): 214302.

5.1 Introduction

The study of inelastic collisions plays a relevant role in the understanding of important processes in different fields, such as atmospheric and astrophysical chemistry and physics. In particular open-shell molecules are crucial, being highly reactive compounds and intermediate in a large number of chemical reactions. A relevant chemical species is the NH radical. This compound serves as a prototype for other collisional studies involving open-shell molecules. Being diatomic it is also preferred for both experimental and theoretical scattering studies, owing to its large rotational energy level spacings. In addition, the magnetic moment of its $^3\Sigma^-$ electronic ground state, makes NH suitable for studies of ultracold molecules (Friedrich and Doyle 2009; Egorov et al. 2004), because it can be easily thermalized at low temperatures through collision with cold buffer gas atoms. In the past, NH has been subject of many theoretical and experimental collisional studies in different electronic states and with a variety of perturbers, such as the rare gases He (Alexander et al. 1991; Rinnenthal and Gericke 2002; Krems et al. 2003; Cybulski et al. 2005; Stoecklin 2009; Toboła et al. 2011; Dumouchel et al. 2012; Ramachandran et al. 2018) and Ne (Rinnenthal and Gericke 2000; Kerenskaya et al. 2005; Bouhafs and Lique 2015).

In our work we focus on the calculation of a new *ab initio* 3D-averaged Potential Energy Surface (PES) and collisional excitation for the NH($^3\Sigma^-$)-Ar system. To our knowledge, there are no theoretical scattering studies for the fine-structure excitation of NH($^3\Sigma^-$) by Ar, while there is only one experimental work performed by Dagdigian (1989), employing a crossed beam apparatus. However, this experiment provides only relative collisional cross sections up to the rotational level $N=4$ and no rate coefficients are available.

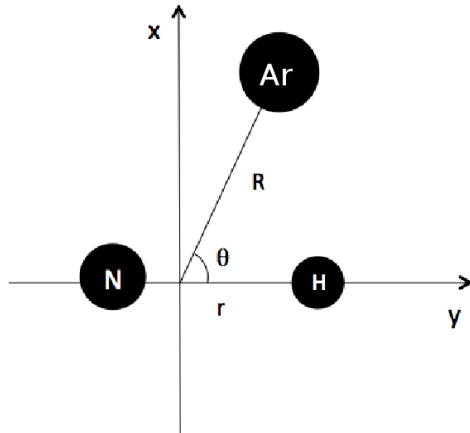


Abbildung 5.1: Definition of the Jacobi coordinate system. The origin of the coordinate system corresponds with the NH center of mass. R is the distance between the origin and the Ar atom, θ is the angle at which the Ar approach the NH molecule and r is the NH bond length.

The most recent PES is given by Kendall et al. (1998). They employed a combination of supermolecular and intermolecular unrestricted Møller-Plesset perturbation theory (UMPPT) (Cybulski et al. 1995; Cybulski 1989) and a selection of monomer-centered basis sets augmented with bond functions. However, the NH bond length was kept frozen at 1.96 bohr. Recent studies Kalugina et al. (2014); Bouhafs and Lique (2015); Lique (2015); Ramachandran et al. (2018) have proven that the use of a 3D PES which takes into account molecular vibration leads to more accurate results when employed in collisional excitation studies of light hydrides by rare gases. Moreover, inclusion of the bond vibrational motion makes it possible to comprise excited vibrational states. Hence, we have computed a new *ab initio* PES for the NH($^3\Sigma^-$)–Ar van der Waals complex including the NH bond vibration.

Then, we present the first fully quantum close-coupling (CC) calculations of rotational inelastic cross sections for the NH($^3\Sigma^-$)–Ar collisional system. In addition, we have taken into account the spin-coupling splitting of the rotational levels and we have included the temperature dependence of the fine-structure resolved rate coefficients in the final results.

5.2 Potential energy surface

The two interacting species are considered in their ground electronic states NH($^3\Sigma^-$) and Ar(1S). The NH($^3\Sigma^-$)–Ar van der Waals system has ${}^3A''$ ground electronic state. In this work, we used the Jacobi coordinate system (see Fig. 5.1). The center of coordinates is placed in the NH center of mass (c.m.), and the vector \mathbf{R} connects the NH c.m. with the Ar atom. The rotation of NH molecule is defined by the θ angle and the r coordinate describes the NH bond length.

We performed the calculations for five NH bond lengths $r = [1.6, 1.8, 1.95, 2.15, 2.5]$ bohr

which allows us to take into account vibrational motion of NH molecule up to $v = 2$. We have carried out *ab initio* calculations of the PES of the NH–Ar van der Waals complex at the partially spin-restricted coupled cluster with single, double and perturbative triple excitations [RC-CSD(T)] (Hampel et al. 1992; Watts et al. 1993) level of theory, using MOLPRO 2015 package (Werner et al., 2019). In order to determine the interaction potential, $V(R, \theta, r)$, the basis set superposition error (BSSE) was corrected at all geometries using the Boys and Bernardi counterpoise scheme (Boys and Bernardi, 1970):

$$\begin{aligned} V(R, \theta, r) &= E_{\text{NH-Ar}}(R, \theta, r) \\ &\quad - E_{\text{NH}}(R, \theta, r) - E_{\text{Ar}}(R, \theta, r) \end{aligned} \quad (5.1)$$

where the energies of the NH and Ar monomers are computed using the full basis set of the complex.

To achieve a good description of the charge-overlap effects we have performed the calculations in a rather large augmented correlation-consistent basis sets aug-cc-pVXZ ($X = T, Q, 5$) (Dunning Jr, 1989a). Then, we have extrapolated the energies to the Complete Basis Set (CBS) limit using the following scheme (Peterson et al., 1994):

$$E_X = E_{\text{CBS}} + A e^{-(X-1)} + B e^{-(X-1)^2}, \quad (5.2)$$

where X is the cardinal number of the aug-cc-pVXZ basis set, E_X is the energy corresponding to aug-cc-pVXZ basis set, E_{CBS} is the energy extrapolated to CBS limit, A and B are the parameters to adjust. We have carried out the calculations for θ angle values from 0° to 180° in steps of 10° . R -distances were varied from 3.0 to 40.0 bohr, yielding 52 points for each angular orientation. Overall ~ 5000 single point energies were calculated for the NH–Ar complex.

5.2.1 Analytical representation of the potential energy surface

The analytical expression employed for the interaction potential $V(R, \theta, r)$ has the following form (Werner et al., 1988):

$$V(R, \theta, r) = \sum_{n=1}^N \sum_{l=1}^L B_{l,n}(R)(r - r_e)^{n-1} d_{m0}^{l+m-1}(\cos(\theta)), \quad (5.3)$$

where

$$\begin{aligned} B_{l,n}(R) &= e^{-a_{l,n}(R - R_{l,n}^{(0)})} \left(\sum_{i=0}^2 b_{l,n}^{(i)} R^i \right) \\ &\quad - \frac{1}{2} \left(1 + \tanh \frac{R - R_{l,n}^{(1)}}{R_{l,n}^{\text{ref}}} \right) \sum_{j=6,8,10} \frac{c_{l,n}^{(j)}}{R^j}. \end{aligned} \quad (5.4)$$

The basis functions $d_{m0}^{l+m-1}(\cos(\theta))$ are Wigner rotation functions, N is the total number of r -distances, and L is the total number of angles. The analytic potential was found to reproduce

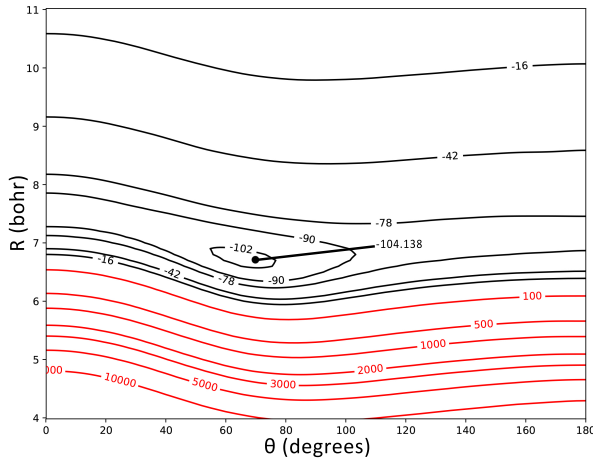


Abbildung 5.2: Contour plot (in cm^{-1}) of the NH–Ar PES averaged over the ground vibrational state $v = 0$ as a function of Jacobi coordinates R and θ .

the calculated energies quite well: the mean difference between the analytic fit and the *ab initio* computed interaction energies is less than 2% over the entire grid.

Previous studies (Kalugina et al., 2014) have shown that averaging of the PES over corresponding vibrational level v leads to a better agreement with experimental results than using a purely two-dimension PES. The newly constructed PES, which takes into account the stretching of the NH molecule, can be averaged over any vibrational state, up to $v = 2$. The averaging is done using the following formula:

$$V_v(R, \theta) = \langle v(r) | V(R, \theta, r) | v(r) \rangle \quad (5.5)$$

The NH vibrational wave functions $|v(r)\rangle$ were those computed in Bouhafs and Lique (2015) that were evaluated using a discrete variable representation (DVR) method (Colbert and Miller, 1992) from *ab initio* calculations of the NH potential function using the internally contracted multireference configuration interaction (MRCI)(Werner and Knowles, 1988) level and a large aug-cc-pV5Z atomic basis set.

Figure 5.2 depicts the contour plot of our 3D PES averaged over the ground vibrational state $v = 0$ as a function of R and θ (hereafter referred as 3D-ave PES). For this weakly-bound system the global minimum in the interaction energy was found to be -104.138 cm^{-1} ($R = 6.7$ bohr, $\theta = 69^\circ$).

Our study is in good agreement with the NH–Ar PES previously published (Kendall et al., 1998). Kendall et al. (1998) carried out calculations for the NH–Ar interaction with the supermolecular unrestricted Møller-Plesset (UMP) perturbation theory and a combination of different basis sets. The NH intermolecular distance was fixed at 1.95 bohr. According to the authors the best results have been obtained with the aug-cc-pVTZ(ext-b) basis set, augmented with bond functions, and the global minimum is found at $R = 6.75$ bohr and $\theta = 67^\circ$, with a well-depth of -100.3 cm^{-1} and an uncertainty within the 5%. These values are very close to our results for

$r = 1.95$ bohr ($R = 6.7$, $\theta = 67^\circ$, 103.787 cm^{-1}) . Furthermore, the results of our 3D-ave PES also agree well with those listed above, confirming the high accuracy of our study. The slightly increased deepness of our well-depth is mostly due to the use of CBS extrapolation, since the energy follows a monotonic trend towards negative values, by approaching the infinite basis set limit.

5.2.2 NH–Ar bound states and dissociation energy

Using the highly correlated 3D-ave PES described in the previous section, we have computed the bound states of NH–Ar complex using a coupled-channel approach, as implemented in the BOUND program (Hutson, 1993). The bound state calculations were performed for the main ^{14}N and ^{40}Ar isotopes.

As a first step we performed bound state calculations neglecting the NH fine structure (i.e. NH was considered as a closed shell molecule). The calculations were performed with a propagator step size of 0.01 bohr, and the other propagation parameters were taken as the default BOUND values. The rotational basis includes the rotational states with $N_{\max} \leq 10$. The bound energy levels of the NH–Ar complex computed with the 3D-ave PES are listed in Table 5.1. From the present calculations, dissociation energy (D_0) of the complex is 73.15 cm^{-1} which is slightly larger than the previously calculated value of Kendall et al. (1998) ($D_0 = 71.5 \text{ cm}^{-1}$). The difference (1.65 cm^{-1}) can be mainly attributed to the difference between the two NH–Ar PESs used in the calculations. Indeed, the well depth of the 3D-ave PES considering the vibration motion is slightly deeper (by few cm^{-1}) than the rigid rotor one of Kendall et al. (1998) and this difference leads to a larger estimated value of the dissociation energy.

In order to derive the rotational constant of the NH–Ar complex, we have fitted the energies of Table 5.1 to the rigid rotor expression: $E_J = E_0 + BJ(J+1) - DJ^2(J+1)^2$ where J corresponds to the total angular momentum of the complex. We have obtained for the rotational and quartic centrifugal distortion constants, $B = 0.1087 \text{ cm}^{-1}$ and $D = 0.000025 \text{ cm}^{-1}$. Such estimates allow generating the energetic structure of the complex and are useful for the interpretation of future experimental spectra.

As previously mentioned, the NH molecule exhibits a fine structure because of the coupling between the rotational angular momentum and the electronic spin. The BOUND program was

Tabelle 5.1: NH–Ar bound energy levels (in cm^{-1}) obtained excluding the NH fine structure. Energies are relative to the ground-state energy of NH. All the levels correspond to the approximate quantum numbers $N = 0$. J and l correspond to the total and orbital angular momentum of the complex, respectively.

J	l	Energy (cm^{-1})
0	0	-73.1507
1	1	-72.9324
2	2	-72.4988
3	3	-71.8479

Tabelle 5.2: NH–Ar bound energy levels (in cm^{-1}) obtained with the inclusion of the NH fine structure. Energies are relative to the ground-state energy of NH. All the levels correspond to the approximate quantum numbers $N = 0, F_1, J$ and l correspond to the total and orbital angular momentum of the complex, respectively.

J	l	Energy (cm^{-1})
1	0	-73.1519
0	1	-72.8964
1	1	-72.9507
2	1	-72.9305
1	2	-72.4804
2	2	-72.5169
3	2	-72.4947
2	3	-71.8333
3	3	-71.8658
4	3	-71.8426

modified to include this fine structure of the NH molecule (Ramachandran et al., 2018). Table 5.2 presents the bound state energies for the first total angular momentum J . The predicted bound energy levels indicate that the coupling of the electron spin to the rotational motion of the complex is very weak. As a consequence, energy levels of NH–Ar are very similar to those obtained by neglecting the fine structure, as already found for the NH–He complex (Ramachandran et al., 2018). The dissociation energy is thus not significantly impacted by the fine structure.

5.3 Scattering calculations

Rotational transitions in the NH($^3\Sigma^-$) electronic ground state show fine-structure splitting, due to spin-rotation coupling. The rotational wave function of NH for $j \geq 1$ in the intermediate coupling scheme can be written as (Gordy and Cook, 1984; Lique et al., 2005):

$$\begin{aligned}
 |F_1 jm\rangle &= \cos \alpha |N = j - 1, S jm\rangle \\
 &\quad + \sin \alpha |N = j + 1, S jm\rangle \\
 |F_2 jm\rangle &= |N = j, S jm\rangle \\
 |F_3 jm\rangle &= -\sin \alpha |N = j - 1, S jm\rangle \\
 &\quad + \cos \alpha |N = j + 1, S jm\rangle
 \end{aligned} \tag{5.6}$$

where $|N, S jm\rangle$ denotes pure Hund's case (b) basis functions and the mixing angle α is obtained by diagonalisation of the molecular Hamiltonian. In this relation corresponding to the Hund's case (b), the total molecular angular momentum j is defined by:

$$\mathbf{j} = \mathbf{N} + \mathbf{S} \tag{5.7}$$

where \mathbf{N} and \mathbf{S} are the nuclear rotational and the electronic spin angular momenta. In the pure case (b) limit, $\alpha \rightarrow 0$, the F_1 level corresponds to $N = j - 1$ and the F_3 level to $N = j + 1$. The levels in the spin multiplets are usually labeled by the nuclear rotational quantum number N and the spectroscopic index F_i . This notation will be used hereafter.

Using the new 3D-ave PES, we have studied the collisional excitation of NH by Ar. The scattering calculations were performed for the main ^{14}N and ^{40}Ar isotopes. The detailed description of the Close-Coupling (CC) calculations that consider the fine structure levels of the colliders is given in Lique et al. (2005). The quantal coupled equations have been solved in the intermediate coupling scheme using the MOLSCAT code (Hutson and Green, 1994) modified to take into account the fine structure of the rotational energy levels.

We used a total energy grid with a variable steps. For the energies below 500 cm^{-1} the step was equal to 1 cm^{-1} , then, between 500 and 1000 cm^{-1} it was increased to 2 cm^{-1} , and to 20 for the interval $1000\text{-}3000 \text{ cm}^{-1}$. Using this energy grid, the resonances (shape and Feshbach) that usually appear in the cross sections at low energies were correctly represented.

In order to ensure convergence of the inelastic cross sections, it is necessary to include in the calculations several energetically inaccessible (closed) levels. At the largest energies considered in this work, the NH rotational basis was extended to $N = 12$ to ensure convergence of the rotational cross sections between levels with $N < 8$. One also needs to converge inelastic cross sections with respect to partial waves. The total angular momentum quantum number J needed for the convergence was set up to 238 for the inelastic cross sections.

Moreover, in MOLSCAT, it is necessary to adjust the propagator's parameters in order to ensure convergence of cross sections calculations. For all the energies, the minimum and maximum integration distances were $R_{min} = 3.0 \text{ bohr}$ and $R_{max} = 50 \text{ bohr}$, respectively. The STEPS parameter was adjusted for each value of energy in order to obtain a step length of the integrator sufficient to achieve the convergence. In our work, the value of the STEPS parameter decreases with increasing energy (from 50 to 7 for our energy range). The reduced mass of the NH–Ar system is $\mu = 10.912 \text{ u}$ and the NH($^3\Sigma^-$) rotational and centrifugal distortion constants have been taken from Lewen et al. (2004).

Figure 5.3 presents the energy variation of the integral cross sections for transitions from the initial rotational level $N = 0, F_1$ of NH. The resonances shown at low collisional energies are related to the presence of a $\sim 104 \text{ cm}^{-1}$ deep attractive potential well. As a consequence, the Ar atom can be temporarily trapped there forming quasi-bond states before dissociation of the complex (Smith et al. 1979; Christoffel and Bowman 1983). However, excitation cross sections are less affected and therefore show few resonances. Indeed, the energy spacing between rotational levels is generally larger than the well depth of the PES.

The magnitude of the cross sections shown in figure 5.3 seems to present the following propensity rules:

(1) Overall decreasing of the cross sections with increasing ΔN , according to the usual trend for rotational excitation. In addition, even ΔN transitions are favored over odd ΔN transitions as a consequence of near-homonuclearity of the PES.

(2) Fine-structure conserving transitions are favored, i.e. $\Delta j = \Delta N$ in the case of pure Hund's case (b).

The same propensity rules are shown in similar systems, such as NH–He and NH–Ne colli-

5. Collisional excitation of $\text{NH}({}^3\Sigma^-)$ by Ar: a new *ab initio* 3D Potential Energy Surface and scattering calculations

60

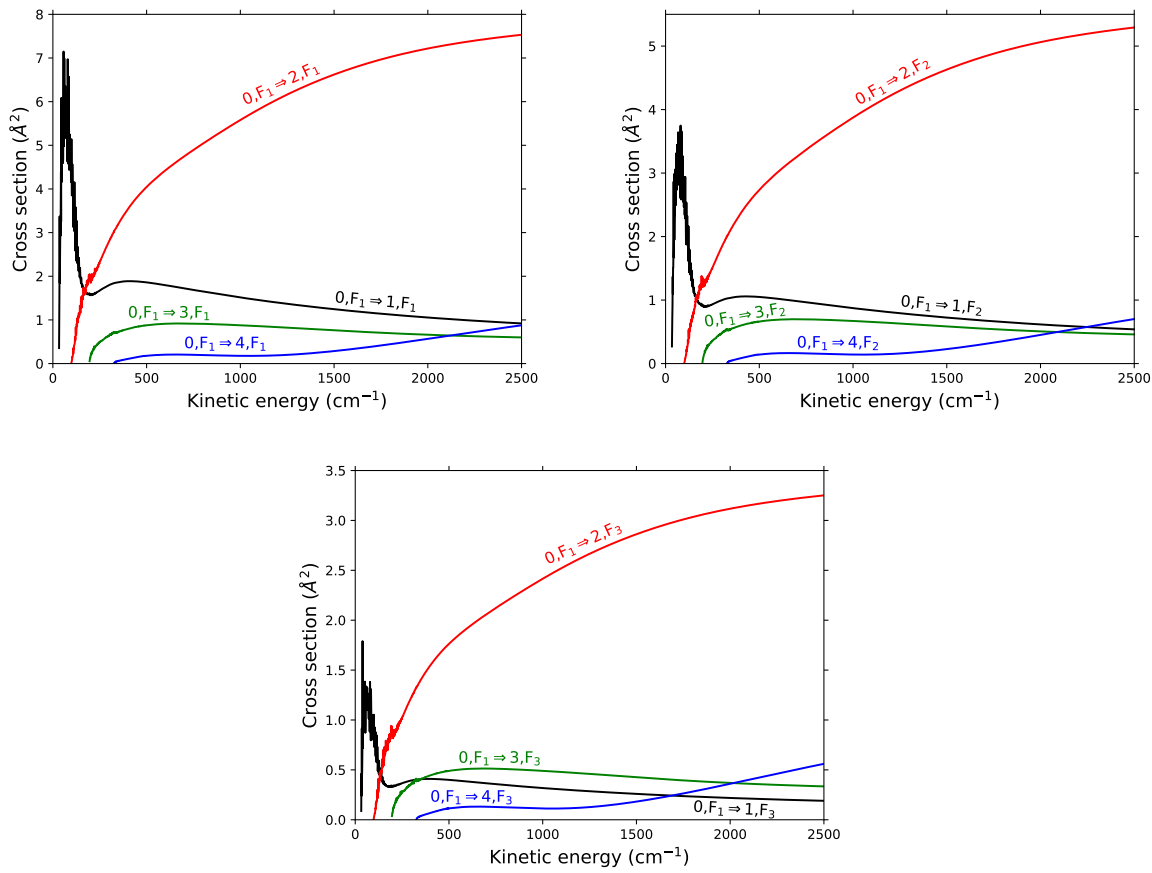


Abbildung 5.3: Collisional excitation cross sections of NH by Ar from $N = 0, F_1$. The upper panel is for fine-structure conserving transitions while the two other panels are for fine-structure changing transitions.

sions (Tobola et al. 2011; Bouhafs and Lique 2015; Ramachandran et al. 2018). In particular, the latter applies in general to molecules in the ${}^3\Sigma^-$ electronic state. Both porpensity rules have been predicted theoretically (Alexander and Dagdigian, 1983) and also observed for the O₂-He (Orlikowski 1985; Lique 2010) or SO(X ${}^3\Sigma^-$)-He (Lique et al., 2005) collisions.

The thermal rate coefficients, $k_{F_i j \rightarrow F'_i j'}(T)$, for excitation and de-excitation transitions between fine-structure levels of NH can be calculated by averaging CC excitation cross sections, $\sigma_{F_i j \rightarrow F'_i j'}$, over a Maxwellian distribution of collision velocities, as follows:

$$\begin{aligned} k_{F_i j \rightarrow F'_i j'}(T) &= \left(\frac{8k_B T}{\pi \mu}\right)^{\frac{1}{2}} \left(\frac{1}{k_B T}\right)^2 \\ &\times \int_0^\infty E_k \sigma_{F_i j \rightarrow F'_i j'}(E_k) e^{\frac{-E_k}{k_B T}} dE_k \end{aligned} \quad (5.8)$$

where k_B is the Boltzmann constant, μ is the reduced mass of the system and E_k is the translational energy.

The thermal dependence of these state-to-state rate coefficients for temperatures up to 350 K is shown in Fig. 5.4 for transitions out of the $N = 0, j = 1, F_1$ level.

The rate coefficients display the same propensity rules as seen for the integral cross sections. In particular, the rate coefficients for F -conserving transitions are generally larger than those for F -changing transitions.

5.4 Comparison with experiments

Our new calculated cross sections can be compared with the previous experimental results, obtained for a collisional energy of 410 cm $^{-1}$ and for rotational levels up to $N=4, F_1$ (Dagdigian, 1989)). Tab. 5.3 shows experimental and theoretical values normalized with respect to the $N = 0, F_1 \rightarrow N' = 1, F_1$ cross section. The F -conserving propensity rule is overall fullfilled in both the experimental and calculated values. The main discrepancy is the trend of the cross sections over increasing ΔN and over even/odd ΔN , as discussed for the first propensity rule in Section 5.3. Furthermore, according to the results of Dagdigian (1989), the largest cross sections are those with $N' = 1$, whereas this is not the case in our study. In fact, larger values are related to the transitions involving $N' = 2$, as also shown in figure 5.3.

It is likely that these discrepancies are due to a particular feature of the experiment. In fact, as declared by the author, the NH beam was not entirely pure, with 68% of the population in the rotational ground state $N = 0, F_1$, and approximately 16% and 9% in the $N = 1, F_1$ and $N = 1, F_2$ levels, respectively. By taking into account this NH beam population composition, the propensity rules observed in the experiment can be reproduced making a convolution of the various cross sections involved. This is shown in Tab. 5.4, which gathers values computed using 68% contribution from inelastic cross section for transitions out of the $N = 0, F_1$, 16% from cross sections involving the $N = 1, F_1$, and 9% from those involving the $N = 1, F_2$. We have also taken into account contributions from elastic collisions when appropriate.

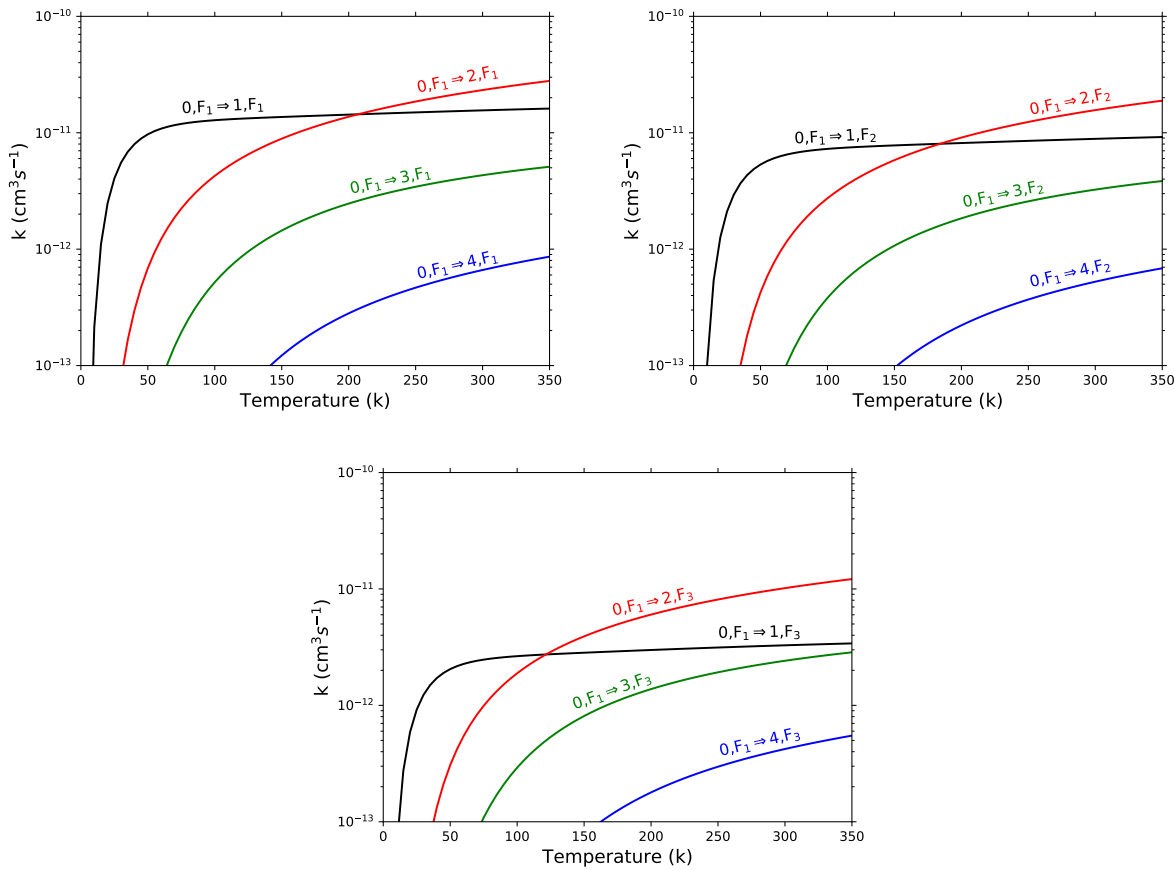


Abbildung 5.4: Thermal dependence of the rate coefficients of NH by Ar from $N = 0, F_1$. The upper panel is for fine-structure conserving transitions while the two other panels are for fine-structure changing transitions.

Tabelle 5.3: Comparison between experimental and our theoretical cross sections at a collisional energy of 410 cm^{-1} and for transitions out of the $N = 0, F_1$ rotational level. All the values are normalized with respect to the cross section for the $N = 0, F_1 \rightarrow N' = 1, F_1$ transition. Experimental error in parenthesis are in units of the last quoted digit.

N'	F_1		F_2		F_3	
	Exp ¹	Theory ²	Exp ¹	Theory ²	Exp ¹	Theory ²
1	1.0	1.0	0.662(40)	0.560	0.255(54)	0.217
2	0.407(54)	1.906	0.284(46)	1.275	0.154(20)	0.833
3	0.068(15)	0.427	0.059(10)	0.321	0.047(08)	0.239
4	0.023(05)	0.061	-	-	-	-

¹ Dagdigian (1989).

² Our work.

It should be pointed out that there is a 7% population with unknown distribution and thus the theoretical results obtained through convolution are still different in magnitude from the experimental ones.

5.5 Conclusions

We have computed a new highly accurate 3D PES for the NH–Ar collisional system by taking into account the stretching of the NH bond. We carried out these *ab initio* calculations at the RCCSD(T) level and a complete basis set extrapolation. The results are in good agreement with the most recent PES available (Kendall et al., 1998).

Employing our new 3D-ave PES we have calculated the dissociation energy of the NH–Ar van der Waals complex and the corresponding rotational and centrifugal distortion constants. We have also performed scattering calculations at the close-coupling level, obtaining collisional cross sections for energies up to 3000 cm^{-1} . We have then determined rate coefficients for temperatures up to 350 K. The resulting values follows the same propensity rules seen in other similar systems (Bouhafs and Lique 2015; Ramachandran et al. 2018), i.e. overall decreasing with increasing ΔN , even ΔN favored over odd ΔN and larger values for F -conserving transitions.

Our theoretical results have been compared to a previous experimental study (Dagdigian, 1989). The discrepancy concerning the ΔN propensity rules can be explained with the impurity of the NH population of the experimental molecular beam, since we have been able to reproduce the results of the experiment through convolution of various cross sections, as discussed in Section 5.4.

We hope that our results will encourage new experimental studies concerning collisional excitation of $\text{NH}(^3\Sigma^-)$ by Ar. In particular it would be interesting to fill the gap of missing data regarding Ar as a collisional partner, with respect to systems involving He or Ne, more widely studied. Furthermore, a complete overview of these systems could also encourage studies with

Tabelle 5.4: Comparison between experimental and convolved theoretical cross sections at a collisional energy of 410 cm^{-1} and for transitions out of the $N = 0, F_1$ rotational level. All the values are normalized with respect to the cross section of the $N = 0, F_1 \rightarrow N' = 1, F_1$ transition. Experimental error in parenthesis are in units of the last quoted digit. The convolution of the theoretical values is described in Section 5.4. As a comparison, we also included the relative values obtained without the elastic contributions in the $N = 0, F_1 \rightarrow N' = 1, F_1$ and $N = 0, F_1 \rightarrow N' = 1, F_2$ cross sections.

N'	F_1				F_2				F_3		
	Exp ¹	Theory ²	Theory ³	Exp ¹	Theory ²	Theory ³	Exp ¹	Theory ²	Theory ³		
1	1.0	1.0	1.0	0.662(40)	0.576	0.842	0.255(54)	0.023	0.365		
2	0.407(54)	0.060	0.954	0.284(46)	0.041	0.654	0.154(20)	0.026	0.411		
3	0.068(15)	0.014	0.224	0.059(10)	0.010	0.172	0.047(08)	0.008	0.123		
4	0.023(05)	0.002	0.037	-	-	-	-	-	-		

¹ Dagdigian (1989).

² Our work. See text for details.

³ Our work. No contribution from the elastic cross sections included in the convolution. See text for details.

ortho- and para-H₂, highly important for astrophysical environments.

Kapitel 6

Conclusions

This thesis focus on three fields of laboratory astrochemistry, namely rotational spectroscopy of molecules in the gas phase, vibrational spectroscopy of molecules in the solid phase and scattering calculations for the collisional excitation of rotational levels. In particular the works presented in the thesis are divided and distributed within 3 main chapters, as follows:

Chapter 3: Since a better understanding of sulphur chemistry is needed to solve the interstellar sulphur depletion problem, new S-bearing molecules must be studied in the laboratory to provide accurate rest frequencies for an astronomical search. Dithioformic acid, HCSSH, being the sulphur analogue of formic acid and being chemically related to CS₂ seemed to be a good candidate for new studies. This chapter presents the spectroscopic results of HCSSH obtained in the laboratory by means of an absorption spectrometer employing the frequency-modulation technique. The molecule, which presented two spectra as a consequence of the two stable isomers, was produced within a cell by high voltage discharge of a gas mixture. Lines belonging to the electronic ground state up to 478 GHz were measured, with a total number of 204 and 139 new rotational transitions, respectively, for *trans* and *cis* isomers. The final dataset also includes lines in the centimetre range available from literature. The measurements were extended in the mm and submm range, leading to an accurate set of rotational and centrifugal distortion constants, with estimated uncertainties on the computed frequencies as low as 5 kHz at 1 mm wavelength, hence perfectly suitable for astronomical search.

The second part of the chapter focuses on the study of solid-phase production of HCSSH. Dithioformic acid, in fact, should mostly form onto solid phase, hence data were required on its possible formation on ice analogues under energetic processes. Employing an infrared spectrometer and an ion bombardement system, it was possible to observe formation of HCSSH within a large range of radiation doses. However, the HCSSH formed was at least 10 times lower than other newly formed S-bearing molecules and could not account for the missing so-called sulphur-residue.

Chapter 4: Complex Organic Molecules (COM) have been a hot topic within the last decades, being strongly related to prebiotic chemistry. In particular nitrogen-bearing COMs are a convenient starting point for synthesis of amino-acids. This chapter focuses on proaprgyl imine, HCCCHNH, studied employing the absorption cell described in chapter 2. The molecule showed two different spectra due to the presence of two energetically separated isomers. In addition, the

nitrogen atom was responsible of the so-called hyperfine splitting, visible and measurable only for almost a third of the transitions. With more than 500 lines recorded per isomer, well in the sub-mm domain, a new set of spectroscopic parameters have been provided for future astronomical search of the compound.

Chapter 5: Collisional excitation of light hydrides is important to fully understand the complex chemical and physical processes of atmospheric and astrophysical environments. This last chapter focuses on the $\text{NH}(\text{X}^3\Sigma^-)\text{-Ar}$ van der Waals system: first by calculation of a new three-dimensional Potential Energy Surface (PES), which explicitly includes the NH bond vibration and then by studying the collisional excitation of $\text{NH}(\text{X}^3\Sigma^-)\text{-Ar}$ at the close-coupling level, employing the new PES. Collisional excitation cross sections of the fine-structure levels of NH by Ar have been calculated for energies up to 3000 cm^{-1} , obtaining then the rate coefficients for temperatures up to 350 K after thermal average. This study was part of a joint work to benchmark a newly developed method.

The future perspective comprise search and hopefully detection in the ISM of the species presented in chapters 3 and 4 and their consequent inclusion in the future chemical models. In addition, further studies on their solid-phase formation would be helpful to understand their chemical paths and better link them to the overall chemical evolution of a given source. On the other hand, the newly tested method for scattering studies can be now employed for complex systems including molecular hydrogen, being proven to be reliable for computationally expensive studies, such as those involving fine and hyperfine splitting of the rotational levels.

Anhang A

HCSSH: theoretical calculations

Dithioformic acid has been the subject of numerous ab initio calculations in the past in which structures and conformational behaviour, isomerization, unimolecular rearrangement and decomposition reaction paths have been studied (Nguyen et al. 1999 and references therein). Apart from Nguyen et al. (1999), who made use of QCISD(T) methods (Pople et al., 1987), the older studies had been carried out at the HF-SCF (Hehre, 1986) or MP2 (Møller and Plesset 1934a, Pople et al. 1976, Krishnan and Pople 1978) levels, also making use of small basis sets and thus leading to less accurate results. In our work, high level quantum-chemical calculations were performed, focussing on an accurate estimation of dipole moments and equilibrium structures.

Geometry optimization was carried out via the CCSD(T) method (Purvis III and Bartlett 1982, Raghavachari et al. 1989, Hampel et al. 1992, Deegan and Knowles 1994). Employing the frozen-core approximation, we used the correlation consistent valence basis sets cc-pVnZ ($n=T, Q, 5$) (Dunning Jr, 1989b) for the hydrogen and carbon atoms and the d -augmented basis sets cc-pV(n+d)Z (Dunning Jr et al., 2001) for the sulphur atoms. We also provide an estimate of the equilibrium energies based on a hierarchical sequence of basis sets, using the complete basis set (CBS) limit extrapolation, as described in Heckert et al. (2006). The molecules have been considered as planar because of the assumption based on the inertial defect (see Chapter 3). The total energies have been obtained as a sum of the Hartree-Fock self-consistent field (HF-SCF) energy, the electron-correlation contribution at the CCSD(T) level, and the core-valence (CV) correlation effect. CBS limit extrapolation has been applied for the first two values as follows:

$$E_{tot} = E_{\infty}^{HF-SCF} + \Delta E_{\infty}^{CCSD(T)} + \Delta E_{CV}. \quad (\text{A.1})$$

The convergence of the Hartree-Fock CBS limit has been evaluated with (Feller 1992, Feller 1993)

$$E^{HF-SCF}(n) = E_{\infty}^{HF-SCF} + Ae^{-Bn}, \quad (\text{A.2})$$

while the function used to extrapolate the value of electron-correlation energy to the CBS limit is (Helgaker et al., 1997) written as

$$\Delta E^{CCSD(T)}(n) = \Delta E_{\infty}^{CCSD(T)} + Cn^{-3}. \quad (\text{A.3})$$

The core-valence correction has been calculated and added as follows:

$$\Delta E_{CV} = E_{ae} - E_{fc}, \quad (\text{A.4})$$

where both the all electron (E_{ae}) and the frozen-core (E_{fc}) energies have been calculated using the cc-pwCVQZ basis set (Peterson and Dunning Jr, 2002), avoiding correlation of 1s electrons of sulphur in any computation. All the calculations have been performed with the CFOUR program package (www.cfour.de).

Tabelle A.1: Equilibrium geometries and energies of *trans*-HCSSH and *cis*-HCSSH are reported. All the values were computed at the CCSD(T) level of theory.

Basis set	Energy (Hartree)	C=S (Å)	C-S (Å)	S-H (Å)	C-H (Å)	$\angle^1\text{S}=\text{C}-\text{S}$ (°)	$\angle \text{C}-\text{S}-\text{H}$ (°)	$\angle \text{H}-\text{C}=\text{S}$ (°)
<i>trans</i> -HCSSH								
cc-pVTZ	-834.692586	1.6259	1.7412	1.3418	1.0896	128.27	95.49	110.23
cc-pVQZ	-834.739631	1.6223	1.7352	1.3421	1.0891	128.09	95.61	110.43
cc-pV5Z	-834.754180	1.6212	1.7332	1.3420	1.0891	128.04	95.64	110.50
CBS ²	-834.767911	1.6201	1.7314	1.3420	1.0891	127.98	95.66	110.54
cc-pwCVQZ(fc)	-834.743529	1.6214	1.7341	1.3415	1.0891	128.09	95.61	110.44
cc-pwCVQZ(ae)	-835.433398	1.6173	1.7297	1.3394	1.0877	128.11	95.61	110.44
CBS+CV ³	-835.457780	1.6161	1.7270	1.3398	1.0877	127.99	95.66	110.54
<i>cis</i> -HCSSH								
cc-pVTZ	-834.690500	1.6247	1.7454	1.3412	1.0881	123.75	96.59	114.16
cc-pVQZ	-834.737690	1.6211	1.7391	1.3413	1.0877	123.58	96.79	114.33
cc-pV5Z	-834.752258	1.6200	1.7370	1.3412	1.0877	123.52	96.83	114.39
CBS ²	-834.765988	1.6189	1.7352	1.3411	1.0877	123.46	96.86	114.45
cc-pwCVQZ(fc)	-834.741583	1.6202	1.7380	1.3407	1.0877	123.56	96.80	114.34
cc-pwCVQZ(ae)	-835.431447	1.6161	1.7336	1.3385	1.0862	123.55	96.82	114.37
CBS+CV ³	-835.455852	1.6149	1.7309	1.3389	1.0862	123.45	96.88	114.48

¹ Bond angle in degree.

² CBS extrapolation using the additivity assumption shown in (A.1) without core-valence correction, ΔE_{CV} .

³ Final best estimated values, calculated using the complete additivity assumption shown in (A.1).

The results show that the *trans* conformer is the most stable and has a difference in energy of 421 cm⁻¹ with respect to the *cis*-HCSSH. This value is in reasonable agreement with the experimental value given by Bak et al. (1978), which differs only by 71 cm⁻¹. Molecular structures were obtained with the same method shown above. All the results are listed in Table A.1.

Dipole moments were also calculated and extrapolated to the CBS limit with a similar procedure (Halkier et al., 1999). For these dipole calculations, we used similar basis sets, but augmented with diffuse functions to ensure correct evaluation of this property: that is, the light atoms used the aug-cc-pVnZ basis sets (Kendall et al., 1992) and the sulphur atoms used the aug-cc-pV(n+d)Z basis sets (Dunning Jr et al., 2001). The computations were carried out using the CBS + CV equilibrium geometries, i.e. the best estimated structure obtained with the additivity assumption from (A.1). The final values are shown in Table A.2. Owing to its higher computational cost, the barrier energy to *trans* – *cis* conversion was computed at the CCSD(T)/cc-pVTZ level, with the frozen-core approximation, giving a value of 3762 cm⁻¹.

Tabelle A.2: Dipole moments of *trans*-HCSSH and *cis*-HCSSH. All the values were computed at the CCSD(T) level of theory.

Basis set	μ_a (Debye)	μ_b (Debye)
<i>trans</i> -HCSSH		
aug-cc-pVTZ	1.4788	0.1950
aug-cc-pVQZ	1.4870	0.1957
aug-cc-pV5Z	1.4807	0.1939
CBS ¹	1.4800	0.1935
aug-cc-pCVQZ(fc)	1.4863	0.1945
aug-cc-pCVQZ(ae)	1.4822	0.1934
CBS+CV ²	1.4766	0.1924
<i>cis</i> -HCSSH		
aug-cc-pVTZ	2.0756	1.6323
aug-cc-pVQZ	2.0896	1.6474
aug-cc-pV5Z	2.0878	1.6448
CBS ¹	2.0861	1.6428
aug-cc-pwCVQZ(fc)	2.0883	1.6489
aug-cc-pwCVQZ(ae)	2.0834	1.6464
CBS+CV ²	2.0829	1.6403

¹ CBS extrapolation using the additivity assumption shown in (A.1) without core-valence correction, ΔE_{CV} .

² Final best estimated values, calculated using the complete additivity assumption shown in (A.1).

Anhang B

HCCCHNH: theoretical calculations

Coupled-cluster (CC) level of theory, with single and double excitations augmented by a perturbative treatment for estimating the effects of triple excitations, i.e. CCSD(T) (Raghavachari et al., 1989), is considered the “gold standard” for obtaining very accurate predictions of molecular structures and spectroscopic parameters (see for example Ramabhadran and Raghavachari, 2013; Puzzarini et al., 2014). Basis-set and wave function truncation biases can be efficiently minimised by adopting composite schemes; these approaches, relying on the additivity approximations, combine the different contributions to provide the best theoretical estimate. In the present investigation, given the size of the molecular system, for determining the equilibrium structures the approach based on the additivity of most relevant terms at the energy-gradient level (Heckert et al., 2006) was employed instead than applying it directly to the geometrical parameters (Charmet et al., 2010; Gambi et al., 2019). Extrapolation to the complete basis set (CBS) limit was performed for both the Hartree–Fock self-consistent-field (HF-SCF) and the valence correlation (evaluated at the frozen-core (fc) CCSD(T) level of theory) terms, using the formulas of Halkier et al. (1999) for the former and the two-parameter correction of Helgaker et al. (1997) for the latter.

At HF-SCF level of theory the correlation consistent polarised basis sets cc-pV_nZ ($n = T, Q, 5$) Dunning Jr (1989b); Woon and Dunning Jr (1995) were used, while the fc-CCSD(T) calculations were carried out by using the cc-pVTZ and cc-pVQZ basis sets. For computing the contribution related to the core-valence (CV) electron correlation, the difference between the all-electron (ae) and frozen-core results using the cc-pCVTZ basis set (Woon and Dunning Jr, 1995) was used, while the contribution due to the diffuse functions was calculated by employing the aug-cc-pVTZ basis set (Kendall et al., 1992). All these terms were evaluated at CCSD(T) level of theory. In this way for the two conformers their overall best-estimate geometries, shortly labelled in the following as CCSD(T)/CBS+CV, were obtained. The energies of these two structures were computed with the same approach but using the cc-pV_nZ ($n = Q, 5, 6$) basis sets. Employing a similar composite approach (see, for example Barone et al. 2015; Pietropolli Charmet et al. 2017) the best-estimate values of the quadratic force fields were derived.

The vibrational corrections to equilibrium rotational constants were calculated at fc-MP2 level of theory (Møller and Plesset, 1934b) and using the aug-cc-pVTZ basis set. The cubic force field data needed for determining the sextic centrifugal distortion constants were obtained at

CCSD(T) level on the basis of its good accuracy reported in the literature (Charmet et al., 2017). Nuclear quadrupole coupling constants for the nitrogen atoms were computed at ae-CCSD(T) level of theory in conjunction with the pw-CV5Z basis set (Dunning Jr, 1989b; Peterson and Dunning Jr, 2002) following the same procedure described previously (Cazzoli et al., 2010; Pietropolli Charmet et al., 2016).

All the calculations carried out at CCSD(T) and MP2 level of theory were performed by using the CFOUR¹ suite of programs and its implementation of analytic second derivatives (Gauss and Stanton, 1997), while the sextic centrifugal distortion constants were computed using an appropriate suite of programs(Charmet and Cornaton, 2018) and the formulas reported in the literature (Aliev and Watson, 1976; Watson, 1977b; Camy-Peyret and Flaud, 1985).

¹CFOUR, Coupled-Cluster techniques for Computational Chemistry, a quantum-chemical program package written by J.F. Stanton, J. Gauss, L. Cheng, M.E. Harding, D.A. Matthews, P.G. Szalay et al., and the integral packages MOLECULE (J. Almlöf and P.R. Taylor), PROPS (P.R. Taylor), ABACUS (T. Helgaker, H.J. Aa. Jensen, P. Jørgensen, and J. Olsen), and ECP routines by A. V. Mitin and C. van Wüllen. For the current version, see <http://www.cfour.de>.

Literaturverzeichnis

- Alexander, Millard H and Paul J Dagdigian (1983), “Propensity rules in rotationally inelastic collisions of diatomic molecules in 3σ electronic states.” *J. Chem. Phys.*, 79, 302–310.
- Alexander, Millard H, Paul J Dagdigian, and Didier Lemoine (1991), “Quantum scattering studies of inelastic collisions of nh (a 3π) with helium: Fine-structure and λ -doublet propensities.” *J. Chem. Phys.*, 95, 5036–5046.
- Aliev, MR and James KG Watson (1976), “Calculated sextic centrifugal distortion constants of polyatomic molecules.” *Journal of Molecular Spectroscopy*, 61, 29–52.
- Altwegg, Kathrin, Hans Balsiger, Akiva Bar-Nun, Jean-Jacques Berthelier, Andre Bieler, Peter Bochsler, Christelle Briois, Ursina Calmonte, Michael R Combi, Hervé Cottin, et al. (2016), “Prebiotic chemicals—amino acid and phosphorus—in the coma of comet 67p/churyumov-gerasimenko.” *Science advances*, 2, e1600285.
- Aponte, Jose C, Jamie E Elsila, Daniel P Glavin, Stefanie N Milam, Steven B Charnley, and Jason P Dworkin (2017), “Pathways to meteoritic glycine and methylamine.” *ACS Earth and Space Chemistry*, 1, 3–13.
- Asplund, Martin, Nicolas Grevesse, A Jacques Sauval, and Pat Scott (2009), “The chemical composition of the sun.” *Annual Review of Astronomy and Astrophysics*, 47, 481–522.
- Bak, B., O. Nielsen, H. Svanholt, and J. J. Christiansen (1979), “Rotational spectra of isotopic dithioformic acids with a structure of trans HCSSH . Ab initio estimates of cis/trans structures, energies, dipole moments, and torsional barrier.” *J. Mol. Spectr.*, 75, 134–143.
- Bak, B., O. J. Nielsen, and H. Svanholt (1978), “Production and microwave spectra of dithioformic acid, HCSSH.” *J. Mol. Spectr.*, 69, 401–408.
- Barone, Vincenzo, Małgorzata Biczysko, and Cristina Puzzarini (2015), “Quantum chemistry meets spectroscopy for astrochemistry: Increasing complexity toward prebiotic molecules.” *Accounts of chemical research*, 48, 1413–1422.
- Birnbaum, George (1967), “Microwave pressure broadening and its application to intermolecular forces.” *Advances in Chemical Physics: Intermolecular Forces*, 487–548.

Bizzocchi, Luca, Filippo Tamassia, Jacob Laas, Barbara M Giuliano, Claudio Degli Esposti, Luca Dore, Mattia Melosso, Elisabetta Canè, Andrea Pietropolli Charmet, Holger SP Müller, et al. (2017), “Rotational and high-resolution infrared spectrum of hc _3 n: global ro-vibrational analysis and improved line catalogue for astrophysical observations.” *arXiv preprint arXiv:1711.08592*.

Bohn, Robert B, G Dana Brabson, and Lester Andrews (1992), “Reaction of atomic hydrogen and carbon disulfide: infrared spectra of hscs and hshcs in solid argon.” *The Journal of Physical Chemistry*, 96, 1582–1589.

Bolatto, Alberto D, Mark Wolfire, and Adam K Leroy (2013), “The co-to-h₂ conversion factor.” *Annual Review of Astronomy and Astrophysics*, 51, 207–268.

Born, Max and Robert Oppenheimer (1927), “Zur quantentheorie der molekeln.” *Annalen der physik*, 389, 457–484.

Bouhafs, Nezha and François Lique (2015), “Collisional excitation of nh (x3σ-) by ne: Potential energy surface, scattering calculations, and comparison with experiments.” *J. Chem. Phys.*, 143, 184311.

Boys, S F_ and Fiorenza de Bernardi (1970), “The calculation of small molecular interactions by the differences of separate total energies. some procedures with reduced errors.” *Mol. Phys.*, 19, 553–566.

Burton, Aaron S, Jennifer C Stern, Jamie E Elsila, Daniel P Glavin, and Jason P Dworkin (2012), “Understanding prebiotic chemistry through the analysis of extraterrestrial amino acids and nucleobases in meteorites.” *Chemical Society Reviews*, 41, 5459–5472.

Calmonte, Ursina, Kathrin Altwegg, Hans Balsiger, Jean-Jacques Berthelier, André Bieler, G Cessateur, F Dhooghe, EF Van Dishoeck, B Fiethe, SA Fuselier, et al. (2016), “Sulphur-bearing species in the coma of comet 67p/churyumov–gerasimenko.” *MNRAS*, 462, S253–S273.

Camy-Peyret, C and JM Flaud (1985), “Molecular spectroscopy: Modern research.” *Vol. III/Ed. K. Narahari Rao. Orlando*, 69.

Cazzoli, Gabriele, Lino Cludi, Cristina Puzzarini, Paolo Stoppa, Andrea Pietropolli Charmet, Nicola Tasinato, Agostino Baldacci, Alessandro Baldan, Santi Giorgianni, René Wugt Larsen, et al. (2010), “Microwave, high-resolution infrared, and quantum chemical investigations of chbrf2: Ground and v4= 1 states.” *The Journal of Physical Chemistry A*, 115, 453–459.

Charmet, Andrea Pietropolli and Yann Cornaton (2018), “Benchmarking fully analytic dft force fields for vibrational spectroscopy: A study on halogenated compounds.” *Journal of Molecular Structure*, 1160, 455–462.

Charmet, Andrea Pietropolli, Paolo Stoppa, Nicola Tasinato, Alessandro Baldan, Santi Giorgiani, and Alberto Gambi (2010), “Spectroscopic study of chbrf 2 up to 9500 cm⁻¹: Vibrational analysis, integrated band intensities, and ab initio calculations.” *The Journal of chemical physics*, 133, 044310.

Charmet, Andrea Pietropolli, Paolo Stoppa, Nicola Tasinato, and Santi Giorgiani (2017), “Computing sextic centrifugal distortion constants by dft: A benchmark analysis on halogenated compounds.” *Journal of Molecular Spectroscopy*, 335, 117–125.

Christoffel, Kurt M and Joel M Bowman (1983), “Complex coordinate calculations of feshbach resonance energies and widths for a collinear triatomic system.” *J. Chem. Phys*, 78, 3952–3958.

Cobb, Alyssa K and Ralph E Pudritz (2014), “Nature’s starships. i. observed abundances and relative frequencies of amino acids in meteorites.” *The Astrophysical Journal*, 783, 140.

Colbert, Daniel T and William H Miller (1992), “A novel discrete variable representation for quantum mechanical reactive scattering via the s-matrix kohn method.” *J. Chem. Phys*, 96, 1982–1991.

Cybulski, H, RV Krems, HR Sadeghpour, A Dalgarno, J Kłos, GC Groenenboom, A van der Avoird, D Zgid, and G Chałasiński (2005), “Interaction of nh (x σ- 3) with he: Potential energy surface, bound states, and collisional zeeman relaxation.” *J. Chem. Phys*, 122, 094307.

Cybulski, Si/awomir M, Rudolf Burcl, Grzegorz Chal/asiński, and MM Szczęśniak (1995), “Partitioning of interaction energy in van der waals complexes involving excited state species: The he (1 s)+ cl2 (b 3π u) interaction.” *J. Chem. Phys*, 103, 10116–10127.

Cybulski, SM (1989), “Trurl 94 package, rochester, mi, 1994. 32 g. chal” asinski, sm cybulski, mm szczesniak, and s. scheiner.” *J. Chem. Phys*, 91, 7048.

Dagdigian, Paul J (1989), “Scaling relations in the rotational excitation of nh (x 3-) n= 0 by argon.” *J. Chem. Phys*, 90, 6110–6115.

Dalgarno, Alexander (2008), “A serendipitous journey.” *Annu. Rev. Astron. Astrophys.*, 46, 1–20.

Danger, G, Fabien Borget, M Chomat, F Duvernay, P Theulé, J-C Guillemin, L Le Sergeant d’Hendecourt, and T Chiavassa (2011), “Experimental investigation of aminoacetonitrile formation through the strecker synthesis in astrophysical-like conditions: reactivity of methanimine (ch2nh), ammonia (nh3), and hydrogen cyanide (hcn).” *Astronomy & Astrophysics*, 535, A47.

Darling, Byron T and David M Dennison (1940), “The water vapor molecule.” *Phys. Rev.*, 57, 128.

Davis, R Wellington, AG Robiette, MCL Gerry, E Bjarnov, and G Winnewisser (1980), “Microwave spectra and centrifugal distortion constants of formic acid containing 13c and 18o: Refinement of the harmonic force field and the molecular structure.” *J. Mol. Spectr.*, 81, 93–109.

Deegan, Miles JO and Peter J Knowles (1994), “Perturbative corrections to account for triple excitations in closed and open shell coupled cluster theories.” *Chem. Phys. Lett.*, 227, 321–326.

Dickens, JE, William M Irvine, CH DeVries, and Masatoshi Ohishi (1997), “Hydrogenation of interstellar molecules: A survey for methylenimine (ch2nh).” *The Astrophysical Journal*, 479, 307.

Dore, Luca (2003), “Using fast fourier transform to compute the line shape of frequency-modulated spectral profiles.” *J. Mol. Spectr.*, 221, 93–98.

Douglas, AE and G Herzberg (1941), “Note on ch⁺ in interstellar space and in the laboratory.” *The Astrophysical Journal*, 94, 381.

Druard, C. and V. Wakelam (2012), “Polysulphanes on interstellar grains as a possible reservoir of interstellar sulphur.” *MNRAS*, 426, 354–359.

Dumouchel, Fabien, Jacek Kłos, Robert Toboła, Aurore Bacmann, Sébastien Maret, Pierre Hily-Blant, Alexandre Faure, and François Lique (2012), “Fine and hyperfine excitation of nh and nd by he: On the importance of calculating rate coefficients of isotopologues.” *J. Chem. Phys.*, 137, 114306.

Dunning Jr, Thom H (1989a), “Gaussian basis sets for use in correlated molecular calculations. i. the atoms boron through neon and hydrogen.” *J. Chem. Phys.*, 90, 1007–1023.

Dunning Jr, Thom H (1989b), “Gaussian basis sets for use in correlated molecular calculations. i. the atoms boron through neon and hydrogen.” *J. Chem. Phys.*, 90, 1007–1023.

Dunning Jr, Thom H, Kirk A Peterson, and Angela K Wilson (2001), “Gaussian basis sets for use in correlated molecular calculations. x. the atoms aluminum through argon revisited.” *J. Chem. Phys.*, 114, 9244–9253.

Egorov, D, WC Campbell, Bretislav Friedrich, SE Maxwell, E Tsikata, LD Van Buuren, and JM Doyle (2004), “Buffer-gas cooling of nh via the beam loaded buffer-gas method.” *Eur. Phys. J. D*, 31, 307–311.

Elsila, Jamie E, Daniel P Glavin, and Jason P Dworkin (2009), “Cometary glycine detected in samples returned by stardust.” *Meteoritics & Planetary Science*, 44, 1323–1330.

Endres, Christian P, Stephan Schlemmer, Peter Schilke, Jürgen Stutzki, and Holger SP Müller (2016), “The cologne database for molecular spectroscopy, cdms, in the virtual atomic and molecular data centre, vamdc.” *Journal of Molecular Spectroscopy*, 327, 95–104.

- Feller, David (1992), “Application of systematic sequences of wave functions to the water dimer.” *J. Chem. Phys.*, 96, 6104–6114.
- Feller, David (1993), “The use of systematic sequences of wave functions for estimating the complete basis set, full configuration interaction limit in water.” *J. Chem. Phys.*, 98, 7059–7071.
- Ferrante, R. F., M. H. Moore, M. M. Spiliotis, and R. L. Hudson (2008), “Formation of Interstellar OCS: Radiation Chemistry and IR Spectra of Precursor Ices.” *ApJ*, 684, 1210–1220.
- Flower, David (2007), *Molecular collisions in the interstellar medium*, volume 42. Cambridge University Press.
- Friedrich, Bretislav and John M Doyle (2009), “Why are cold molecules so hot?” *ChemPhysChem*, 10, 604–623.
- Gambi, Alberto, Andrea Pietropolli Charmet, Paolo Stoppa, Nicola Tasinato, Giorgia Ceselin, and Vincenzo Barone (2019), “Molecular synthons for accurate structural determinations: the equilibrium geometry of 1-chloro-1-fluoroethene.” *Physical Chemistry Chemical Physics*, 21, 3615–3625.
- Gardner, FF and G Winnewisser (1975), “The detection of interstellar vinyl cyanide/acrylonitrile.” *The Astrophysical Journal*, 195, L127–L130.
- Garozzo, M., D. Fulvio, Z. Kanuchova, M. E. Palumbo, and G. Strazzulla (2010), “The fate of S-bearing species after ion irradiation of interstellar icy grain mantles.” *A&A*, 509, A67.
- Gauss, Jürgen and John F Stanton (1997), “Analytic ccSD (t) second derivatives.” *Chemical physics letters*, 276, 70–77.
- Godfrey, PD, RD Brown, BJ Robinson, and MW Sinclair (1973), “Discovery of interstellar methanimine (formaldimine).” *Astrophysical Letters*, 13, 119.
- Gordy, Walter (1948), “Microwave spectroscopy.” *Reviews of Modern Physics*, 20, 668.
- Gordy, Walter and Robert L Cook (1984), *Microwave molecular spectra*. Wiley.
- Halkier, Asger, Wim Klopper, Trygve Helgaker, and Poul Joergensen (1999), “Basis-set convergence of the molecular electric dipole moment.” *J. Chem. Phys.*, 111, 4424–4430.
- Hamada, Yoshiaki, Masamichi Tsuboi, Harutoshi Takeo, and Chi Matsumura (1984), “Pyrolysis of amines: Infrared spectrum of propargylimine.” *Journal of Molecular Spectroscopy*, 106, 175–185.
- Hampel, C., K. A. Peterson, and H.-J. Werner (1992), “A comparison of the efficiency and accuracy of the quadratic configuration interaction (qcisd), coupled cluster (ccsd), and brueckner coupled cluster (bccd) methods.” *Chem. Phys. Lett.*, 190, 1–12.

- Hampel, Claudia, Kirk A Peterson, and Hans-Joachim Werner (1992), “A comparison of the efficiency and accuracy of the quadratic configuration interaction (qcisd), coupled cluster (ccsd), and brueckner coupled cluster (bccd) methods.” *Chem. Phys. Lett.*, 190, 1–12.
- Hasegawa, T. I., E. Herbst, and C. M. Leung (1992), “Models of gas-grain chemistry in dense interstellar clouds with complex organic molecules.” *ApJS*, 82, 167–195.
- Heckert, Miriam, Mihály Kállay, David P Tew, Wim Klopper, and Jürgen Gauss (2006), “Basis-set extrapolation techniques for the accurate calculation of molecular equilibrium geometries using coupled-cluster theory.” *J. Chem. Phys.*, 125, 044108.
- Hehre, Warren J. (1986), *Ab initio molecular orbital theory*. Wiley-Interscience.
- Heisenberg, W (1927), “Über den anschaulichen inhalt der quantentheoretischen kinematik und mechanik.” *Z. Phys.*, 43, 172–198.
- Helgaker, Trygve, Wim Klopper, Henrik Koch, and Jozef Noga (1997), “Basis-set convergence of correlated calculations on water.” *J. Chem. Phys.*, 106, 9639–9646.
- Herbst, Eric and Ewine F Van Dishoeck (2009), “Complex organic interstellar molecules.” *Annual Review of Astronomy and Astrophysics*, 47, 427–480.
- Hutson, J. M. (1993). BOUND computer code, version 5 (1993), distributed by Collaborative Computational Project No. 6 of the Science and Engineering Research Council (UK).
- Hutson, J. M. and S. Green (1994). MOLSCAT computer code, version 14 (1994), distributed by Collaborative Computational Project No. 6 of the Engineering and Physical Sciences Research Council (UK).
- Irvine, W. M., P. Friberg, N. Kaifu, H. E. Matthews, Y. C. Minh, M. Ohishi, and S. Ishikawa (1990), “Detection of formic acid in the cold, dark cloud L134N.” *A&A*, 229, L9–L12.
- Jackson, W. M., A. Scodinu, D. Xu, and A. L. Cochran (2004), “Using the Ultraviolet and Visible spectrum of Comet 122P/de Vico to Identify the Parent Molecule CS₂.” *ApJ*, 607, L139–L141.
- Jefferts, K. B., A. A. Penzias, R. W. Wilson, and P. M. Solomon (1971), “Detection of interstellar carbonyl sulfide.” *ApJ*, 168, L111–L113.
- Jenkins, Edward B (1987), “Element abundances in the interstellar atomic material.” In *Interstellar Processes*, 533–559, Springer.
- Jiménez-Escobar, A. and G. M. Muñoz Caro (2011), “Sulfur depletion in dense clouds and circumstellar regions. I. H₂S ice abundance and UV-photochemical reactions in the H₂O-matrix.” *A&A*, 536, A91.
- Jiménez-Escobar, A., G. M. Muñoz Caro, and Y.-J. Chen (2014), “Sulphur depletion in dense clouds and circumstellar regions. Organic products made from UV photoprocessing of realistic ice analogs containing H₂S.” *MNRAS*, 443, 343–354.

- Kalugina, Yulia, François Lique, and Sarantos Marinakis (2014), “New ab initio potential energy surfaces for the ro-vibrational excitation of oh ($x 2 \pi$) by he.” *Phys. Chem. Chem. Phys.*, 16, 13500–13507.
- Kawaguchi, Kentarou, Shuro Takano, Masatoshi Ohishi, Shin-Ichi Ishikawa, Keisuke Miyazawa, Norio Kaifu, Koichi Yamashita, Satoshi Yamamoto, Shuji Saito, Yasuhiro Ohshima, et al. (1992), “Detection of hnccc in tmc-1.” *The Astrophysical Journal*, 396, L49–L51.
- Kendall, Rick A, Grzegorz Chałasiński, Jacek Kłos, Robert Bukowski, Mark W Severson, MM Szczęśniak, and Sławomir M Cybulski (1998), “Ab initio study of the van der waals interaction of nh ($x 3 \sigma$ -) with ar ($1 s$).” *J. Chem. Phys.*, 108, 3235–3242.
- Kendall, Rick A, Thom H Dunning Jr, and Robert J Harrison (1992), “Electron affinities of the first-row atoms revisited. systematic basis sets and wave functions.” *J. Chem. Phys.*, 96, 6796–6806.
- Kerenskaya, Galina, Udo Schnupf, Michael C Heaven, Ad van der Avoird, and Gerrit C Groenenboom (2005), “Experimental and theoretical investigation of the a 3π -x 3σ - transition of nh/d-ne.” *Phys. Chem. Chem. Phys.*, 7, 846–854.
- King, William C and Walter Gordy (1954), “One-to-two millimeter wave spectroscopy. iv. experimental methods and results for ocs, c h 3 f, and h 2 o.” *Physical Review*, 93, 407.
- Koch, Denise M, Celine Toubin, Gilles H Peslherbe, and James T Hynes (2008), “A theoretical study of the formation of the aminoacetonitrile precursor of glycine on icy grain mantles in the interstellar medium.” *The Journal of Physical Chemistry C*, 112, 2972–2980.
- Kolesniková, Lucie, B Tercero, J Cernicharo, JL Alonso, AM Daly, BP Gordon, and ST Shipman (2014), “Spectroscopic characterization and detection of ethyl mercaptan in orion.” *ApJ*, 784, L7.
- Krems, RV, HR Sadeghpour, A Dalgarno, D Zgid, J Kłos, and G Chałasiński (2003), “Low-temperature collisions of nh ($x 3 \sigma$ -) molecules with he atoms in a magnetic field: An ab initio study.” *Phys. Rev. A*, 68, 051401.
- Krim, Lahouari, Jean-Claude Guillemin, and David E Woon (2019), “Formation of methyl ketenimine ($\text{ch}_3\text{ch}=\text{c}=\text{nh}$) and ethylcyanide ($\text{ch}_3\text{ch}_2\text{c}\equiv\text{n}$) isomers through successive hydrogenations of acrylonitrile ($\text{ch}_2=\text{ch}-\text{c}\equiv\text{n}$) under interstellar conditions: The role of $\text{ch}_3\text{c}-\text{c}\equiv\text{n}$ radical in the activation of the cyano group chemistry.” *Monthly Notices of the Royal Astronomical Society*, 485, 5210–5220.
- Krishnan, R and John A Pople (1978), “Approximate fourth-order perturbation theory of the electron correlation energy.” *Int. J. Quantum Chem.*, 14, 91–100.
- Kroto, Harold W, Don McNaughton, and Osman I Osman (1984), “The detection of the new molecule prop-2-ynylideneamine, h-c [triple bond, length half m-dash] c-ch [double bond,

- length half m-dash] nh, by microwave spectroscopy.” *Journal of the Chemical Society, Chemical Communications*, 993–994.
- Laas, JC and P Caselli (2019), “Vizier online data catalog: Modeling interstellar sulfur depletion (laas+, 2019).” *VicieR Online Data Catalog*, 362.
- Landau, LD and EM Lifšits (1978), “Fisica teorica, vol. iv.” *Teoria quantistica relativistica*, 148.
- Lewen, Frank, Sandra Brünken, Gisbert Winnewisser, Marie Šimečková, and Štěpán Urban (2004), “Doppler-limited rotational spectrum of the nh radical in the 2 thz region.” *Journal of Molecular Spectroscopy*, 226, 113–122.
- Linke, R. A., M. A. Frerking, and P. Thaddeus (1979), “Interstellar methyl mercaptan.” *ApJ*, 234, L139–L142.
- Lique, F, A Spielfiedel, M-L Dubernet, and N Feautrier (2005), “Rotational excitation of sulfur monoxide by collisions with helium at low temperature.” *J. Chem. Phys*, 123, 134316.
- Lique, François (2010), “Temperature dependence of the fine-structure resolved rate coefficients for collisions of o 2 (x σ 3 g-) with he.” *J. Chem. Phys*, 132, 044311.
- Lique, François (2015), “Communication: Rotational excitation of hcl by h: Rigid rotor vs. reactive approaches.”
- Loomis, Ryan A, Daniel P Zaleski, Amanda L Steber, Justin L Neill, Matthew T Muckle, Brent J Harris, Jan M Hollis, Philip R Jewell, Valerio Lattanzi, Frank J Lovas, et al. (2013), “The detection of interstellar ethanimine (ch3chnh) from observations taken during the gbt primos survey.” *The Astrophysical Journal Letters*, 765, L9.
- Lovas, Francis J, JM Hollis, Anthony J Remijan, and PR Jewell (2006), “Detection of ketenimine (ch2cnh) in sagittarius b2 (n) hot cores.” *The Astrophysical Journal Letters*, 645, L137.
- McGuire, Brett A, Ryan A Loomis, Cameron M Charness, Joanna F Corby, Geoffrey A Blake, Jan M Hollis, Frank J Lovas, Philip R Jewell, and Anthony J Remijan (2012), “Interstellar carbodiimide (hncnh): A new astronomical detection from the gbt primos survey via maser emission features.” *The Astrophysical Journal Letters*, 758, L33.
- McKellar, Andrew (1940), “Evidence for the molecular origin of some hitherto unidentified interstellar lines.” *Publications of the Astronomical Society of the Pacific*, 52, 187–192.
- McNaughton, D, OI Osman, and HW Kroto (1988), “The microwave spectrum and structure of z-prop-2-ynylideneamine, hc c ch nh.” *Journal of Molecular Structure*, 190, 195–204.
- Møller, Chr and Milton S Plesset (1934a), “Note on an approximation treatment for many-electron systems.” *Phys. Rev.*, 46, 618.
- Møller, Chr and Milton S Plesset (1934b), “Note on an approximation treatment for many-electron systems.” *Physical review*, 46, 618.

- Nguyen, Minh Tho, Thanh Lam Nguyen, and Hung Thanh Le (1999), “Theoretical study of dithioformic acid, dithiohydroxy carbene and their radical cations: unimolecular and assisted rearrangements.” *J. Phys. Chem. A*, 103, 5758–5765.
- Oppenheimer, M. and A. Dalgarno (1974), “The Chemistry of Sulfur in Interstellar Clouds.” *ApJ*, 187, 231–236.
- Orlikowski, Tadeusz (1985), “Theoretical studies of rotationally inelastic collisions of molecules in 3σ electronic states: O₂ (x 3σ g-) + he.” *Mol. Phys.*, 56, 35–46.
- Osman, Osman I., Donald McNaughton, Roger J. Suffolk, John D. Watts, and Harold W. Kroto (1987), “Photoelectron, infrared, and theoretical study of the thermolysis of 4-azahepta-1, 6-diyne: spectra of prop-2-ynylideneamine, h–c [triple bond, length half m-dash] c–ch [double bond, length half m-dash] nh, and penta-3, 4-diene-1-yne, ch 2 [double bond, length half m-dash] c [double bond, length half m-dash] chc [triple bond, length half m-dash] ch.” *Journal of the Chemical Society, Perkin Transactions 2*, 683–688.
- Papousek, Dusan and Mamed Ragimovich Aliev (1982), “Molecular vibrational-rotational spectra.”
- Penzias, A. A., P. M. Solomon, R. W. Wilson, and K. B. Jefferts (1971), “Interstellar Carbon Monosulfide.” *ApJ*, 168, L53.
- Persic, Massimo and Paolo Salucci (1992), “The baryon content of the universe.” *Monthly Notices of the Royal Astronomical Society*, 258, 14P–18P.
- Peterson, Kirk A and Thom H Dunning Jr (2002), “Accurate correlation consistent basis sets for molecular core–valence correlation effects: The second row atoms al–ar, and the first row atoms b–ne revisited.” *J. Chem. Phys.*, 117, 10548–10560.
- Peterson, Kirk A, David E Woon, and Thom H Dunning Jr (1994), “Benchmark calculations with correlated molecular wave functions. iv. the classical barrier height of the h+ h₂ h₂+ h reaction.” *J. Chem. Phys.*, 100, 7410–7415.
- Pickett, H. M. (1991), “The fitting and prediction of vibration-rotation spectra with spin interactions.” *J. Mol. Spectr.*, 148, 371–377.
- Piel, Alexander (2017), *Plasma physics: an introduction to laboratory, space, and fusion plasmas*. Springer.
- Pietropolli Charmet, Andrea, Paolo Stoppa, Santi Giorgianni, Julien Bloino, Nicola Tasinato, Ivan Carnimeo, Małgorzata Biczysko, and Cristina Puzzarini (2017), “Accurate vibrational–rotational parameters and infrared intensities of 1-bromo-1-fluoroethene: a joint experimental analysis and ab initio study.” *The Journal of Physical Chemistry A*, 121, 3305–3317.

- Pietropolli Charmet, Andrea, Paolo Stoppa, Nicola Tasinato, Santi Giorgianni, and Alberto Gambi (2016), “Study of the vibrational spectra and absorption cross sections of 1-chloro-1-fluoroethene by a joint experimental and ab initio approach.” *The Journal of Physical Chemistry A*, 120, 8369–8386.
- Planck, Planck Collaboration et al. (2013), “results. xvi. cosmological parameters.” *Preprint at http://arxiv.org/abs/1303.5076*.
- Pople, John A, J Stephen Binkley, and Rolf Seeger (1976), “Theoretical models incorporating electron correlation.” *Int. J. Quantum Chem.*, 10, 1–19.
- Pople, John A, Martin Head-Gordon, and Krishnan Raghavachari (1987), “Quadratic configuration interaction. a general technique for determining electron correlation energies.” *J. Chem. Phys.*, 87, 5968–5975.
- Posener, DW (1959), “The shape of spectral lines: Tables of the voigt profile.” *Australian Journal of Physics*, 12, 184–196.
- Pratap, P, JE Dickens, Ronald L Snell, MP Miralles, EA Bergin, William M Irvine, and FP Schloerb (1997), “A study of the physics and chemistry of tmc-1.” *the Astrophysical Journal*, 486, 862.
- Pugh, LA and K Narahari Rao (1976), “Molecular spectroscopy: Modern research.” *II (New York: Academic)*.
- Purvis III, George D and Rodney J Bartlett (1982), “A full coupled-cluster singles and doubles model: The inclusion of disconnected triples.” *J. Chem. Phys.*, 76, 1910–1918.
- Puzzarini, Cristina, Małgorzata Biczysko, Julien Bloino, and Vincenzo Barone (2014), “Accurate spectroscopic characterization of oxirane: A valuable route to its identification in titan’s atmosphere and the assignment of unidentified infrared bands.” *The Astrophysical journal*, 785, 107.
- Raghavachari, Krishnan, Gary W Trucks, John A Pople, and Martin Head-Gordon (1989), “A fifth-order perturbation comparison of electron correlation theories.” *Chem. Phys. Lett.*, 157, 479–483.
- Ramabhadran, Raghunath O and Krishnan Raghavachari (2013), “Extrapolation to the gold-standard in quantum chemistry: Computationally efficient and accurate ccSD (t) energies for large molecules using an automated thermochemical hierarchy.” *Journal of chemical theory and computation*, 9, 3986–3994.
- Ramachandran, R, J Kłos, and F Lique (2018), “A new ab initio potential energy surface for the nh–he complex.” *J. Chem. Phys.*, 148, 084311.
- Rinnenthal, Jan Leo and Karl-Heinz Gericke (2000), “State-to-state studies of ground state nh (x 3 σ-, v= 0, j, n)+ ne.” *J. Chem. Phys.*, 113, 6210–6226.

- Rinnenthal, Jan Leo and Karl-Heinz Gericke (2002), “State-to-state energy transfer of nh (χ 3 σ^- , $v = 0, j, n$) in collisions with he and n 2.” *J. Chem. Phys.*, 116, 9776–9791.
- Rivilla, VM, J Martín-Pintado, I Jiménez-Serra, S Zeng, S Martín, J Armijos-Abendano, MA Requena-Torres, R Aladro, and D Riquelme (2018), “Abundant z-cyanomethanimine in the interstellar medium: paving the way to the synthesis of adenine.” *Monthly Notices of the Royal Astronomical Society: Letters*, 483, L114–L119.
- Ruffle, DP, TW Hartquist, P Caselli, and DA Williams (1999), “The sulphur depletion problem.” *MNRAS*, 306, 691–695.
- Savage, Blair D and Kenneth R Sembach (1996), “Interstellar abundances from absorption-line observations with the hubble space telescope.” *Annu. Rev. Astron. Astrophys.*, 34, 279–329.
- Schuchardt, Karen L, Brett T Didier, Todd Elsethagen, Lisong Sun, Vidhya Gurumoorthi, Jared Chase, Jun Li, and Theresa L Windus (2007), “Basis set exchange: a community database for computational sciences.” *Journal of chemical information and modeling*, 47, 1045–1052.
- Shingledecker, Christopher N, Thanja Lamberts, Jacob C Laas, Anton Vasyunin, Eric Herbst, Johannes Kästner, and Paola Caselli (2020), “Efficient production of s8 in interstellar ices: The effects of cosmic-ray-driven radiation chemistry and nondiffusive bulk reactions.” *The Astrophysical Journal*, 888, 52.
- Sinclair, M. W., N. Fourikis, J. C. Ribes, B. J. Robinson, R. D. Brown, and P. D. Godfrey (1973), “Detection of interstellar thioformaldehyde.” *Aust. J. Phys.*, 26, 85.
- Slater, John C (1951), “A simplification of the hartree-fock method.” *Physical review*, 81, 385.
- Smith, Leslie N, David J Malik, and Don Secrest (1979), “Rotational compound state resonances for an argon and methane scattering system.” *J. Chem. Phys.*, 71, 4502–4514.
- Smith, Robert G (1991), “A search for solid h2s in dense clouds.” *Monthly Notices of the Royal Astronomical Society*, 249, 172–176.
- Snyder, Lewis E, Francis J Lovas, JM Hollis, Douglas N Friedel, PR Jewell, A Remijan, Vadim V Ilyushin, EA Alekseev, and SF Dyubko (2005), “A rigorous attempt to verify interstellar glycine.” *The Astrophysical Journal*, 619, 914.
- Stoecklin, T (2009), “Combining electric and magnetic static fields for the tuning of the lifetime of zero energy feshbach resonances: Application to he 3+ nh (χ 3) collisions.” *Phys. Rev. A*, 80, 012710.
- Sugie, Masaaki, Harutoshi Takeo, and Chi Matsumura (1985), “Microwave spectra, nuclear quadrupole coupling constants, dipole moments, and rotational isomers of propargylimine.” *Journal of Molecular Spectroscopy*, 111, 83–92.

- Sullivan, Woodruff Turner (2004), *The early years of radio astronomy: Reflections fifty years after Jansky's discovery*. Cambridge University Press.
- Suzuki, Hiroko, Satoshi Yamamoto, Masatoshi Ohishi, Norio Kaifu, Shin-Ichi Ishikawa, Yasuhiro Hirahara, and Shuro Takano (1992), “A survey of ccs, hc3n, hc5n, and nh3 toward dark cloud cores and their production chemistry.” *The Astrophysical Journal*, 392, 551–570.
- Thaddeus, P., M. L. Kutner, A. A. Penzias, R. W. Wilson, and K. B. Jefferts (1972), “Interstellar Hydrogen Sulfide.” *ApJ*, 176, L73.
- Theulé, Patrice, Fabien Borget, Florent Mispelaer, Grégoire Danger, Fabrice Duvernay, Jean-Claude Guillemin, and Thierry Chiavassa (2011), “Hydrogenation of solid hydrogen cyanide hcn and methanimine ch2nh at low temperature.” *Astronomy & Astrophysics*, 534, A64.
- Tieftrunk, A., G. Pineau des Forets, P. Schilke, and C. M. Walmsley (1994), “SO and H2S in low density molecular clouds.” *A&A*, 289, 579–596.
- Tobola, Robert, Fabien Dumouchel, Jacek Kłos, and François Lique (2011), “Calculations of fine-structure resolved collisional rate coefficients for the nh (x 3 σ)-he system.” *J. Chem. Phys.*, 134, 024305.
- Trambarulo, Ralph, Arthur Clark, and Charles Hearns (1958), “Planarity of the formic acid monomer.” *J. Chem. Phys.*, 28, 736–737.
- Troe, J (1985), “Statistical adiabatic channel model of ion-neutral dipole capture rate constants.” *Chem. Phys. Lett.*, 122, 425–430.
- van Dishoeck, Ewine F (2017), “Astrochemistry: overview and challenges.” *Proceedings of the International Astronomical Union*, 13, 3–22.
- Vidal, Thomas HG, Jean-Christophe Loison, Adam Yassin Jaziri, Maxime Ruaud, Pierre Gratier, and Valentine Wakelam (2017), “On the reservoir of sulphur in dark clouds: chemistry and elemental abundance reconciled.” *MNRAS*, 469, 435–447.
- Wakelam, V., P. Caselli, C. Ceccarelli, E. Herbst, and A. Castets (2004), “Resetting chemical clocks of hot cores based on S-bearing molecules.” *A&A*, 422, 159–169.
- Wakelam, V., P. Caselli, C. Ceccarelli, E. Herbst, J. Mascetti, and A. Castets (2005), “Searching for sulphur polymers in young protostars with Herschel and ALMA.” In *ESA Special Publication* (A. Wilson, ed.), volume 577 of *ESA Special Publication*, 435–436.
- Wakelam, Valentine and Eric Herbst (2008), “Polycyclic aromatic hydrocarbons in dense cloud chemistry.” *ApJ*, 680, 371.
- Watanabe, Naoki and Akira Kouchi (2002), “Efficient formation of formaldehyde and methanol by the addition of hydrogen atoms to co in h2o-co ice at 10 k.” *The Astrophysical Journal Letters*, 571, L173.

- Watson, J. K. G. (1977a). In *Vibrational Spectra and Structure* (J. Durig, ed.), volume 6, 1–89, Elsevier, Amsterdam.
- Watson, James KG (1977b), “A planarity relation for sextic centrifugal distortion constants.” *J. Mol. Spectr.*, 65, 123–133.
- Watts, John D, Jürgen Gauss, and Rodney J Bartlett (1993), “Coupled-cluster methods with noniterative triple excitations for restricted open-shell hartree–fock and other general single determinant reference functions. energies and analytical gradients.” *J. Chem. Phys*, 98, 8718–8733.
- Werner, H.-J., P. J. Knowles, G. Knizia, F. R. Manby, M. Schütz, et al. (2019), “Molpro, version 2019.2, a package of ab initio programs.”
- Werner, Hans-Joachim, Bernd Follmeg, and Millard H Alexander (1988), “Adiabatic and diabatic potential energy surfaces for collisions of cn ($x\ 2\sigma^+$, $a\ 2\pi$) with he.” *J. Chem. Phys*, 89, 3139–3151.
- Werner, Hans-Joachim and Peter J Knowles (1988), “An efficient internally contracted multiconfiguration–reference configuration interaction method.” *J. Chem. Phys*, 89, 5803–5814.
- Whittet, Douglas (2017), *Origins of Life: A Cosmic Perspective*. Morgan & Claypool Publishers.
- Wilson, Stephen, John Courtney Decius, Paul C Cross, et al. (1992), *Molecular vibrations*. Plenum Press.
- Winnewisser, Manfred, Brenda P Winnewisser, Monika Stein, Manfred Birk, Georg Wagner, Gisbert Winnewisser, Koichi MT Yamada, Sergey P Belov, and Oleg I Baskakov (2002), “Rotational spectra of cis-hcooh, trans-hcooh, and trans-h 13 cooh.” *J. Mol. Spectr.*, 216, 259–265.
- Woods, P. M., A. Occhiogrosso, S. Viti, Z. Kaňuchová, M. E. Palumbo, and S. D. Price (2015), “A new study of an old sink of sulphur in hot molecular cores: the sulphur residue.” *MNRAS*, 450, 1256–1267.
- Woon, David E (2002), “Pathways to glycine and other amino acids in ultraviolet-irradiated astrophysical ices determined via quantum chemical modeling.” *The Astrophysical Journal Letters*, 571, L177.
- Woon, David E and Thom H Dunning Jr (1995), “Gaussian basis sets for use in correlated molecular calculations. v. core-valence basis sets for boron through neon.” *The Journal of chemical physics*, 103, 4572–4585.
- Zaleski, Daniel P, Nathan A Seifert, Amanda L Steber, Matt T Muckle, Ryan A Loomis, Joanna F Corby, Oscar Martinez Jr, Kyle N Crabtree, Philip R Jewell, Jan M Hollis, et al. (2013), “Detection of e-cyanomethanimine toward sagittarius b2 (n) in the green bank telescope primos survey.” *The Astrophysical Journal Letters*, 765, L10.

Ziegler, James F (2004), “Srim-2003.” *Nuclear instruments and methods in physics research section B: Beam interactions with materials and atoms*, 219, 1027–1036.

Zuckerman, B., J. A. Ball, and C. A. Gottlieb (1971), “Microwave Detection of Interstellar Formic Acid.” *ApJ*, 163, L41.